Between the Stars: The multiphase turbulent ISM

A Thesis

Submitted to the

Tata Institute of Fundamental Research, Mumbai
(A Deemed University)

for the degree of Doctor of Philosophy
in Physics

by

Nirupam Roy

National Centre for Radio Astrophysics
TATA INSTITUTE OF FUNDAMENTAL RESEARCH
2009

Dedication

"And how shall you speak of her except she be the weaver of your speech?"

My Dear Friend,

Most probably you will never come to know of this dedication. I do not know whether the offerings are lost in vain if the flowers do not reach you, but the devotion is unquestionable. Thanks to you, I have seen, with ecstasy, life unvailing Her holy face. I remain grateful, for I have learned to bleed willingly and joyfully.

Please allow me to dedicate
this small work of my passion
to you
who has taught me
the eternity of beauty and life.

Nirupam

"আমি কী দিলেম কারে জানে না সে কেউ, ধুলায় রহিল ঢাকা।"

(*"No one knows what I have given to whom, it remained buried in dust."*)

Declaration

This thesis is a presentation of my original research work. Wherever contributions of others are involved, every effort is made to indicate this clearly, with due reference to the literature, and acknowledgement of collaborative research and discussions.

The work was done under the guidance of Prof. Jayaram N. Chengalur, at the National Centre for Radio Astrophysics (Pune) of the Tata Institute of Fundamental Research, Mumbai.

.....

(Nirupam Roy)

In my capacity as supervisor of the candidate's thesis, I certify that the above statements are true to the best of my knowledge.

.....

(Prof. Jayaram N. Chengalur)

Date: October 20, 2009

Acknowledgments

Over the last few years, borrowing poet's words, *I have loved the stars too fondly to be fearful of the night.*[1] But then it was time to write the thesis. And the only pleasant part of writing a thesis is probably writing this acknowledgements section. At the end of a long journey, this is the time to look back, and tell myself that it was not really as dark as it may have seemed to be at times. I take this opportunity to say a word or two of sincere gratefulness to those who have made life a lot more easier for me.

I first of all convey my heartfelt gratitude to Rajaram Nityananda. I have bothered him time and again with my questions and have never come back unsatisfied. He has managed to find time for me from his busy schedule and has always been very encouraging. All the discussion sessions with him were very useful and his insightful comments always turned out to be very helpful and have significantly improved this work. I also express my gratitude to Raghunathan Srianand. Anand has always encouraged me, has provided the necessary guidance at different stages and has spent his valuable time discussing various things. I sincerely acknowledge the crucial encouraging role of Prof. Govind Swarup in my academic life. His words are always so inspiring and motivating. I also consider myself fortunate to come in touch with Prof. Probir Roy (Dept. of Theoretical Physics, TIFR) as early as in my school days. Since then, through all these years he has motivated and inspired me very much.

I am grateful to Dipankar Bhattacharya, K. S. Dwarakanath, Dave Green, Gopal Krishna, Ranjeev Misra, P. Padoan, D. Pogosyan, A. Pramesh Rao, D. J. Saikia, Kandaswamy Subramanian and V. E. Tarasov for useful discussions and many helpful comments on various aspects this work. I also thank Dipanjan, Ishwara, Tarun, Nimisha, Prasad, Ramana, Vasant, Yaswant and Yogesh for all their encouragements.

I sincerely thank all the staff members of NCRA and GMRT. I have always looked forward to go to GMRT for observation. Everyone there has been very friendly to me. Without their help, it would not have been

[1] Sarah Williams in The Old Astronomer

possible to carry out all the observations that I have done for this thesis work. I also acknowledge the hospitality of all the staff members of the Centre for Theoretical Studies (Indian Institute of Technology, Kharagpur) during my stay there. I am thankful to the ASTRON staff members who have contributed a lot by helping me with the WSRT observations. Special thanks to Annabhat, Hemant, Reena and Sunita for extending their helping hands. I have enjoyed a lot working with Arnab, Leshma, Manoharan, Pavan, Prasun and Somnath-*da*. I thank them for this nice experience and look forward for more collaborative work with them in near future.

I must thank all my NCRA and IUCAA friends. From Ayesha, Dharam, Samir and Subhashis I have learned a lot. I have never felt alone and bored, thanks to my NCRA friends Ananda, Aritra, Babita, Bhaswati, Chiranjib, Ekta, Jayanta, Jayanti, Moumita, Neeraj, Sabyasachi, Sambit, Sudeep, Ujjwal, Vishal and Yogesh. Thanks to my friends *from the other side of the road* Atul, Gaurang, Maryam, Moumita, Nisha, Sanjit, Sudipta and Tapan who have always taken me as one of them. Alka, Atish, Laxmikant, Sagar, Saravanan, Senorita, Shruti and Shweta have added extra colour to my life during their long or short visits to NCRA and IUCAA. Unfortunately, I cannot thank my friend Himan, but I will always cherish her memory and remain grateful for I have learned a lot from her.

A special thanks to Ratna, Samir, Saumya, Subharthi, Supratik and Ujjaini for all the good food that we have had together, to Naren and Rahul for the movies that we have watched together, to Chandreyee and Sumana for all the melodious *adda* sessions, to Maryam et al. for the pleasant night-walks, to Viswesh for providing the excellent background scores in our office, to Chandreyee and Sanhita for all the pleasant torture and ragging sessions and to Chandreyee for the perpetual supply of *anything* (but her century-old badminton racket) *one needs at anytime*. Sincere thanks to Sanhita for the exquisite cups of coffee with *honey* and to Chandreyee for the charmer of our idle hours - all the *classic*s.

I have always been encouraged by many of my teachers, friends, relatives and well-wishers. Here I must acknowledge the contribution of

my school teachers, especially Shri Chittaranjan Roy and Shri Sukumar Nandi; of my professors Dr. Debasis Datta and Dr. Ajit Kr. Chattopadhyay; of my school friends Jayashri, Rajesh, Shankar and Sourav; of my college friends Maidul, Shovan, Tarak and Anuja; of all my relatives, especially of Shrikanta *kaku*, Pushpal and young Poulami. A very special thanks to Jiten *babu* (Shri Jitendranath Sinha) who helped me realize the unquestionable supremacy of Physics, to Sayan for a non-stop supply of Bengali literature which remains my first love, and to Arup, Abhijit, Arpita and Debabrata for all the *adda*s. I cannot convey my gratitude to my respected teacher, my mentor, my affectionate "*dadu*" Narayan Chandra Chakrabortty for he is no more with us. He played the most significant role in shaping my rational point of view in life.

This work has made use of the NASA's Astrophysics Data System, the National Radio Astronomy Observatory VLA archival data, data from the millennium Arecibo 21 cm absorption-line survey and from the The Leiden/Argentine/Bonn Galactic H I Survey. I acknowledge MNRAS, MNRAS Letters, the Royal Astronomical Society and Blackwell Publishing for allowing me to reuse some of the materials and figures from my articles published by them. I also acknowledge support from the TIFR research fellowship and partial support from the Kanwal Rekhi scholarship program of the TIFR Endowment Fund. Thanks to Sanhita, Chandreyee, Yogesh and Nimisha for carefully (and painfully) proof reading the whole thesis! Much of the credit for the LaTeX style goes to Jamie Stevens. There are many other friends and well-wishers who have helped me in various ways and I remain grateful to all of them. I also very sincerely acknowledge the contribution of everyone who are playing an important role in scientific research by paying tax to the government.

There are some friends to whom I must not say a "thank you", because no amount of thanks will ever be adequate for them to convey my appreciation. I better not say anything about Jayaram for I do not have words to express my gratitude. To be honest, I would not like to go for a second Ph.D.; but if I ever do that again, it can only be if Jayaram be my super-

visor. Nissim also played a very important role in shaping up this thesis. Without his continuous turbulent driving (critical, harsh, encouraging), it would have been very hard, if not impossible, for me to do much of what I have done in the last few years. Throughout, Susmita was always there with me; something that was required most on those days. And above all, my grandmother, my *Maa* (Mashimoni), my sister Mahua and my parents, Aparajita Roy and Kajal Kanti Roy have always been supportive and helpful. They remain my main source of inspiration. I will not thank them, but I would like to sincerely acknowledge their crucial contribution to this work.

Nirupam Roy

List of Publications

(Publications related to works which are part of this thesis are marked with ★.)

Refereed publications:

1. **N. Roy**, J. N. Chengalur and R. Srianand, A multiwavelength investigation of the temperature of the cold neutral medium, 2006, **MNRAS Letters**, 365, L1

2. **N. Roy**, On spherically symmetrical accretion in fractal media, 2007, **MNRAS Letters**, 378, L34

3. **N. Roy** and A. K. Ray, Critical properties of spherically symmetric accretion in a fractal medium, 2007, **MNRAS**, 380, 733

4. **N. Roy**, P. K. Manoharan and P. Chakraborty, Occultation observation to probe the turbulence scale size in the plasma tail of comet Schwassmann-Wachmann 3-B, 2007, **ApJ Letters**, 668, L67

5. S. Scarano Jr., F. R. H. Madsen, **N. Roy** and J. R. D. Lépine, H I aperture synthesis and optical observations of the pair of galaxies NGC 6907 and 6908, 2008, **MNRAS**, 386, 963

★6. **N. Roy**, L. Peedikakkandy and J. N. Chengalur, Turbulence measurements from H I absorption spectra, 2008, **MNRAS Letters**, 387, L18

★7. **N. Roy**, S. Bharadwaj, P. Dutta and J. N. Chengalur, Magnetohydrodynamic turbulence in supernova remnants, 2009, **MNRAS Letters**, 393, L26

8. **N. Roy** and A. K. Ray, Fractal features in accretion discs, 2009, **MNRAS**, 397, 1374

In preparation:

★1. **N. Roy**, J. N. Chengalur, S. Bharadwaj and P. Dutta, H I opacity fluctuations towards Cassiopeia A, 2009 (in preparation)

★2. **N. Roy**, R. Srianand and J. N. Chengalur, On C II radiative cooling of the diffuse interstellar medium, 2009 (in preparation)

★3. **N. Roy**, N. Kanekar, J. N. Chengalur and R. Braun, The temperature of the diffuse H I in the Milky Way, 2009 (in preparation)

Others:

1. **N. Roy**, J. N. Chengalur and R. Srianand, A multi-wavelength investigation of the temperature of the cold neutral ISM, 2005, Proceeding of the 23rd Meeting of the ASI in **BASI**, 33, 389

2. **N. Roy** and N. Kanekar, Frequency-switched bandpass calibration at the GMRT, 2007, **NCRA Technical Report**, R00228

3. S. Chakraborti, P. Chandra, **N. Roy** and A. Ray, Radio monitoring of SN 2007gr by GMRT in the L-band, 2007, **The Astronomer's Telegram**, #1222

★4. **N. Roy**, J. N. Chengalur, S. Bharadwaj and P. Dutta, Turbulence in the cold neutral ISM and in supernova remnants, 2009, Proceedings of the conference *The Low-Frequency Radio Universe*, **ASP Conference Series**, Vol. 407, p.272

★5. **N. Roy**, S. Bharadwaj, P. Dutta and J. N. Chengalur, MHD turbulence in supernova remnants, 2009, to appear in Proceeding of the 27th Meeting of the ASI in **BASI**

Contents

List of Figures

List of Tables

Abstract

The process of star formation through the collapse of baryonic matter (protostellar clouds) captured in a dark matter halo is never totally efficient. This leads to the existence of residual gas around the stars or the primordial interstellar medium (ISM). The radiation and mechanical energy input from the stars influences the properties of the ISM. Processes like stellar winds, ejection of the outer mantle in the late stages of stellar evolution and supernova explosions transfer material and energy from the stars to the ISM. Similarly, ultraviolet radiation from hot, young stars and cosmic rays heat and ionize the ISM. All these processes couple the ISM with the stars and leads to the ISM playing a crucial coupling role between stellar and galactic scales. Hence, the study and understanding of the properties of the ISM is very important from many considerations in astronomy and astrophysics.

Multiple phases and turbulence are two of the key ingredients of ISM physics. Our present understanding is that multiple phases of the ISM in a galaxy are in rough thermal pressure equilibrium (e.g. Field, 1965; Field et al., 1969; McKee & Ostriker, 1977; Wolfire et al., 1995, 2003). In a multiphase medium, the cold dense neutral gas (cold neutral medium or CNM) is embedded in either neutral or ionized low density warm gas (warm neutral/ionized medium or WNM and WIM), which again may be embedded in much lower density hot ionized gas (hot ionized medium or HIM). Considering the details of different cooling and heating processes, it can be shown that the neutral hydrogen gas (H I) can be in thermal steady state in one of the two stable ranges of temperature: (i) $\sim 40 - 200$ K for CNM and (ii) $\sim 5000 - 8000$ K for WNM. The H I at intermediate temperatures is unstable and is expected to quickly move to one of the stable phases (McKee & Ostriker, 1977; Wolfire et al., 2003). The ISM is also known to have a clumpy self-similar hierarchical structure over several orders of magnitude in scale (Larson, 1981; Falgarone et al., 1992; Heithausen et al., 1998). Direct H I absorption observations and interstellar scintillation measurements suggest that the structure extends down to 10 AU scales

(e.g. Hill et al., 2005). On the theoretical front, the ISM is known to be turbulent and hence is expected to exhibit density structures and velocity fluctuations on a wide range of spatial scales (Crovisier & Dickey, 1983; Green, 1993; Lazarian & Pogosyan, 2000).

The thermal steady state model forms the basis of our theoretical understanding of the temperature of the diffuse atomic ISM. Recently, however, there have been some observational indications of the existence of a large fraction of H I in the intermediate temperature unstable state (Dwarakanath et al., 2002; Heiles & Troland, 2003a,b; Kanekar et al., 2003). This has raised doubts about the validity of the thermal equilibrium model. Given the serious implication of these observations on our understanding of ISM physics, it is very important to critically test the above-mentioned observational results. The H I 21 cm emission line width is sometimes used for a direct measurement of temperature (Heiles & Troland, 2003a). One of the major issues in this regard is the determination of temperature in the presence of non-thermal line broadening due to turbulence in the ISM. Hence, to get the actual temperature of the gas from H I 21 cm observations, it is crucial to understand the nature of the turbulence in the diffuse atomic ISM. This will allow one to quantify the contribution of turbulence to the observed line width, to get better estimates of the temperature and the fraction of gas in thermally stable or unstable states. In this thesis, I have presented my work on the ISM temperature, turbulence and the interplay of these two, concentrating mostly on the science of the diffuse atomic ISM.

H I 21 cm absorption and emission observations are often used to derive the spin temperature (T_s) which is found to be coupled to the kinetic temperature (T_k) of the gas (Field, 1958; Radhakrishnan et al., 1972; Mebold et al., 1982; Heiles & Troland, 2003a,b; Roy et al., 2006). However, the temperature can also be inferred independently from the observed H I 21 cm line width (Heiles & Troland, 2003a). This gives an upper limit to the kinetic temperature (T_{kmax}) if the non-thermal broadening of the line due to processes like turbulence is significant. On the other hand, measuring

both T_s and T_{kmax} will allow one to quantify the non-thermal line width and derive some understanding of the turbulence in the ISM.

This strategy is used to estimate the non-thermal contribution to the observed H I line width using published data from the millennium Arecibo 21 cm absorption-line survey measurements (Heiles & Troland, 2003a). It is found that the non-thermal line width has a power law scaling with the derived length scale and the power law index is consistent with what one would expect from a turbulent medium with a Kolmogorov scaling (Kolmogorov, 1941). This scaling relation is used to estimate the "true" kinetic temperature of all the H I components detected in the Arecibo survey. It is also found that $\sim 30\%$ of the total H I column density is in the warm unstable phase.

These results are, however, based completely on single dish observations of H I emission and absorption spectra. Single dish spectra are known to be affected by stray radiation entering via the side-lobes of the telescope beam, self-absorption of background emission by foreground gas and an inaccurate subtraction of the emission in the beam to obtain the H I absorption spectra. Interferometric absorption studies of lines of sight towards compact sources are not affected by the above issues.

Keeping this in mind, high resolution and high sensitivity interferometric H I absorption observations have been carried out towards 18 compact sources to obtain estimates of the distribution of the atomic ISM in different thermal phases. Based on the upper limits of the kinetic temperature derived from the line widths, it is found that more than 80% of neutral gas has $T_{kmax} > 500$ K and $\sim 65\%$ gas is in the unstable thermal phase. After correcting for the non-thermal line width, approximately half of the gas is found to in the unstable phase. This large observed fraction of gas in the unstable phase is a strong indication of the possibility that the thermal steady state has not been achieved in the diffuse ISM. In light of these results, it is, hence, a necessary and urgent exercise to check if alternative (time-dependent supernova-dominant or turbulence dominated) models of the ISM can explain the observations properly.

ABSTRACT

The possibility that thermal steady state models are not applicable for the ISM may be related to the turbulent nature of the ISM (Vázquez-Semadeni et al., 2000). Hence, this exercise of temperature measurements from H I observations is very much coupled with understanding the nature of turbulence in the ISM. Turbulence in two different components of the ISM (namely in supernova remnants and in the cold diffuse neutral gas) is probed as a part of this thesis work.

At the galactic scale, supernovae and supernova remnants play a very important role as a link between the gaseous and stellar components of the Galaxy. In addition to the large scale shell-like or filled-centre structures, supernova remnants show a very rich and complicated structure over a wide range of scales. A useful statistic both for quantifying these structures as well as for comparison with theoretical models is the power spectrum of the intensity fluctuations. A simple but robust visibility based method (Begum et al., 2006; Dutta et al., 2008) is used to provide, for the first time, a quantitative estimate of the fine scale structures for two supernova remnants. The synchrotron radiation intensity fluctuation power spectra for the shell type supernova remnant Cas A and the filled-centre Crab Nebula can both be described as a power law with index -3.24 ± 0.03. This power law spectrum is consistent with magnetohydrodynamic turbulence in the synchrotron emitting plasma (Cho & Lazarian, 2002a,b). For Cas A, there is a break in the power spectrum and the power law index changes from -3.2 to -2.2 at angular scales larger than that corresponds to the shell thickness of Cas A. This is interpreted as a transition from three to two dimensional turbulence on scales larger than the shell thickness.

The same formalism is used to estimate the H I 21 cm opacity fluctuation towards Cas A. The power spectrum of the opacity fluctuation has a power law index of $\sim 2.86 \pm 0.10$ over the scales of $0.07 - 3.6$ pc. This is consistent with previously reported observational results based on both H I emission (over somewhat larger scales) and absorption studies (over a similar range of scales) (Crovisier & Dickey, 1983; Green, 1993; Desh-

pande et al., 2000). Power spectra derived for the gas from the Perseus spiral arm and from the solar neighbourhood show no significant difference. The variation of the power law index with the velocity width of the channel is also within the estimation error ruling out any significant effect of averaging over velocity. The limit on the power law index of the velocity structure function ($\beta = 0.2 \pm 0.6$) is consistent with the value of $\beta = 2/3$ predicted for Kolmogorov turbulence (Kolmogorov, 1941).

Finally, an illustrative example is considered to demonstrate the importance of measuring the temperature of the diffuse ISM. This is related to the technique of computing the star formation rate (in our Galaxy as well as in extragalactic sources including high redshift damped Lyman-α systems) from the observed C II* column density. CII 157.7 μm is a major coolant of the diffuse interstellar gas. The observed C II* column density is a direct measure of the cooling rate of the gas (Pottasch et al., 1979). In steady state, the cooling rate is equal to the heating rate, which in turn depends on the star formation rate. Thus, observations of the flux in the C II* line allow one to determine the star formation rate (Wolfe et al., 2003). However, the inferred heating rate (or equivalently, the star formation rate) estimated from CII* radiative cooling crucially depends on the physical conditions like temperature of the gas (Lehner et al., 2004; Wolfe et al., 2003). If the CII* line arises in the WNM, the inferred star formation rate is almost an order of magnitude more than if it arises in the CNM.

One way to resolve the issue would be to directly measure the temperature of the gas giving rise to the C II* absorption. Direct H I 21 cm emission and absorption observations can be used to determine the spin temperature which, as already mentioned, is known to be a good proxy of the kinetic temperature of the gas. H I observations of seven high Galactic latitude lines of sight with C II* absorption were carried out with the GMRT. From these observations, it appears that even at high Galactic latitudes, gas in both cold and warm phases contribute to the observed C II* absorption.

Chapter 1

An introduction to Interstellar Medium

The word *astronomy* literally means "the laws of stars". Dictionaries, however, define astronomy as "the study of objects and matter outside the earth's atmosphere and of their physical and chemical properties" [1]. This includes the study of the interstellar medium (ISM) also. Loosely speaking, the interstellar medium is the medium in the region between the stars. The interstellar space in a galaxy is far from empty. Even if the density is very low, these regions are filled with gas (mostly hydrogen and helium), dust (silicate and graphite), charged particles and magnetic fields. The total mass of the gas and dust in the ISM is approximately $10 - 15\%$ of the total visible mass of the Galaxy.

The study and understanding of the properties of ISM is very important from many considerations in astronomy and astrophysics. The process of star formation through the collapse of baryonic matter (protostellar clouds) captured in a dark matter halo is never totally efficient. This leads to the existence of residual gas around the stars (primordial ISM). The local radiation field of the stars influences the properties of ISM to some extent. Processes like stellar winds, ejection of the outer mantle in late stages of stellar evolution and supernova explosions transfer material and energy

[1] Merriam-Webster Online (`http://www.merriam-webster.com/dictionary/astronomy`)

from the stars to the ISM. All these processes couple stars and the ISM and hence it plays a crucial coupling role between stellar and galactic scales.

Astronomers inferred the existence of interstellar gas after the discovery of stationary absorption lines of ionized calcium (Ca II) towards the spectroscopic binary δ-Orionis (Hartmann, 1904). Any spectral line from stars of a spectroscopic binary system should have a periodic wavelength shift due to the Doppler effect for the motion of the stars. The stationary Ca II absorption line was hence taken as an indication of interstellar gas. Edward Emerson Barnard (1857 – 1923) was the first astronomer who carried out a systematic study of the Galactic ISM. Even though initially it was not clearly established, he first proposed the existence of "intervening opaque masses" between the stars to explain these observed "dark nebula". He used his expertise of astrophotography to produce the first images of dark nebulae and published the first catalogue (Barnard, 1919) of such dark clouds. Very soon, from more imaging and spectroscopic observations, the existence of widespread interstellar material including gas and dust clouds was quite evident.

1.1 General Properties

The ISM is known to exhibit a vast range of physical and chemical properties like densities, temperatures, ionization fractions and molecular abundances. Discrete "clouds" (dark clouds made of compact, cold molecular gas at temperature $\sim 10 - 20$ K and diffuse clouds made of cold atomic gas at temperature $\sim 50 - 100$ K) occupy about $\sim 1 - 2\%$ of the interstellar space and account for half of the total ISM mass. The rest of the ISM between these "clouds" are in warm neutral (atomic), warm ionized and hot ionized phases. The basic properties of these different components are summarized in Table 1.1.

The observed chemical composition of the ISM is very much like the "cosmic composition". It is composed mainly of hydrogen (70.4% by mass), helium (28.1%) and trace amounts of heavier elements (1.5%). However, a

Table 1.1: Basic properties of different components of the ISM[a]

Component of ISM	Density (cm^{-3})	Temperature (K)	Fractional volume	Total mass $10^9 M_\odot$
Cold molecular gas	$10^2 - 10^6$	$10 - 20$	$< 1\%$	$\sim 1.3 - 2.5$
Cold neutral gas	$20 - 50$	$50 - 100$	$1 - 5\%$	$\} \gtrsim 6.0$
Warm neutral gas	$0.2 - 0.5$	$6000 - 10000$	$10 - 20\%$	
Warm ionized gas	$0.2 - 0.5$	~ 8000	$20 - 50\%$	$\gtrsim 1.6$
Hot ionized gas	~ 0.0065	$\sim 10^6$	$30 - 70\%$	not known

[a] Adapted from Ferrière (2001)

significant fraction of these heavier elements (or "metals") is locked up in solid dust grains. About $0.5 - 1\%$ of the total mass of the interstellar matter is in the form of dust.

1.2 Multiphase ISM

Our understanding of the structure of the ISM has evolved from modelling it as consists of homogeneous "standard clouds" (which are typically of about 10 pc diameter), coexisting with "large clouds" of ~ 70 pc diameter (Spitzer, 1978), to the present widely accepted multiphase turbulent ISM (McKee & Ostriker, 1977; Wolfire et al., 1995, 2003). Field et al. (1969) presented a static two phase equilibrium model of the ISM. This, with further inputs from more observations and a better theoretical understanding of thermal and mechanical energy balance, has evolved to the present model of multiphase ISM (Wolfire et al., 2003). In a multiphase medium, the cold dense neutral gas is embedded in either neutral or ionized low density warm gas, which again may be embedded in much lower density hot ionized gas. The typical cold neutral medium (CNM) temperature is ~ 100 K while the typical temperature of warm neutral medium (WNM) and warm ionized medium (WIM) is $\sim 10^4$ K. The hot ionized medium (HIM) is at a

temperature of $\sim 10^6$ K. Typical size (over which the physical parameters are not drastically changing) of CNM cloud is $\sim 1-20$ pc (McKee & Ostriker, 1977). This is significantly smaller than the scale on which the turbulent pressure in the WNM begins to dominate the thermal pressure (~ 215 pc). Below this scale, the gas will be in approximate thermal pressure equilibrium (Wolfire et al., 2003). The CNM clouds, hence, can be considered to be embedded in an isobaric medium. Similarly, in the inner regions of the CNM, the gas will be in thermal pressure equilibrium on scales $<\sim 0.3$ pc.

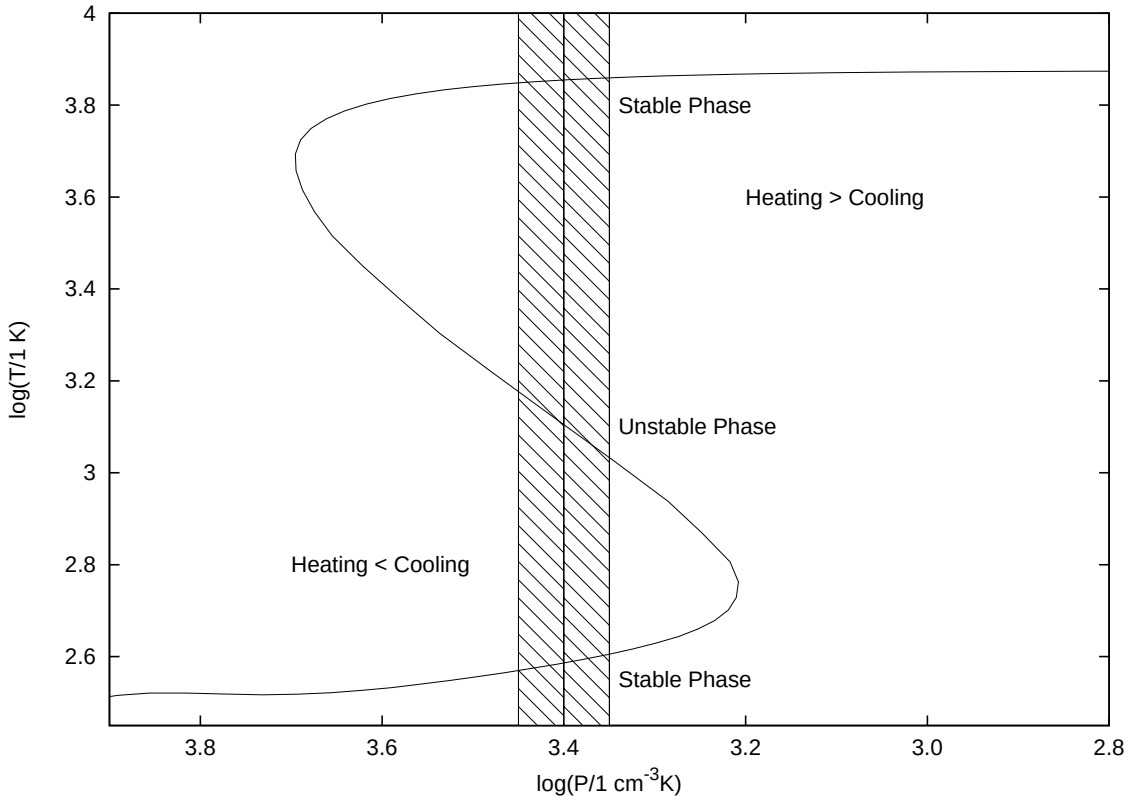

Figure 1.1: A schematic phase diagram of multiphase interstellar medium showing the relation between pressure and temperature in steady states for a simplified toy model. The 'S'-shaped curve is the thermal equilibrium curve, i.e. where the heating and cooling rates are equal. The stable CNM and WNM phases are shown to be coexisting in a rough thermal pressure equilibrium. Any thermal disturbance in the unstable gas at intermediate temperature will cause runaway heating or cooling and move it to one of the stable phases.

All these different phases of the ISM in a galaxy are in a rough thermal pressure equilibrium (Field et al., 1969; Wolfire et al., 2003) and the typical pressure is $P/k \sim 10^3$ cm^{-3}K. Considering the details of different cooling and heating processes, it can be shown that the neutral hydrogen gas (denoted by H I as opposed to H II for ionized hydrogen gas) can be in pressure equilibrium in one of the two stable ranges of temperature: (i) $\sim 40-200$ K for CNM and (ii) $\sim 5000-8000$ K for WNM (Wolfire et al., 1995). This is simply because of multi-valued nature of thermal equilibrium curve in pressure – temperature space. A schematic phase diagram of multiphase ISM in steady state for a simplified toy model is shown in Figure (1.1). The H I at intermediate temperatures is unstable and is expected to quickly move to one of the stable phases, unless energy is intermittently being injected into the medium.

This multiphase model has successfully explained the the properties of ISM inferred from observations using a wide range of wavelengths, a variety of techniques and various tracers. But, it should be noted that, even after almost 50 years of study, several details like the exact relative proportion of different phases, the subdivisions of these phases (if any), the observational evidence of the existence of very very small sized neutral hydrogen clouds or observational indications of a significant fraction of neutral gas being in the thermally unstable region are not well understood.

1.3 Structures in the ISM

The ISM is believed to have a self-similar hierarchical structure over several orders of magnitude in scale (Larson, 1981; Falgarone et al., 1992; Heithausen et al., 1998). Direct H I absorption observations and interstellar scintillation measurements suggest that the structure extends down to 10 AU scales (Crovisier, Dickey & Kazès, 1985; Langer et al., 1995; Faison et al., 1998) and possibly even to sub-AU scale (Hill et al., 2005). However, the latter is limited by the spatial resolution of the observations. Hence the issue is far from being definite even after observational detection of the

lower limit of self-similarity scale in some ISM components (~ 0.1 pc for low-mass star-forming regions reported by Goodman, Barranco, Wilner & Heyer, 1998). On the theoretical front, the ISM is known to be turbulent and hence is expected to exhibit density structures and velocity fluctuations on a wide range of spatial scales. But a detailed model, which is capable of providing a complete quantitative understanding of the observations, is lacking. Numerous theories have attempted to explain the origin, evolution and mass distribution of these clouds (beginning with the hierarchical fragmentation picture, Hoyle, 1953) and it has been established, from both observations (Elmegreen & Falgarone, 1996) and numerical simulations (e.g., Burkert, Bate & Bodenheimer, 1997; Klessen, Burkert & Bate, 1998; Semelin & Combes, 2000), that the ISM has a clumpy hierarchical structure. Even if the details are not clearly understood, it is well-accepted that it is most likely to arise due to turbulent processes in the medium.

1.4 Observational techniques

As mentioned above, the global properties of the ISM are determined by the balance of different physical processes. The two most important among them are the mechanical balance keeping different phases of the ISM in approximate thermal pressure equilibrium, and the thermal balance equating the local heating and cooling rates making the coexistence of stable phases at different temperature possible. In a similar spirit, the concept of balance between other dynamical processes (ionization and recombination, excitation and de-excitation of atomic and molecular levels etc) is very useful to determine the physical properties of the ISM.

On the observational front, the physical conditions in the ISM have been traditionally determined using spectral lines from a variety of tracers including the 21 cm line and recombination lines of hydrogen in the radio regime, Lyman lines of H I, the Lyman and Werner bands of H_2 and the atomic fine-structure lines such as C I in the UV as well as a host of rotational lines from molecules in the mm wavelength regime. For example

the kinetic temperature of the gas can be determined using either the H I 21 cm line or the H_2 UV lines (Roy et al., 2006), the pressure and cooling rates can be determined from the fine structure lines of C I (Pottasch et al., 1979), etc. Since many of these tracers co-exist in the diffuse ISM, multiwavelength observations allow one to cross check different observational techniques as well as to derive a more complete understanding of the physical state of the ISM.

Despite the obvious advantage, astronomers have started multiwavelength observations of the Galactic ISM very recently though multiwavelength observations of extragalactic sources like high redshift Damped Lyman-α systems are fairly routine. Instead we picture the ISM of our own Galaxy as an amalgam of the average properties as determined from studies at different wavelengths. Part of the reason for this is that a given line of sight is rarely amenable to observations at more than one wavelength. For example, UV observations are generally made towards bright nearby stars. However these stars have no detectable radio emission ruling out complimentary 21 cm studies. However, the large scale high sensitivity and high angular resolution surveys (e.g. NVSS, Condon et al., 1998) have partially solved this problem by identifying either two or more sources with small angular separation suitable for observations at different wavelength (like radio sources that happen to be close to the line of sight to UV bright stars) or large number of sources (like radio-loud quasars) suitable for multiwavelength observation. This allows one to probe very close (or same) lines of sight using different tracers at different wavelength and has given a whole new dimension to the subject.

1.4.1 H I 21 cm radiation

In the radio frequencies, the most useful tracer of the ISM is the H I 21 cm line. This is not only because hydrogen is the most abundant element in the ISM but also because it is possible to extract a lot of useful information (like gas temperature, density, velocity, magnetic field strength etc) about the physical properties of the ISM from H I 21 cm observation. In 1944,

Hendrik van de Hulst predicted the possibility of detecting H I 21 cm radiation of celestial origin and it was first observed by Ewen & Purcell (1951). This line emission or absorption is caused by the transition between the two hyperfine states of the $1^2S_{\frac{1}{2}}$ ground state of hydrogen. As the proton and electron spins are each $\frac{1}{2}\hbar$, the total spin angular momentum F, which is the sum of proton and electron spins, takes the value of 0 and 1 for anti-parallel and parallel spin configurations respectively. In a magnetic field, F = 1 state is further split into three and hence called a triplet while F = 0 is called a singlet. The energy of these two states are different due to different orientation of electron and proton magnetic moment (parallel in the singlet and anti-parallel in the triplet), the higher energy state being that of the triplet. The triplet state energy is more than that of the singlet state by an amount $h\nu$ with $\nu = 1420.405752$ MHz corresponding to 21.1 cm. The energy levels for atomic hydrogen are shown schematically in Figure (1.2). The 21 cm transition of neutral hydrogen has an extremely small probability of $2.9 \times 10^{-15}\mathrm{s}^{-1}$. So, the natural lifetime of the excited state for a single isolated atom is about 10 million years. But, because of the processes like collisions and interaction with the background radiation field, the lifetime can be considerably shortened. This, and the fact that the total number of atoms in the ISM is quite large, the 21 cm emission (or absorption against some background source) is easily observed by radio telescopes.

There are two kinds of mechanisms, collisional and radiative, which cause the transitions between these two hyperfine states. Each of these can cause the transition directly by exchange of a quantum of energy equal to $h\nu$. Another possibility is that, higher levels of hydrogen atom can be excited from one of the hyperfine states followed by de-excitation to the alternate hyperfine state via Ly-α or higher Lyman lines transitions (see Figure (1.2)). We need not consider high energy collisions because the number of particles which can excite Ly-α collisionally and the number of particles which can ionize the hydrogen atom are comparable. Hence the regions hot enough for high energy collisions will be ionized. So the possible mechanisms are only low energy collisions and both the low- and

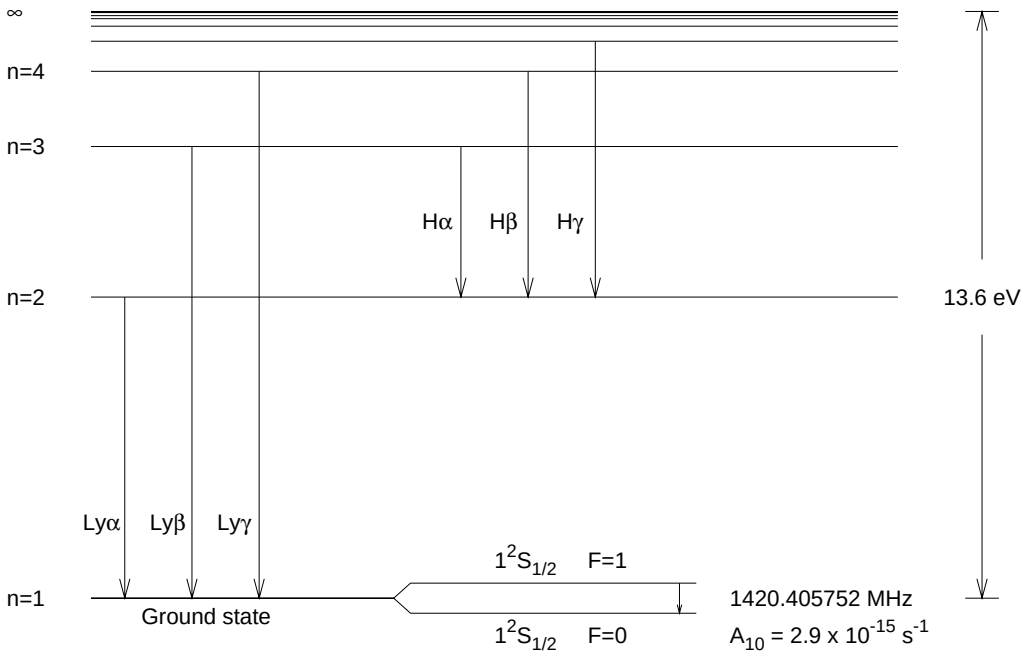

Figure 1.2: A simplified representation of the energy levels (not to scale) of atomic hydrogen showing the hyperfine splitting of the ground state. Higher energy level transitions, particularly Ly-α transition, play a crucial role in bringing equilibrium between the hyperfine states (see text for details).

the high energy radiative transitions (Field, 1958).

The probability of transition via Ly-α photons depends on the intensity profile of radiation near Ly-α frequency. Radiation which has been scattered many times in the ISM will have a profile dependent on the Doppler effects in the medium and hence on the kinetic temperature. For a cloud near H II region these Ly-α photons will play an important role to couple the spin temperature and the kinetic temperature. This is particularly true for low density gas. In high density regions, the collisional mechanism dominates, and there this coupling comes in, since collisions tend to bring the singlet and triplet H I into a thermal equilibrium characterized

by the kinetic temperature (Field, 1958).

The number of atoms in the singlet state (n_0) and that in the triplet state (n_1) are related by the Boltzmann distribution law,

$$\frac{n_1}{n_0} = \frac{g_1}{g_0} \exp\left(-\frac{h\nu_{10}}{kT}\right) \tag{1.1}$$

for a cloud in thermodynamic equilibrium, g_1 and g_0 being the statistical weights of the triplet and the singlet levels respectively and are given by $g = 2F + 1$. Therefore, we get, $n_1 = 3n_0 \exp(-h\nu_{10}/kT)$. Even if the cloud is not in thermodynamic equilibrium, we can define a temperature called spin or excitation temperature (T_s) that satisfies this number distribution of atoms between the two spin states.

If we express the observed intensity as the brightness temperature (T_B), which is a common term in radio astronomy, then it can be shown that for a constant T_s along the line of sight, $T_B(\nu) = T_s[1 - e^{-\tau(\nu)}]$ where $T_B(\nu) = I(\nu)c^2/2k\nu^2$ is the brightness temperature, $\tau(\nu)$ is the optical depth at frequency ν, $I(\nu)$ is the intensity, k is the Boltzmann constant and c is the speed of light. For low optical depth, the spin temperature will be $T_s(\nu) = T_B(\nu)/\tau(\nu)$.

1.4.2 Temperature and column density

For an isothermal cloud, the line of sight column density (i.e. the integrated number density along the line of sight) of hydrogen atom is given by,

$$\begin{aligned} N_{HI} &= 3.88 \times 10^{17} T_s \int \tau(\nu) d\nu \\ &= 1.823 \times 10^{18} T_s \int \tau(V) dV \\ &= 1.823 \times 10^{18} \int T_B(V) dV \end{aligned} \tag{1.2}$$

where N_{HI} is in cm^{-2}, ν is in kHz and V is in km s^{-1} (Kulkarni & Heiles, 1988; Dickey J. M. & Lockman F. J., 1990). The spin temperature, T_s is given by,

$$T_s = \frac{N_{HI}}{1.823 \times 10^{18} \int \tau(V) dV} = \frac{\int T_B(V) dV}{\int \tau(V) dV} \tag{1.3}$$

where N_{HI} can be either determined from H I emission spectrum or independently estimated from observations of the Ly-α line for the same line of sight and the optical depth $\tau(\nu)$ can be determined from H I absorption spectrum towards a background continuum source.

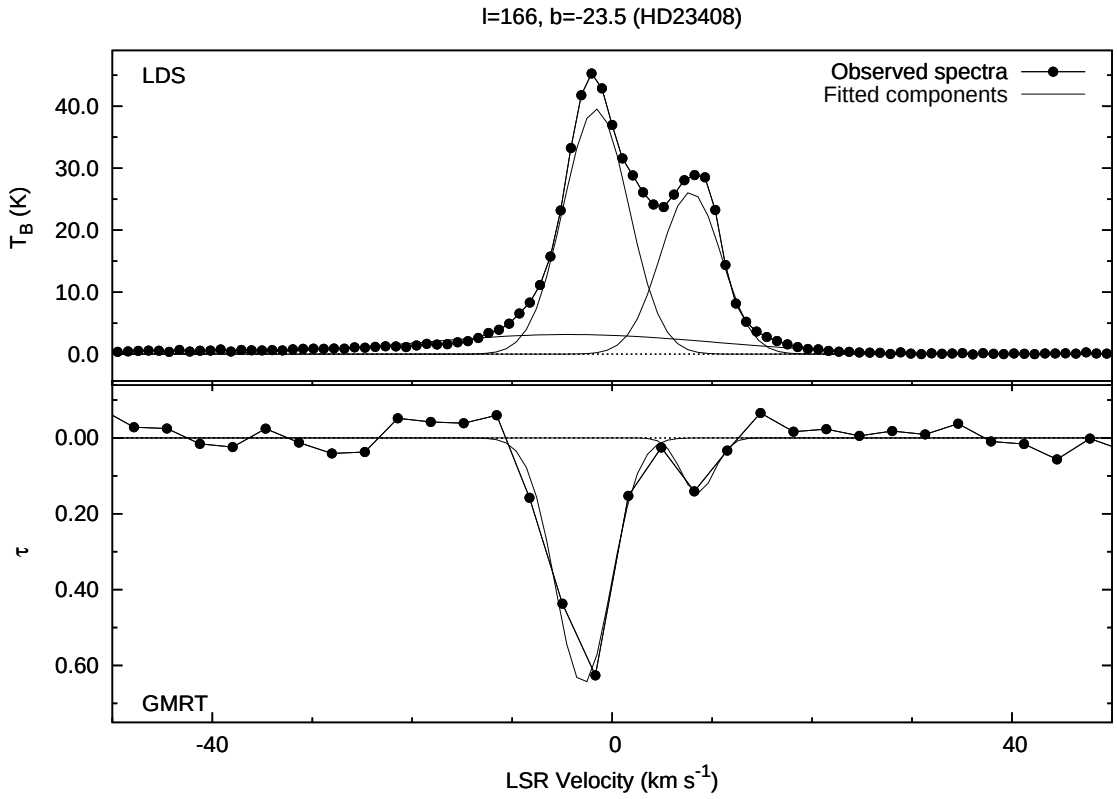

Figure 1.3: Profiles of the observed H I 21 cm emission and absorption towards $l = 166°$, $b = 23°.5$ (towards background radio source J034440+243622 and close to the line of sight towards the star HD23408). The top panel is the emission spectrum taken from Leiden-Dwingeloo Survey (LDS). The bottom panel is the absorption spectrum obtained with the GMRT.

In the real-life situation where the gas is not homogeneous, but instead has density and temperature structures, both along as well as transverse to the line of sight, the determination of 'the' spin temperature from radio observations is non-trivial. As an example, the application of equation (1.3) to the observed spectrum produced by a set of optically thin multiple

components along the line of sight will yield a column-density-weighted harmonic mean temperature of the individual components. If the optical depths are large or there is structure both along and transverse to the line of sight, then in general there is no unique interpretation of the data, although several approaches to modelling the spectra as a collection of multiple Gaussian components have been attempted (e.g., Mebold, 1972; Mebold et al., 1982; Heiles & Troland, 2003a,b). Although there is no mathematically unique and physically robust procedure that can be used to interpret the spectra in this case, much of what we have learned about the neutral atomic medium has come from the relatively simplistic assumptions underlying equation (1.3).

Figure (1.3) illustrates the technique of extracting physical information from H I 21 cm study. It shows the H I emission spectrum (top panel) towards $l = 166°$, $b = 23°.5$ (in Galactic coordinate system) taken from Leiden-Dwingeloo Survey (LDS) and the H I absorption spectrum (bottom panel) for the same direction towards a background radio source observed using the Giant Metrewave Radio Telescope (GMRT). It is possible to determine the integrated H I column density and the average spin temperature for the line of sight following the procedure described earlier. Both the emission and absorption spectra can also be modelled as a set of multiple Gaussian components as shown in Figure (1.3). In this particular case, the emission spectrum shows three components but only two components are detected in absorption. The broad component in emission is not detected in absorption. The traditional interpretation of this is that wide emission components arise from gas with too high a spin temperature to produce measurable absorption (Radhakrishnan et al., 1972; Heiles & Troland, 2003a,b), i.e. the warm neutral medium (WNM), although of course it could also arise from multiple weak narrow CNM components. The width of individual Gaussian components will be a measure of the kinetic temperature if the broadening of the line is purely thermal. But, in general, it will only give an upper limit of the kinetic temperature if there is any other mechanism like turbulence or differential rotation of the gas that

may contribute to the width. One can also determine the column density and the spin temperature for individual components. Moreover, in some cases we can also infer, with the help of a prior knowledge of the Galactic rotation curve, the distance to the H I cloud from the central velocity of each Gaussian component.

1.5 Thesis outline

The multiphase nature and turbulence are two of the key ingredients of the ISM physics. The thermal equilibrium model described in Sec.(1.2) form the basis of our theoretical understanding of the temperature of the diffuse neutral ISM. Recently, however, there have been some observational indications of the existence of a large fraction of H I in the intermediate temperature unstable state. This has raised doubts about the validity of the thermal equilibrium model. Given the serious implication of these observational evidences on our understanding of the ISM physics, it is very important to critically test the above-mentioned observational results.

H I 21 cm emission line width is sometimes used for a direct measurement of temperature (e.g., Heiles & Troland, 2003a; Kanekar et al., 2003). One of major issues in this regard is the determination of temperature in the presence of non-thermal broadening of line width due to turbulence in the ISM. Hence, to get the actual temperature of the gas from H I 21 cm observations, it is crucial to understand the nature of the turbulence in the diffuse ISM. This will allow one to quantify the contribution of turbulence to the observed line width, to get better estimates of the temperature and the fraction of gas in thermally stable or unstable states.

Measuring the temperature and understanding the nature of turbulence has a variety of implications. In this thesis, I have presented my work on the ISM temperature and turbulence and also on the interplay of these two, concentrating mostly on the diffuse neutral ISM. First, the issue of the non-thermal broadening of linewidth, its implications on temperature measurements and the distribution of diffuse gas in different thermal

phases have been investigated using both single dish and interferometric observations. Next, the nature of turbulence in two different components of the ISM (namely in supernova remnants and in diffuse neutral gas) have been studied. Finally, an illustrative example has been considered to show the importance of knowing the physical conditions including the temperature of the gas. This is related to the technique of computing the star formation rate from the observed C II* column density. C II 157.7μm transition is a major coolant of the diffuse ISM. The observed C II* column density is a direct measure of the cooling rate of the gas. In the steady state the cooling rate is equal to the heating rate, which in turn depends on the star formation rate. The star formation rate required to maintain a given heating rate, however, crucially depends on whether the gas is in the CNM or WNM phase. So, a direct measurement of temperature is important to deduce the star formation rate.

In the first two chapters of this thesis, works related to the temperature of the diffuse ISM are presented. The interplay of the turbulence and the temperature measurement in the context of millennium Arecibo survey results is discussed in Chapter 2. In Chapter 3, the results of the GMRT and WSRT diffuse H I 21 cm absorption line survey are summarized. This survey was carried out to detect warm neutral gas directly in H I absorption, to study the temperature distribution and the nature of turbulence of the diffuse neutral gas, and to critically re-examine the issue of diffuse gas in unstable phase. In the next two chapters, works related to turbulence in different ISM components are presented. The nature of turbulence in supernova remnants and in diffuse H I from the intensity fluctuation power spectra study are discussed in Chapter 4 and Chapter 5 respectively. In chapter 6, the particular case of the importance of direct temperature measurements of the diffuse ISM to relate the star formation rate to the observed C II* column density is discussed. Finally, in Chapter 7, the main results of all the work presented in this thesis are summarized.

Chapter 2

Turbulence measurements from H I absorption spectra

2.1 Introduction

The classical description of the Galactic atomic interstellar medium (ISM) is that it consists of the cold neutral medium (CNM) and the warm neutral medium (WNM), in rough pressure balance with each other (e.g. Field, 1965; Field et al., 1969; Wolfire et al., 2003). Detailed modeling of the energy balance in a multi-phase medium (e.g. Wolfire et al., 1995) shows that the pressure equilibrium can be maintained for H I in one of two stable ranges of kinetic temperature (T_K), viz. ~ 40K -200K for the CNM and ~ 5000K -8000 K for the WNM. H I at intermediate temperatures is unstable and is expected to quickly migrate into one of the stable phases, unless energy is intermittently being injected into the medium. Recent observations and simulations indicate that in our Galaxy a significant fraction of the atomic ISM is in the thermally unstable region (e.g. Vázquez-Semadeni et al., 2000; Heiles, 2001; Hennebelle & Audit, 2007; Hennebelle et al., 2007).

The classical method of determining the temperature of the atomic ISM is to compare the H I 21 cm line in absorption towards a bright continuum source with the emission spectrum along a nearby line of sight. Assuming

that the physical conditions are the same along both the lines of sight, one can measure the spin temperature (T_S) (or excitation temperature) of H I (see e.g. Kulkarni & Heiles, 1988, for details). While the H I spin temperature, strictly speaking, characterizes the population distribution between the two hyperfine levels of the hydrogen atom, it is often used as a proxy for the kinetic temperature of the gas. This is because, in high density regions, T_S is expected to be tightly coupled to the kinetic temperature via collisions, while in low density regions, resonant scattering of Lyman-α photons is generally expected to couple the spin temperature to the kinetic temperature (Field, 1958).

The 21 cm optical depth of the WNM is extremely low (typically $< 10^{-3}$) which makes it very difficult to measure H I absorption from gas in the WNM phase. Consequently, emission-absorption studies usually provide only a lower limit to T_S. If the particle and the Lyman-α number densities are low, T_S could in turn be significantly lower than T_K. On the other hand, one could use the 21 cm emission line width to determine an upper limit to the kinetic temperature. The line width is an upper limit to the temperature because in addition to thermal motions of the atoms, both bulk motion of the gas (e.g. differential rotation) as well as turbulence contribute to the observed line width.

The presence of turbulence in the atomic ISM of our own Galaxy can be detected through, for e.g., the scale free nature of the power spectrum of the intensity fluctuations in H I 21 cm emission (Crovisier & Dickey, 1983; Green, 1993). In a turbulent medium, one would also expect the velocity dispersion to increase as a power of the length scale. Such a power law velocity width length scale scaling has been observed in the atomic ISM of the Large Magellanic Cloud (LMC) (Kim et al., 2007). To the best of our knowledge it has not been observed in the atomic ISM of our own Galaxy. Here, we show that, assuming that the atomic ISM is in rough pressure equilibrium, the data from the millennium Arecibo 21 cm absorption-line survey (Heiles & Troland, 2003a,b) is consistent with a velocity-length scale relation of the form $\sigma_v^2 \propto l^\alpha$. We also show that this

scaling is, to zeroth order, consistent with that expected from turbulence in an medium with magnetic field of the order of few μGauss.

Once one has an estimate of the turbulent velocity contribution to the observed velocity width, one can correct for it, to derive a tighter limit to the kinetic temperature. We show that this correction leads to a substantially smaller fraction of the gas being in the WNM phase than if one does not take turbulence into account.

2.2 The millennium Arecibo survey data

The data we use are taken from the millennium Arecibo 21 cm absorption-line survey and consist of emission and absorption spectra with a velocity resolution of ~ 0.4 km s^{-1} towards a total of 79 background radio sources. The observational and analysis techniques are discussed in detail by Heiles & Troland (2003a) and the astrophysical implications are discussed in Heiles & Troland (2003b); In short, the absorption spectra were corrected for emission from gas in the telescope beam by interpolating multiple off-source spectra, after which both the emission and absorption spectra were modeled as a collection of multiple Gaussian components. For each component, the spin temperature, upper limits on kinetic temperature, column densities and velocities were derived using these fits. There are several systematic uncertainties in such an analysis, discussed for example in Heiles & Troland (2003a), in particular those associated with estimating and subtracting the emission, simultaneous multi-component fitting of emission and absorption spectra, and the assumption that each Gaussian component is a physically distinct entity. While a more robust measurement of the absorption spectra can be done using interferometric observations (e.g. Kanekar et al., 2003), here we work with the fit parameters provided as part of the survey. All the systematic uncertainties relevant to the Arecibo millennium absorption survey hence also apply to our results.

The survey lists a total of 374 Gaussian components in the emission spectra towards the 79 continuum sources. Out of these, 205 components

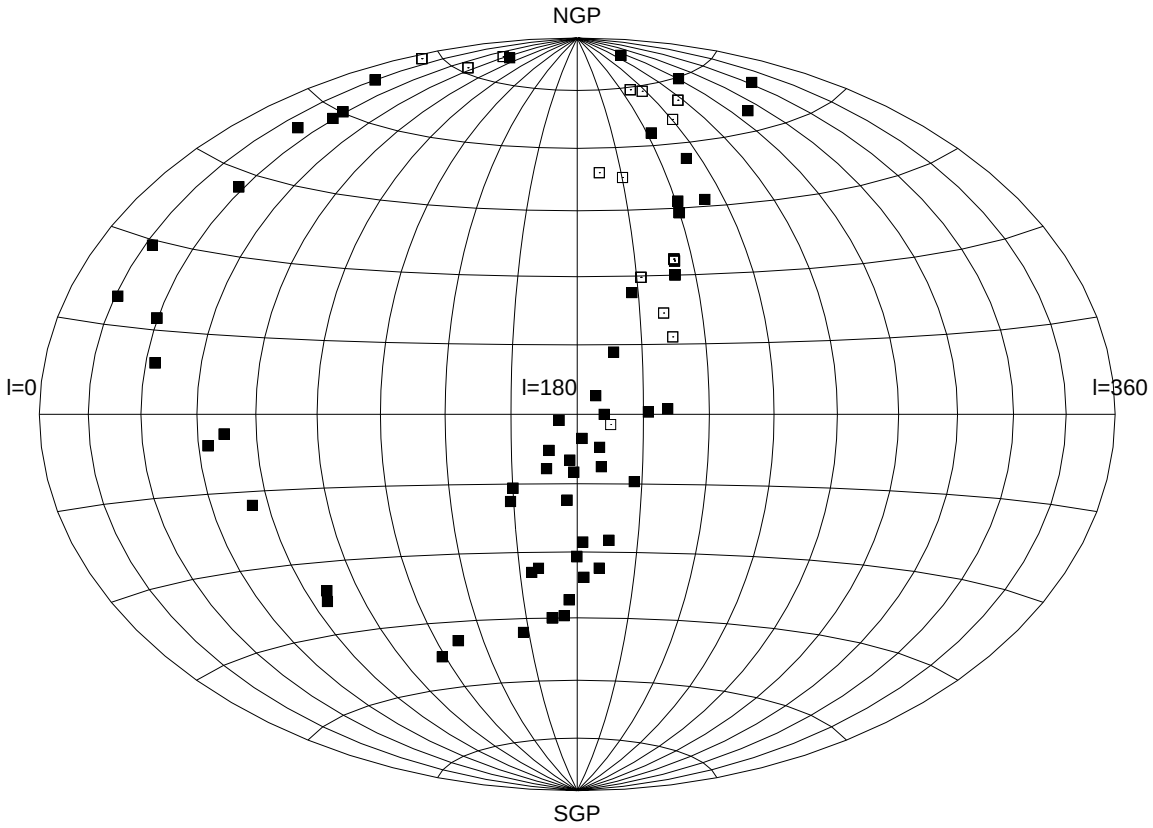

Figure 2.1: Sky coverage of the millennium Arecibo 21 cm absorption-line survey shown in Galactic coordinate system. The filled squares are lines of sight for which H I absorption was detected, and empty squares represent lines of sight with no detected H I absorption.

are also detected in H I absorption and have T_S measurements. For 21 of these components either the spin temperature had to be set to zero (by hand) in order to attain convergence of the fit (Heiles & Troland, 2003a) or the upper limit of the kinetic temperature computed from the line width is less than the spin temperature (or the lower limit of the spin temperature). These inconsistencies are most likely largely due to the constrained simultaneous fitting of emission and absorption spectra, and may partly be due to inaccurate estimation and subtraction of the emission, contribution of stray radiation etc. The derived parameters for these components are clearly unphysical, and we do not use them in our analysis. We are hence

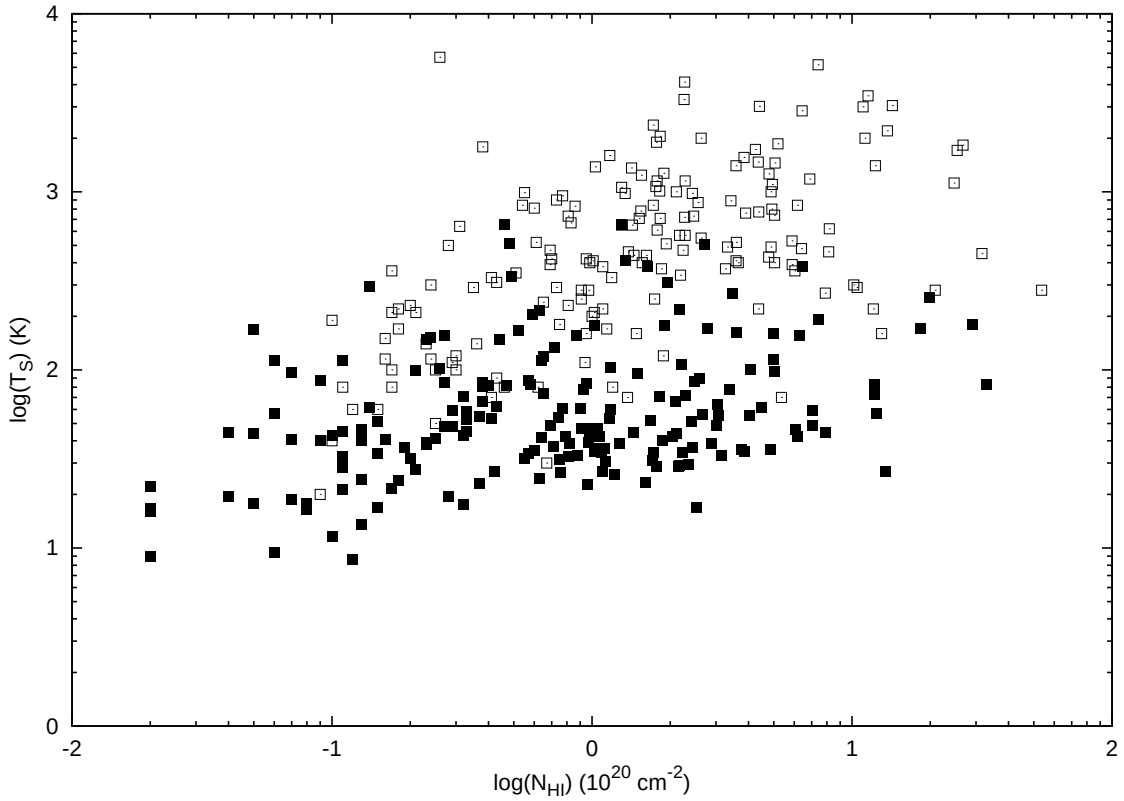

Figure 2.2: $N_{HI} - T_S$ plot for Gaussian components from the millennium Arecibo 21 cm absorption-line survey data. The filled squares are components detected both in emission and absorption and the empty squares are components detected only in emission giving a lower limit for T_S.

left with a total of 353 Gaussian components consisting of 188 components detected both in emission and absorption and 165 components detected only in emission. Figure (2.1) shows the sky coverage of the millennium Arecibo 21 cm absorption-line survey in Galactic coordinate system. Figure (2.2) is a scatter plot of the spin temperature T_S against the column density N_{HI}; filled squares are components that have been detected in both emission and absorption while empty squares are components that have been detected only in emission. It is clear from the plot that the survey did not detect much gas with $T_S \lesssim 10$ K. Much of the gas below 10 K will be in molecular phase or will be associated with cold molecular clouds. But,

another plausible reason for this may again be the technique of fitting emission and absorption spectra simultaneously and thus missing these cold gas with very little emission.

2.3 Analysis and results

For a homogeneous cloud at temperature T, the pressure $P = nkT$, with $n = \mathrm{N_{HI}}/l$, where N_{HI} is the column density and l is the length of the cloud. Putting these together we have $l = \mathrm{N_{HI}}kT/P$. For the CNM clouds detected in absorption, it is quite reasonable to assume that the kinetic temperature is the same as the spin temperature $\mathrm{T_S}$. If we further assume that the pressure is roughly constant across clouds, then we have $l \propto \mathrm{N_{HI}\ T_S}$. Though the density and temperature of neutral ISM vary over a few orders of magnitude, this assumption is justified because the pressure changes, in most of the cases, only by a factor of a few since the turbulence in the gas is at most transonic. Further, for these components, the non-thermal component of the line width is given by $v_{nt}^2 \propto (\mathrm{T_{K}}_{max} - \mathrm{T_S})$, where $\mathrm{T_{K}}_{max}$ is the measured line width of this component. Figure (2.3) shows a scatter plot of $(\mathrm{T_{K}}_{max} - \mathrm{T_S})$ against $\mathrm{N_{HI}T_S}$. As discussed above, to zeroth order this can be regarded as a plot of the non thermal velocity against the length scale. The filled squares show components with $|b| < 30^\circ$ and the open squares are for $|b| > 30^\circ$. The solid line in the figure is a dual power law fit; at large length scales ($\log(\mathrm{N_{HI}T_S}) \geq 21.4 \pm 0.2$) the power law index is 0.7 ± 0.1, while at small length scales, the power law index is consistent with zero. The dotted line shows a fit which assumes that the measured $\mathrm{T_{K}}_{max}$ is larger than the true $\mathrm{T_{K}}_{max}$ by 60K. Both these models provide a reasonable fit to the data over five orders of magnitude in $\mathrm{N_{HI}\ T_S}$. The goodness of fit based on the rms of the residuals is similar for both these models but the residual is higher for a single power law model. The length scale corresponding to a pressure of 2000 $\mathrm{cm^{-3}K}$, as well as the non thermal velocity width in km $\mathrm{s^{-1}}$ are also indicated in the figure.

The correlation between the cloud scale length and the non-thermal

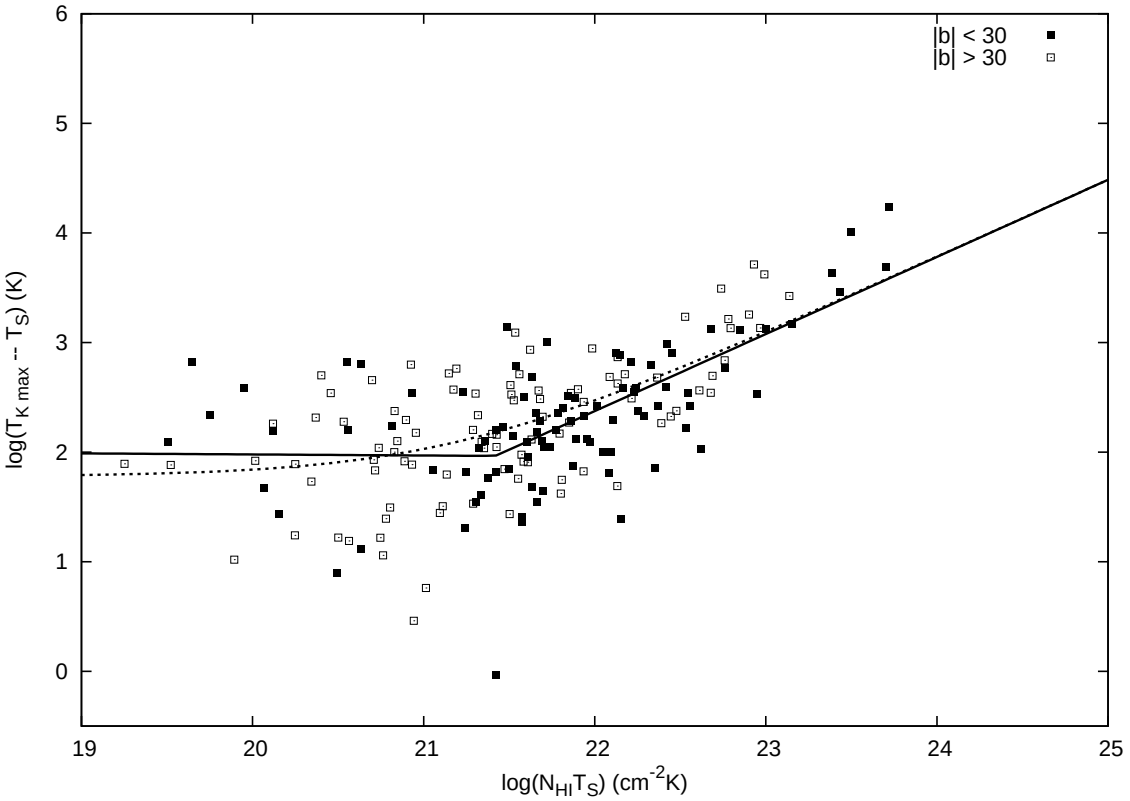

Figure 2.3: $N_{HI}T_S$ vs. ($T_{Kmax} - T_S$) plot for Gaussian components (detected both in emission and absorption) from the millennium Arecibo 21 cm absorption-line survey data. The filled and the open squares show components with $|b| < 30^\circ$ and $|b| > 30^\circ$ respectively. The solid line is a fit to the data using two power laws. The dotted line is the model with a 60 K overestimation of T_{Kmax} (see §2.2 for details).

line width that we see at long length scales is consistent with a turbulence driven velocity line-width relation. The assumptions we have made (viz., homogeneous clouds, constant pressure) are fairly naive, and are certainly not exactly valid in the current situation. The large scatter around the fit would be partly due to a break down of the assumptions (e.g. variations in the pressure) and partly due to measurement errors. If variations in pressure were a dominant factor for the scatter, one would expect to see a systematic variation of the scatter plot for components in different Galactic latitude ranges. However, as shown Figure (2.3), in no such variation is

observed.

The ISM is known to have clumpy density and velocity structures and is believed to be turbulent at scales ranging from AU to kpc (Dieter et al., 1976; Larson, 1981; Deshpande et al., 2000). Incompressible hydrodynamic turbulence leads to the famous Kolmogorov scaling $\sigma_v^2 \propto l^{2/3}$ (Kolmogorov, 1941), similar to what we see at large length scales. However, the Galactic ISM cannot be modeled simply as an incompressible fluid. Recent theoretical studies and numerical simulations have investigated in details the turbulence of multi-phase medium (Koyama & Inutsuka, 2002; Audit & Hennebelle, 2005; Gazol et al., 2005; Vázquez-Semadeni et al., 2006; Hennebelle et al., 2007). In some of these cases (Vázquez-Semadeni et al., 2006; Hennebelle et al., 2007), synthetic H I spectra are computed to study the effect of turbulence. In general, these analytical and numerical works predict a Kolmogorov-like turbulence in two-phase neutral ISM. Hennebelle et al. (2007) also report, based on simulation results, a power law scaling $\sigma_v^2 \propto l^{0.8}$ consistent with our observation.

Now, since fractional ionization couples the H I to the magnetic field, the turbulence is expected to be magnetohydrodynamic (MHD) in nature. Though simple and ingenious models (e.g. Goldreich & Sridhar, 1995) of incompressible MHD turbulence have been proposed, most of the insights into incompressible and compressible MHD turbulence again come from numerical simulations (Cho et al., 2002, and references therein). Models (like Goldreich & Sridhar, 1995) predict a Kolmogorov-like energy spectrum, $E(k) \propto k^{-5/3}$, for incompressible MHD turbulence and this is supported by both numerical simulations and observations (see Cho et al. (2002) for details). In case of compressible MHD turbulence, Alfvén modes are least susceptible to damping mechanisms (Minter & Spangler, 1997) and hence the energy transfer in Alfvén waves is of major interest. Again, numerical simulations show that the energy spectra of Alfvén modes follow a Kolmogorov-like spectrum. There is no clear theoretical explanation for the fact that even if turbulence in the ISM is compressible and magnetohydrodynamic in nature, both the simulated and observed power spectra

are very close to the Kolmogorov spectrum.

The Alfvén velocity in the medium is $v_{\rm A} = B/\sqrt{4\pi\mu n_{\rm H} m_{\rm H}}$, where $\mu = 1.4$ is the effective mass of the H+He gas with cosmic abundance, $m_{\rm H}$ is the mass of the hydrogen atom, n_H is the H I number density and B is the magnetic field strength. It is usually assumed that the magnetic perturbation amplitude $\delta B \sim B$. In a situation where the bulk of the energy transfer is via Alfvén waves, the non-thermal velocity dispersion δv is related to δB as $\delta v \approx v_{\rm A}(\delta B/B) = \delta B/\sqrt{4\pi\mu n_{\rm H} m_{\rm H}}$ (Arons & Max, 1975; Roshi, 2007). Using this relation, the magnetic field is found to be of the order of few μG (column density weighted mean and median values are 11.7 and 10.2 μG respectively) with no significant trend related to the "cloud" size. We note that there are various uncertainties to the derived equipartition magnetic field. But the estimate from this work is broadly consistent with the observed magnetic field in the diffuse neutral ISM and matches, within a factor of 2, with the median magnetic field estimated for a subsample of these components using Zeeman splitting measurements (Heiles & Troland, 2005).

The break that is clearly seen in Figure (2.3) requires some attention. This change in the power law index cannot be explained just in terms of lower signal to noise on the physical quantities at low $N_{\rm HI}T_{\rm S}$ end. However, as shown in the figure, the data fit well by a model in which the line width is overestimated by about ~ 60 K. There are three systematic effects that may contribute to the overestimation of the line width without affecting $N_{\rm HI}$ and $T_{\rm S}$ much: (i) the finite spectral resolution, (ii) blending of two or more narrow components and (iii) velocity (but not $T_{\rm S}$) fluctuations in the gas within the Arecibo beam. The contribution from the first effect is quantified by estimating the width of a Gaussian signal after smoothing it to a spectral resolution of 0.4 km s^{-1} and adding noise similar to that in the actual spectra. The effect is found to be almost negligible because of the high spectral resolution. A similar numerical exercise with two Gaussian components was done to check the effect of blending of narrow components and ambiguities in Gaussian fitting. In this case, the effect is most

significant when the blended lines are of comparable amplitudes and have separations comparable to their widths. For example, blending of components with $T_{\mathrm{K}max} = 60$ K (width of the Gaussian ~ 0.7 km s^{-1}) with a separation of ~ 1.2 km s^{-1} results in typically 20 – 30 K overestimation of $T_{\mathrm{K}max}$. When the amplitudes of the two Gaussian profiles are comparable, the line width is overestimated by upto 60 K.

The third possibility, that is a fine scale structure in the velocity (but not in the temperature), has been proposed earlier (e.g. Brogan et al., 2005; Roy et al., 2006) to explain the observed fine scale H I opacity fluctuations (Dieter et al., 1976; Crovisier et al., 1985). Such velocity fluctuations within the Arecibo beam will also cause an overestimation of $T_{\mathrm{K}max}$. However, it should be noted that the scale length (inferred from N_{HI} and T_{S}) of the components below the break is very small. Although the existence of tiny "clouds" is supported by observations and numerical simulations (e.g. Braun & Kanekar, 2005; Stanimirović & Heiles, 2005; Nagashima et al., 2006; Vázquez-Semadeni et al., 2006; Hennebelle & Audit, 2007), their origin and physical properties are still unknown. The evaporation timescale for these clouds are ~ 1 Myr. These structures can survive if either the ambient pressure around the clouds is much higher than the standard ISM pressure or they are formed continuously with a comparable timescale. While we have presented plausible arguments for the break that we see not corresponding to a physical phenomena, the lack of detailed understanding of these tiny H I structures means that we cannot rule out the possibility of some physical phenomenon being responsible for the break.

2.4 A new indicator of the temperature

For a multi-phase medium if the turbulent velocity dispersion scaling is similar for coexisting phases, then this scaling relation can be exploited to get a handle on the physical temperature of the gas that is detected only in H I emission but not in absorption. Since one only has a lower limit on T_{S} for these components, they lie, as expected, systematically on

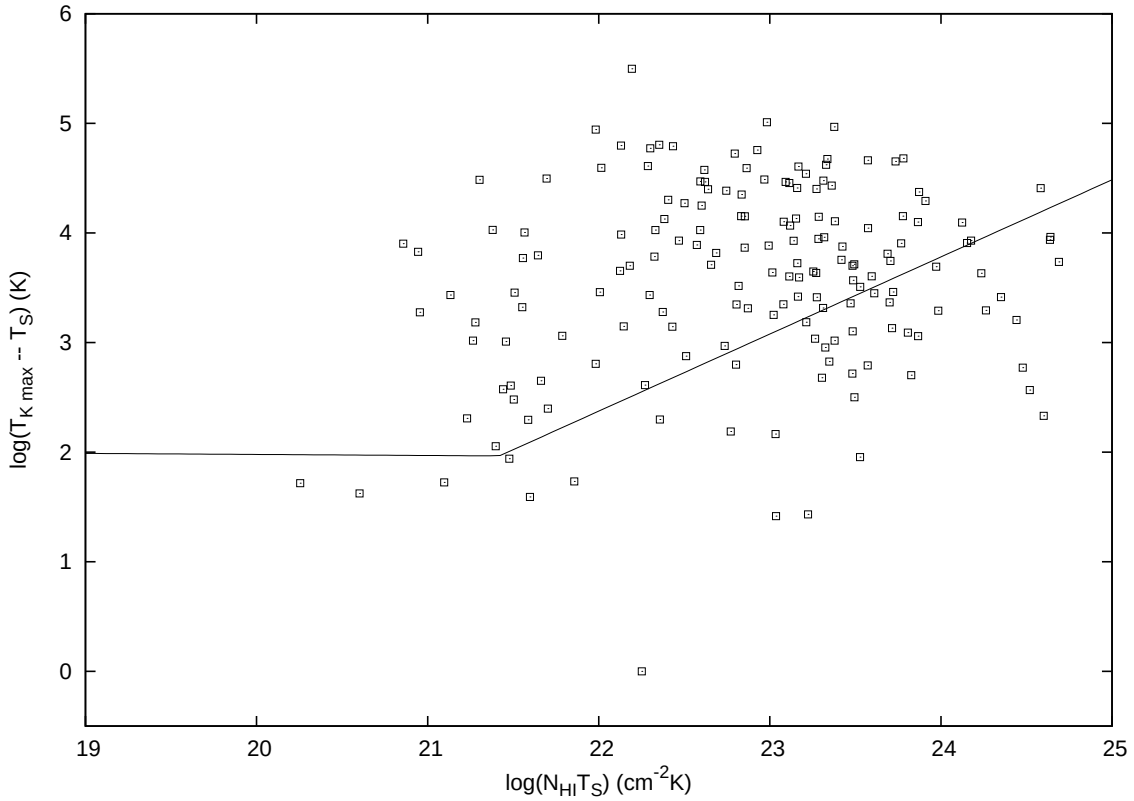

Figure 2.4: $N_{HI}T_S$ vs. ($T_{Kmax} - T_S$) plot for Gaussian components from the millennium Arecibo 21 cm absorption-line survey data. Components detected only in emission and not in absorption are shown here and T_S is the lower limit for these components. The solid line is derived from the components detected both in emission and absorption.

the top left side of the fit to the components detected in both emission and absorption (Figure (2.4)). For these components we define a proxy temperature T_L that will restore the component back to this power law correlation. Given the measured N_{HI} and T_{Kmax} from the emission spectra, one can uniquely compute this proxy temperature. Since T_L corresponds to the velocity width after correction for the turbulent velocity, it is a better estimate of the actual physical temperature of the cloud than that of T_{Kmax}. Note that since most of the components in Figure (2.4) are beyond the break in the fitted function the derived T_L is independent of whether the

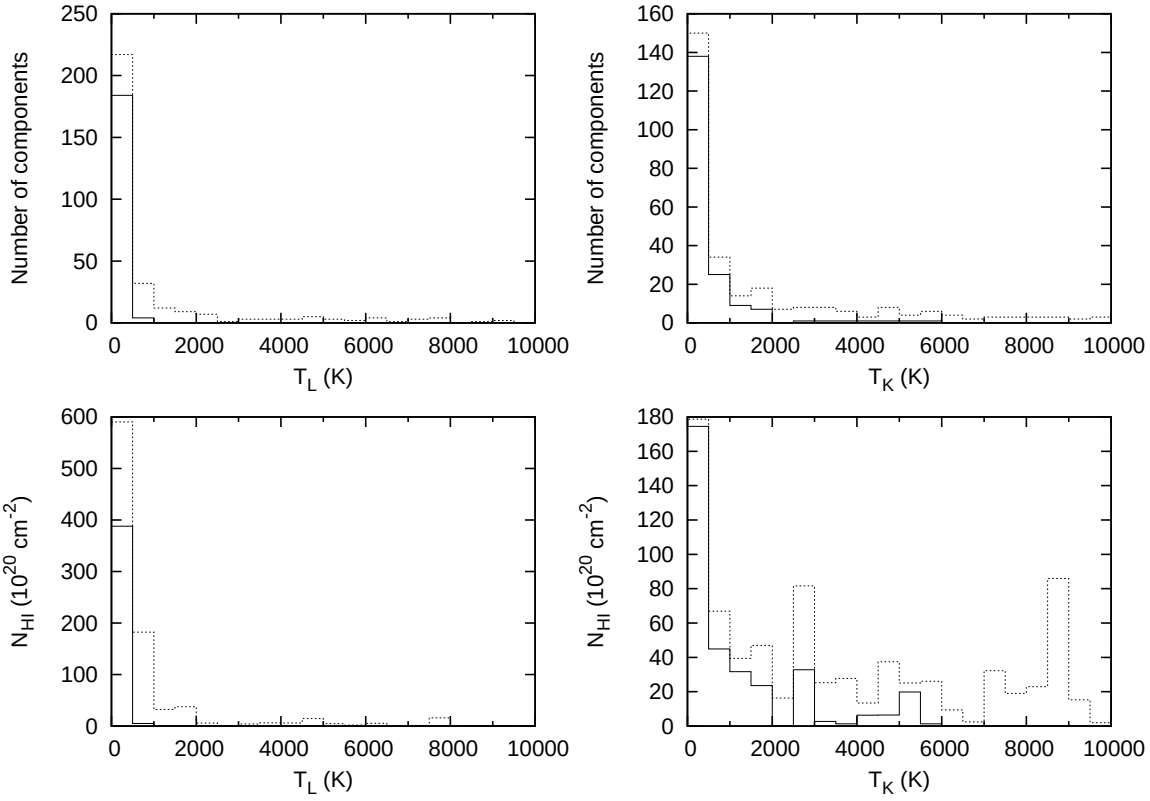

Figure 2.5: Histograms of derived temperatures T_L and T_K. The solid lines only include components detected both in emission and absorption and the dotted lines include all the components. The top panels give the number of Gaussian components and the bottom panels give the H I column density. The left panels are histogram of T_L and the right panels are that of T_{Kmax}.

break arises due to any underlying physical reason.

For all except 2 of the 165 components detected only in emission, T_L was calculated as described above. For two components, no meaningful solution for T_L could be found. This may reflect some problem with the measurements or the fitting techniques, and these components are hence not included in the further analysis. For the components detected both in emission and absorption, T_S is taken to be the same as T_L. With this, we have T_L and T_{Kmax} for a total of 351 Gaussian components. Figure (2.5) shows the histogram of T_L and T_{Kmax} in terms of both the number

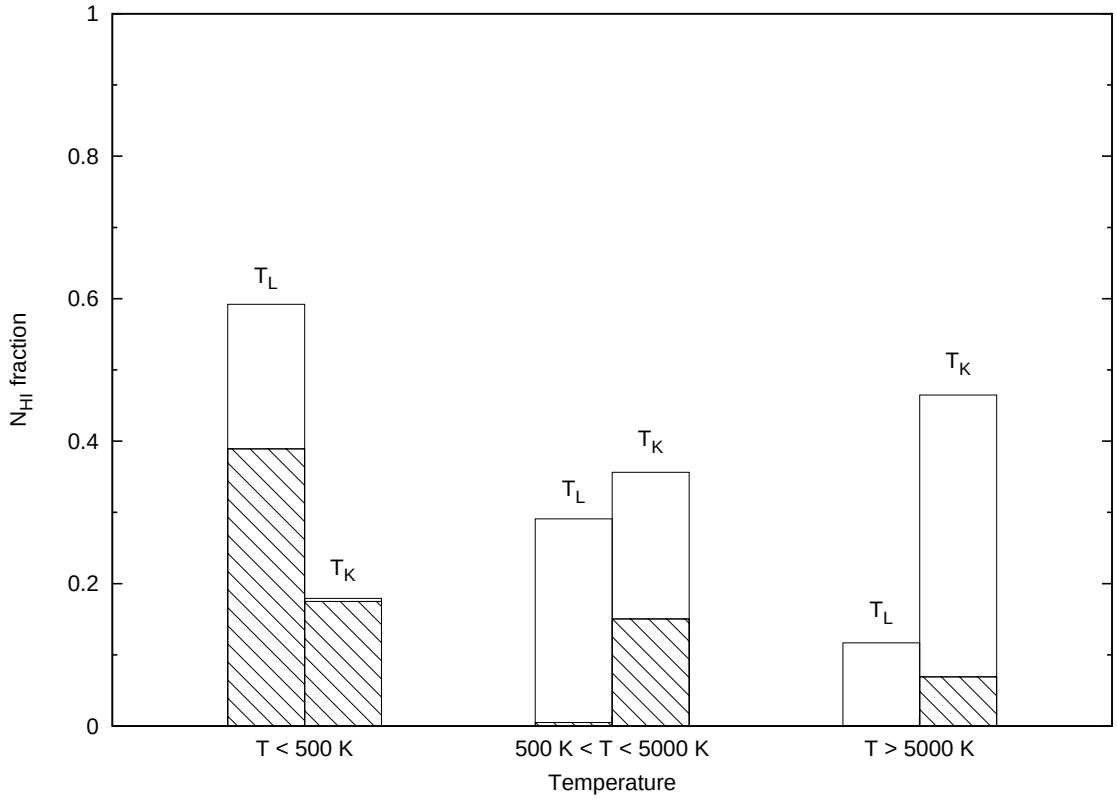

Figure 2.6: N_{HI} fraction, for components detected both in emission and in absorption (hatched histogram) and components detected only in emission but not in absorption (empty histogram), in different temperature range using T_L and T_{Kmax} as the proxy for the actual physical temperature.

of "clouds" and the H I column density. The top panels show the number of Gaussian components and the bottom panels show the H I column density in different temperature bins. From the histograms, it is evident that the results qualitatively confirm the earlier detection of a significant fraction of gas in the thermally unstable region. Quantitatively, however, a significant fraction of the gas with high T_{Kmax}, after correction for turbulent broadening corresponds to gas in the stable phase. This quantitative difference is illustrated in Figure (2.6) which shows the N_{HI} fraction for both the population (components detected both in emission and absorption and components detected only in emission) in different temperature

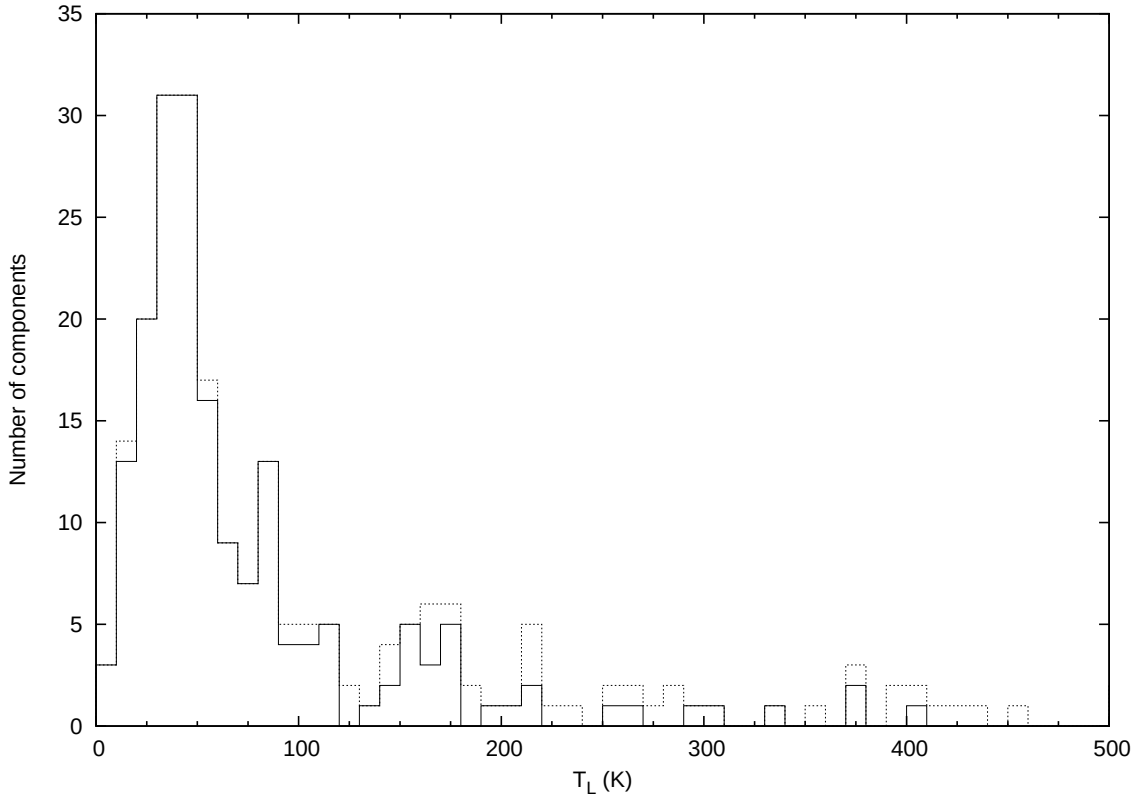

Figure 2.7: The histogram of derived temperatures for $T_L < 500$ K. The solid line includes only components detected both in emission and absorption and the dotted line includes all the components.

range using T_L instead of T_{Kmax} as the proxy for actual physical temperature. Further, while Heiles & Troland (2003b) find that 60% of all H I is in the WNM phase, we find that only 40% of the gas has temperature higher than 500 K.

A closer examination of the components with $T_L < 500$ shows a clear peak near $T_L \sim 50$ K in the number distribution and that the major fraction of the gas is below $T_L \sim 100$ K as shown in Figure (2.7). Figure (2.8) shows the histogram of scale length $L \sim N_{HI}\ T_S$. This clearly shows a bi-modal statistical distribution of the "cloud" size for the neutral ISM. As expected, the dominant contribution to the the peak at lower L is from the cold components and to the peak at higher L is mostly from the warm components.

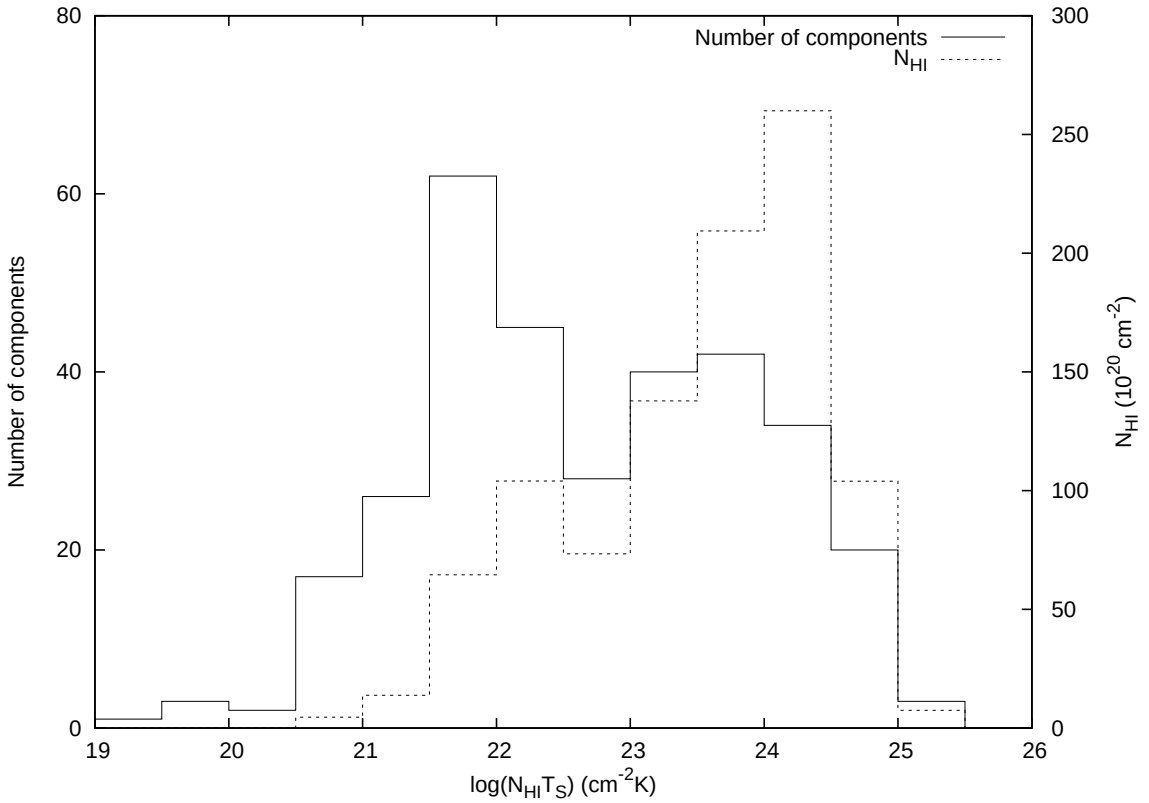

Figure 2.8: The histogram of the scale length, $L \sim \mathrm{N_{HI}\ T_S}$, in terms of the number of components (solid line) and N(H I) (dotted line) showing two distinct peaks.

If N is the number of clouds along the lines of sight, R is the typical size of a cloud and n is the H I number density, then $\mathrm{N(H\ I)}_X \propto N_X R_X n_X$ where X stands for CNM or WNM. From the observed N(H I) and N for all the components used for this analysis we find, using this relation, $R_{\rm WNM}/R_{\rm CNM} \sim 110$ for typical $n_{\rm CNM}/n_{\rm WNM} \sim 100$. This is consistent with the ratio of the length scale corresponding to two peaks in the bi-modal distribution.

2.5 Conclusions

Here I have presented a new phenomenology based technique to address the issue of non-thermal line width and the temperature of the diffuse neutral hydrogen of our Galaxy assuming a rough pressure equilibrium

between different phases of the ISM. A possible connection between the observed Kolmogorov-like scaling of the non-thermal velocity dispersion in the Galactic H I and the turbulence of the interstellar medium is discussed. This scaling relation is used to re-examine the issue of the temperature of the Galactic ISM with the help of the millennium Arecibo 21 cm absorption-line survey measurements. The distribution of the derived temperature is found to be significantly different from the distribution of the upper limits of the kinetic temperature. A considerable fraction ($\sim 29\%$) of the gas is found to be in the thermally unstable phase, qualitatively confirming earlier results. However, about 60% of all the neutral diffuse gas, a much higher fraction than that reported earlier, has temperature below 500 K. The CNM temperature distribution shows a clear peak near T ~ 50 K and the cloud size for the neutral ISM shows a bi-modal statistical distribution. Derived magnetic field from the non-thermal velocity dispersion matches, within a factor of 2, with the magnetic field value estimated from the Zeeman splitting measurements. The Kolmogorov-like scaling is consistent with the existing theoretical prediction, numerical simulations and earlier observational results.

Chapter 3

The temperature of the diffuse H I in the Milky Way

3.1 Introduction

A cornerstone of the classical models of the Galactic ISM is that H I exists in two stable phases, in a rough thermal pressure equilibrium with one another and with the hot ionized medium (e.g. Field, 1965; Field et al., 1969; McKee & Ostriker, 1977; Wolfire et al., 1995, 2003). Observationally, it has been established that H I indeed has two phases, (1) a cold phase (the CNM), with high density ($n \approx 20 - 50$ cm^{-3}) and a high 21 cm optical depth, giving rise to the narrow absorption features seen towards continuum sources, and (2) a warm diffuse phase ($n \approx 0.2 - 0.5$ cm^{-3}), the WNM, which contributes to the emission, but is extremely difficult to detect in absorption due to its low optical depth (Radhakrishnan et al., 1972; Heiles & Troland, 2003a,b). Theoretical models (e.g. Wolfire et al., 1995) find that thermal steady state, i.e., a balance between the net heating and cooling rates, can be maintained for H I in two stable temperature ranges, $\sim 40 - 200$ K (CNM) and $\sim 5000 - 8000$ K (WNM). The thermal timescale derived from the heating or cooling rate for the CNM is $\sim 2 \times 10^4$ yr and is about 100 times longer for the WNM (Wolfire et al., 1995). On the other hand, the timescale of disturbance (typical time interval between signifi-

cant pressure fluctuations) from the propagation of supernova shock front is 4×10^5 yr (McKee & Ostriker, 1977; Wolfire et al., 1995). So, CNM can be assumed to be in the thermal steady state. For WNM, even if the thermal balance is not necessarily achieved, the physical conditions will evolve towards the steady state, and the steady state conditions are thought to "represent an average of the conditions to be expected in the actual WNM" (Wolfire et al., 1995). H I at intermediate temperatures is unstable and such gas is expected to quickly settle into one of the stable phases. The estimated e-folding time for the instability due to runaway heating or cooling of the thermally unstable gas is only $\sim 10^6$ years (Field et al., 1969). Hence, warm gas at intermediate temperature exists "only as a transient phenomenon" (Field et al., 1969) and most of the H I is expected to be found in one of the two stable phases. Decades of study have established that the CNM has temperatures in the expected range, $\sim 40 - 200$ K (e.g. Dickey et al., 1978; Heiles & Troland, 2003a; Roy et al., 2006); however, direct measurement of WNM temperature is quite rare (Carilli et al., 1998; Dwarakanath et al., 2002; Kanekar et al., 2003) and very little is as yet known about physical conditions in the WNM.

Recently, there have been claims that the measured kinetic temperatures of the warm gas is in the unstable range, $500 - 5000$ K (Heiles & Troland, 2003a,b; Kanekar et al., 2003). Kanekar et al. (2003) carried out high velocity resolution interferometric H I absorption studies along the lines of sight towards two compact southern sources from the Australia Telescope Compact Array (ATCA). A significant fraction of gas is found to be in the thermally unstable phase for both the lines of sight. On the other hand, Heiles & Troland (2003a) used the Arecibo Telescope to carry out high velocity resolution 21 cm absorption and emission studies towards 79 compact radio sources. The spectra were modelled as thermally-broadened Gaussians and a fit to the emission spectra was used to estimate the kinetic temperature of WNM components. A substantial fraction ($\sim 48\%$) of the warm gas was found to be in the thermally unstable phase, $T_k \sim 500 - 5000$ K. These results are very interesting as they suggest that

the steady state may not be attained in the WNM. This may be due to the longer timescales ($\sim 2 \times 10^6$ yr) required for the WNM phase to reach the steady state compared to the timescale of intermittent injection of energy into the medium and significant pressure fluctuations from the propagation of supernova shock front (4×10^5 yr; McKee & Ostriker, 1977; Wolfire et al., 1995). However, it is critical to test these claims, given the importance of the WNM in the interstellar medium and the repercussions of the above results for our understanding of the ISM.

A concern with the results presented by Heiles & Troland (2003a) is that they were obtained using a single-dish telescope, where the absorption spectrum contains contributions from the H I emission in the beam. This emission has to be modelled and subtracted out, using off-source emission spectra, in order to obtain the "true" H I absorption spectrum. It is very difficult to do this correction accurately as it is based on the assumption that the H I distribution is smooth on scales larger than the size of the telescope beam; this is often not true for the CNM and may also be incorrect for the WNM. Single-dish emission studies also require assumptions about the spatial distribution of H I clouds along the line of sight (which is unknown, *a priori*), to correct for absorption of background H I emission by foreground CNM. Finally, emission spectra are affected by stray radiation entering via the side-lobes of the telescope beam. The effect of all these uncertainties on the results is not well-understood.

Carilli et al. (1998) and Dwarakanath et al. (2002) used interferometric H I absorption studies to detect weak, broad absorption features towards Cygnus A and 3C 147. But, they had used the corresponding H I emission spectra to derive the spin temperature for the components. Hence, these studies could also be affected by the above mentioned issues. The modest spectral resolution of these studies (~ 2.1 km s^{-1} per channel) also prevents one from ruling out the possibility of blending of narrow CNM components.

It should be emphasized that it is the H I *emission* spectra that are affected by the above issues like stray radiation, non-uniformity of H I clouds across the beam, self-absorption, etc. Interferometric 21 cm ab-

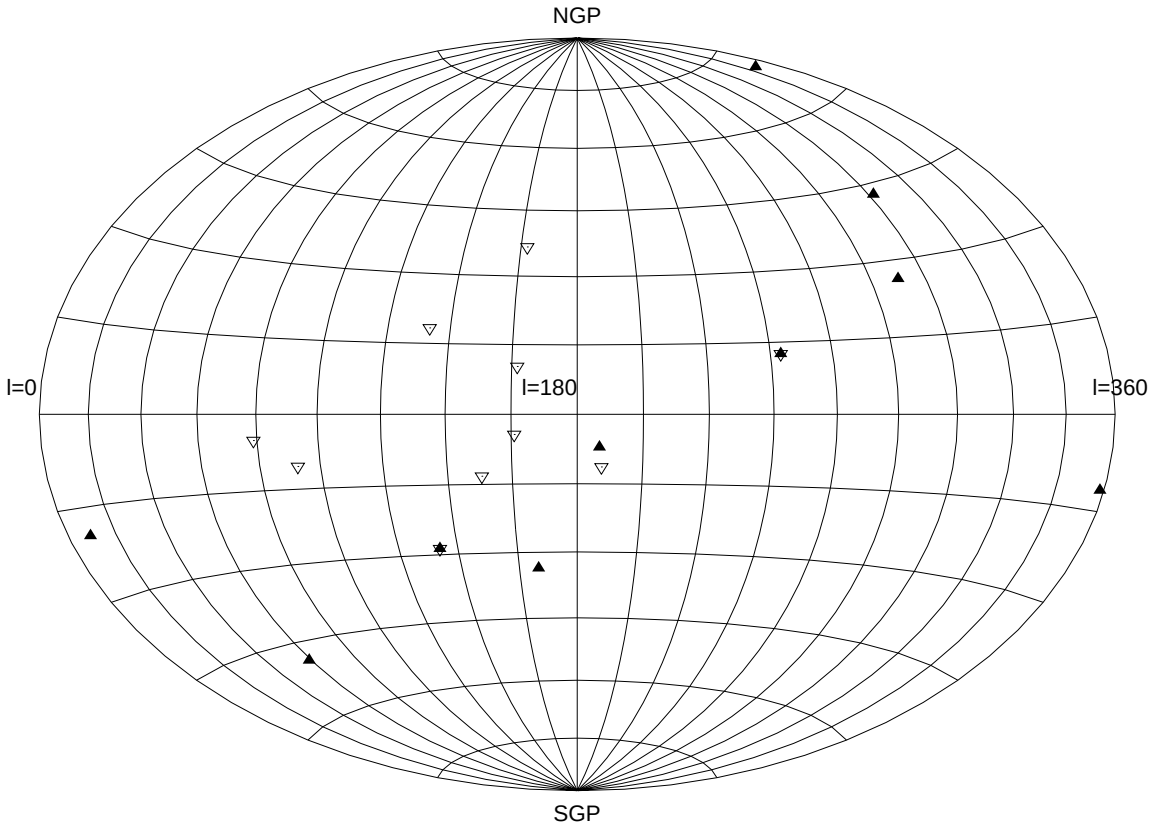

Figure 3.1: Sky coverage of the WNM 21 cm absorption-line survey shown in the Galactic coordinates. The filled and empty triangles are for the lines of sight observed with the GMRT and the WSRT respectively.

sorption studies of compact sources resolve out the foreground H I emission (thus avoiding the above difficulties) and trace narrow lines of sight through the intervening clouds, providing an uncontaminated measure of the absorption profile, which might then be examined for wide WNM features Carilli et al. (e.g., 1998); Dwarakanath et al. (e.g., 2002); Kanekar et al. (e.g., 2003). The fact that the WNM must be searched for in the midst of strong CNM absorption features can be mitigated by using high velocity resolution observations to resolve and subtract out the narrow CNM components. A simultaneous multi-Gaussian fit to the absorption spectrum then allows one to measure the velocity widths of the different components and to thus estimate their kinetic temperatures. Of course, the WNM op-

tical depth is very low and a high sensitivity and a high spectral dynamic range are needed to detect it in absorption.

The above strategy was followed by Kanekar et al. (2003) for two compact southern sources and resulted in the detection of the WNM in absorption (in the unstable phase) along both the lines of sight. The main assumption here (as also in Heiles & Troland, 2003a) is that the decomposition of the absorption profiles into thermally-broadened Gaussians is physically meaningful. Note that, strictly speaking, the velocity width, in both approaches, places an upper limit on the kinetic temperature, as turbulent motions might also contribute to the observed line width (see Chapter 2 and Roy et al., 2008, for details). The critical difference between the two approaches is that Kanekar et al. (2003) worked entirely with absorption spectra and were hence not affected by emission-related issues. However, while Kanekar et al. (2003) found that it was indeed possible to measure the WNM kinetic temperature from interferometric absorption spectra, they only obtained results for two directions in the Galaxy.

In this Chapter, I report the results from deep, high-resolution interferometric 21 cm observations of a large sample of compact sources. I have obtained absorption-based estimates of WNM kinetic temperatures from a statistically significant number of lines of sight and can thus test whether a large fraction of the WNM indeed has temperatures in the unstable range.

3.2 Observation and data analysis

3.2.1 The sample

A H I 21 cm absorption survey using the GMRT and the WSRT have been carried out, towards a large sample of sources to measure the kinetic temperature of the WNM along each line of sight. The complete sample consists of the 54 VLA L-band calibrators (unresolved in at least the VLA B-array), with L-band flux densities higher than 3 Jy. In this on-going survey, it is planned to use the GMRT and the WSRT to obtain deep, high velocity resolution absorption spectra of all 54 sources and, as a part of

this, deep 21 cm absorption spectra of 10 sources with the GMRT and of 12 with the WSRT are already obtained . The L-band continuum flux densities for all the sources in this subsample are more than or equal to 5 Jy. While selecting this subsample, those lines of sight are excluded along which the H I 21 cm emission spectra, obtained from the Leiden/Argentine/Bonn (LAB) Galactic H I Survey (Hartmann & Burton, 1997; Arnal et al., 2000; Bajaja et al., 2005; Kalberla et al., 2005), are extremely complicated. Two of the sources are observed with both the GMRT and the WSRT to cross-check the instrumental behaviour. For two lines of sight, the 21 cm absorption spectra are very complicated and it was not possible to derive a reasonable fit of the spectra even with a large number of Gaussian components. So, in this work, further analysis is restricted to a total of 18 sources. The position of these sources on the sky is shown in Figure (3.1) in the Galactic coordinate system.

3.2.2 Observation

For the GMRT observations of 10 of these sources, a baseband bandwidth of 0.5 MHz, sub-divided into 256 channels was used, yielding a total velocity coverage of ~ 105 kms^{-1} and a velocity resolution of ~ 0.4 kms^{-1}. A total bandwidth of 2.5 MHz, sub-divided into 2048 channels yielding a velocity coverage of ~ 525 kms^{-1} and a resolution of ~ 0.26 kms^{-1}, was used for the observation of 10 sources with the WSRT.

For these observations, the "standard" route towards bandpass calibration using a bandpass calibrator does not work because of two reasons. (1) It is not possible to find a source without spectral features in the observing band where H I 21 cm absorption is likely to be present towards any possible bandpass calibrator. In this situation, the final spectrum towards the target source (with standard bandpass calibration) would be corrupted by the absorption against the calibrator, making it impossible to detect features weaker in optical depth than those towards the calibrator. (2) The target sources are also so strong that a large fraction of the total time is needed on a (weaker) bandpass calibrator to reach a signal-

to-noise ratio comparable to that on the target. We solve this problem by employing an alternative approach to bandpass calibration, involving frequency-switching.

We note that frequency-switching is routinely used at radio interferometers such as the ATCA and the WSRT and that it has been possible to achieve spectral dynamic ranges of > 1000 at both these telescopes, with frequency-switching on a timescale of five minutes (e.g. Braun & Kanekar, 2005; Kanekar et al., 2003). In the case of the GMRT, to the best of our knowledge, the only detailed study based on this technique is that of Mohan et al. (2001). These authors achieved a spectral dynamic range of $\sim 50 - 140$ per ~ 3.3 kms^{-1} channel along 14 lines of sight, with frequency-switching carried out every two hours, at the fourth (or baseband) local oscillator. Further, these observations were carried out in the early days of the GMRT, in 1999, with only $8 - 10$ working antennas. As a preliminary to this H I absorption survey, a series of observations were carried out with the full GMRT array to test the quality of spectral baselines that can be achieved with frequency-switching at the GMRT. It is found that the spectral baseline obtained by switching at the first local oscillator (using a frequency throw of 5 MHz) is quite flat (Roy & Kanekar, 2007). The resulting spectral dynamic range is $\gtrsim 1000$ for narrow features and $\sim 1000 \times N^{1/2}$ for features that are N channels wide (where N is significantly smaller than the total number of channels).

So, bandpass calibration for the GMRT observations was carried out with frequency-switching at the first local oscillator, using a frequency throw of 5 MHz. For the WSRT observations, bandpass calibration was carried out with in-band frequency-switching. Total observation time including all calibrations was 10 and 12 hours per source for the GMRT and WSRT observations respectively.

3.2.3 Analysis

All data were analysed in NRAO AIPS, using standard procedures. Some of the data were edited out for a variety of reasons (e.g. correlator spikes

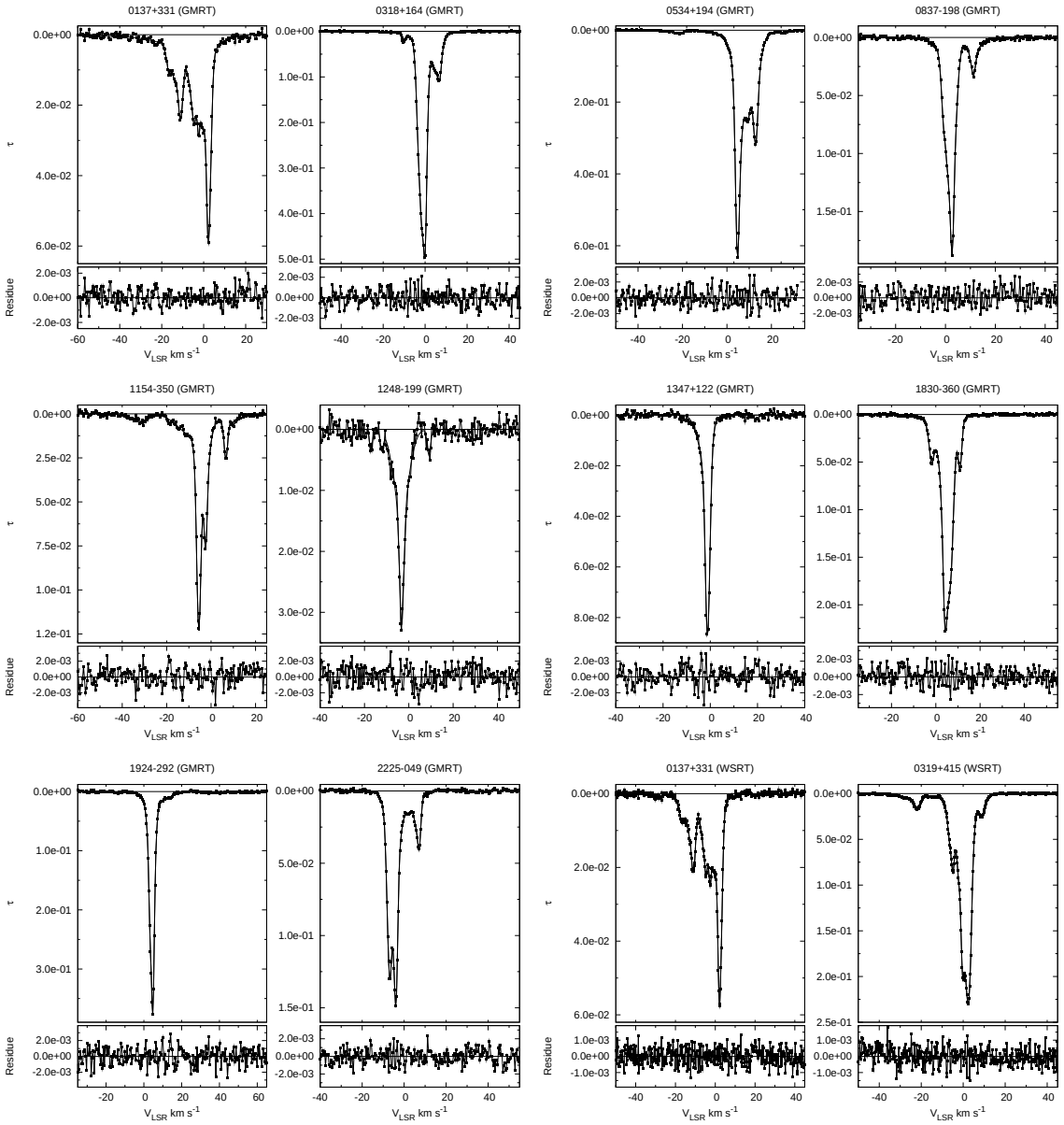

Figure 3.2: H I 21 cm absorption spectra obtained using the GMRT and the WSRT. The observed spectrum with the best fit multi-Gaussian model is shown in the top panel and the residual after subtracting the model from the data is shown in the bottom panel for each of the 20 lines of sight. The name of the background source and the telescope (GMRT/WSRT) is mentioned for each case at the top of the panels. Only the relevant LSR velocity range containing H I 21 cm absorption is shown in the plots. See Section 3.2.3 for a detailed discussion of analysis and model fitting procedure (continued ...).

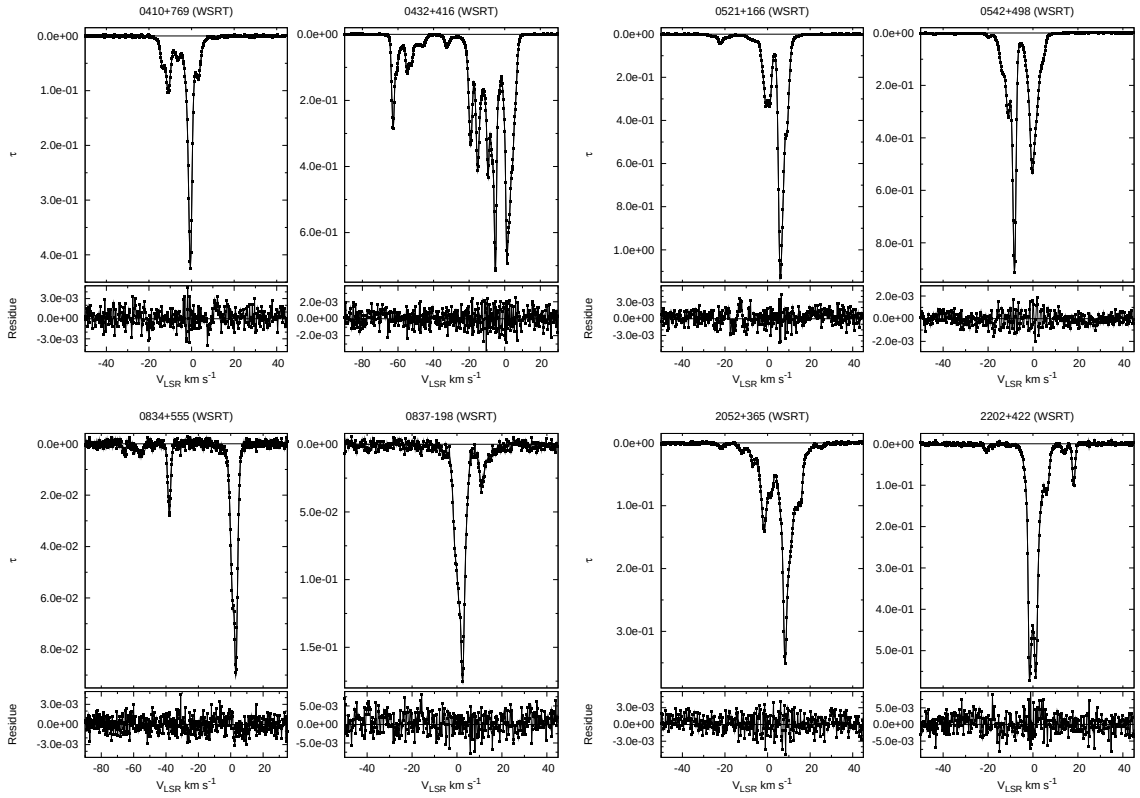

Figure 3.2: continued ...

in one side-band for GMRT data). Special care was taken to remove the narrow spikes originating from frequency dependent radio frequency interference. After removing unwanted and bad data, the standard calibration procedure was followed to obtain the antenna-based complex gains. Bandpass calibration was applied using interpolation between bandpass solutions (i.e. DOBAND=3 in AIPS). In all of the cases the background continuum source remains unresolved or just barely resolved with most of the flux being in the compact component. Next, continuum subtraction was carried out using the line-free channels to estimate the continuum flux, and the task CVEL then used to shift the residual U-V data to the LSR frame. The residual data were imaged in all channels, and the final spectrum then was obtained by a cut through the dirty cube at the loca-

tion of the target source. This was converted into optical depth spectrum using the flux value estimated from the continuum image of the line-free channels.

The optical depth spectra were modelled as a combination of multiple Gaussian components. Modelling the absorption spectra as a collection of Gaussian components has been done routinely for Galactic H I 21 cm absorption studies (e.g., Mebold, 1972; Radhakrishnan et al., 1972; Mebold et al., 1982; Heiles, 2001; Heiles & Troland, 2003a). But, this is a valid approach only if (1) the damping wings are negligible (as in the case of H I 21 cm line), (2) the the absorbing "cloud" is homogeneous and (3) the broadening of the line is dominantly thermal. The last two conditions may not be necessarily true for the diffuse ISM. Particularly, when the broadening is dominantly non-thermal, the line can have Gaussian shape only when there is a contribution to the width from a large number of turbulent elements. There have been attempts of using simple model of non-Gaussian line profiles in some cases (e.g., Braun & Kanekar, 2005). Another critical issue is that the fits are not unique since the Gaussian functions are not orthogonal. Although there is no mathematically unique and physically robust procedure that can be used to interpret the spectra, it may be noted that: (1) most of the spectra can easily and conveniently be decomposed into Gaussians, (2) though there are some doubts on the exactness of the physical model, empirically it works quite well and (3) much of what we have learned about the neutral atomic medium has come from this relatively simplistic assumption. In the analysis presented below, the same tradition had been continued.

The best fit model parameters and the errors were derived by the standard technique of minimization of the reduced chi-square. For each spectra, it was tried to achieve a reasonable fit (reduced chi-square as close to one as possible and a noise-like residual) with a minimum number of components. The optical depth spectra and the models as well as the residuals for each of the 20 lines of sight are shown in Figure (3.2). A summary of the fit with the number of Gaussian components for the model, the value of the

reduced chi-square (χ^2_r) and the residual RMS for each case is also given in Table (3.1). For all of the spectra, the value of the reduced chi-square is very close to one implying that the model is a good representation of the observed optical depth spectrum. The residuals are also noise-like with no significant spectral baseline and the RMS of the residual is consistent with the spectral noise estimated from the line-free channels.

3.2.4 Comparing Arecibo/GMRT/WSRT spectra

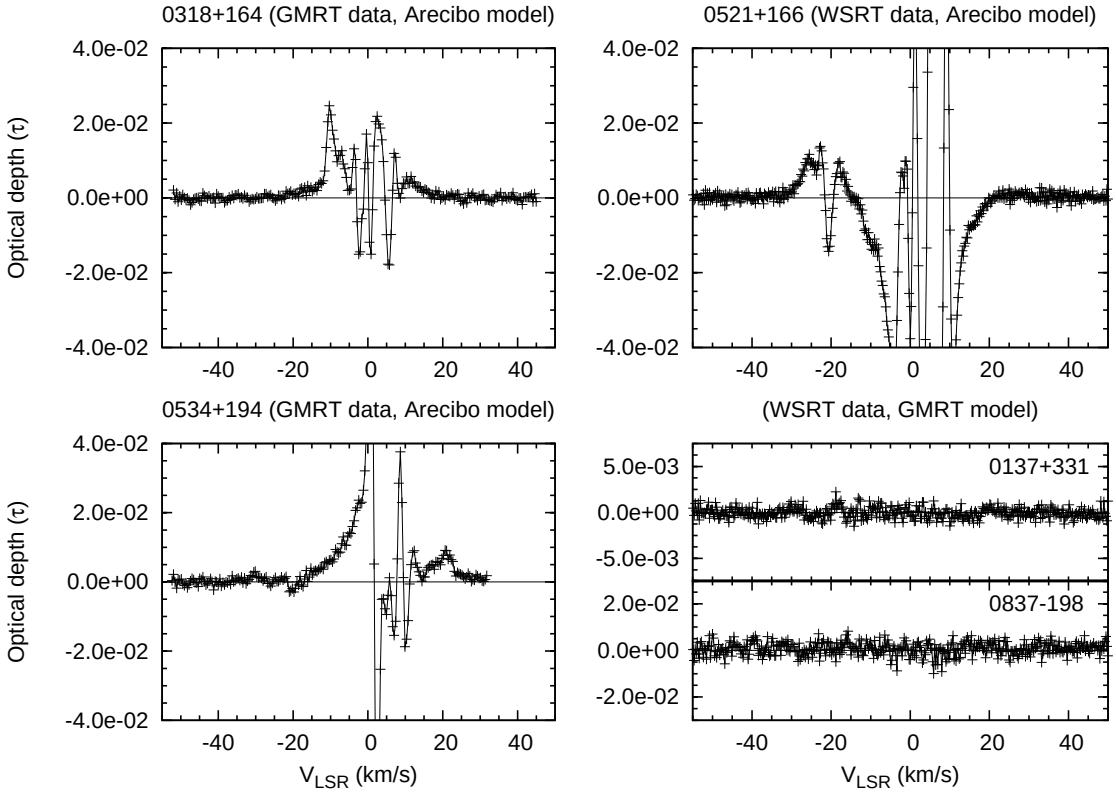

Figure 3.3: The residuals of the H I 21 cm absorption spectra obtained with one telescope after subtracting the (scaled) model of the spectra obtained with another telescope for the same line of sight. Names of the telescopes used to obtain the spectra and the best-fit model are mentioned at the top of each panel.

As mentioned earlier, the H I absorption spectra obtained from the

Table 3.1: Details of the GMRT and the WSRT sources and model fitting

Source	Coordinate		S_ν[b]	N(H I)[c]	Fit summary[d]		
Name[a]	l	b	Jy	cm^{-2}	n	χ^2_r	RMS
The GMRT sources:							
0137+331	134.0	−28.7	16.5	0.428E+21	11	1.099	0.00062
0318+164	166.6	−33.6	07.8	0.944E+21	10	1.141	0.00075
0534+194	186.8	−07.1	06.8	0.266E+22	11	1.071	0.00099
0837−198	243.3	+12.6	05.0	0.715E+21	07	1.046	0.00108
1154−350	289.9	+26.3	05.0	0.775E+21	07	1.083	0.00105
1248−199	302.0	+42.9	05.3	0.382E+21	05	1.047	0.00123
1347+122	347.2	+70.2	05.2	0.196E+21	02	1.020	0.00107
1830−360	358.3	−11.8	06.9	0.817E+21	06	1.055	0.00089
1924−292	009.3	−19.6	06.0	0.732E+21	07	1.086	0.00102
2225−049	059.0	−48.8	05.7	0.456E+21	07	1.051	0.00079
The WSRT sources:							
0137+331	134.0	−28.7	16.5	0.428E+21	11	1.030	0.00053
0319+415	150.6	−13.3	23.9	0.131E+22	11	1.031	0.00049
0410+769	133.4	+18.3	05.8	0.110E+22	07	1.024	0.00116
0432+416	161.0	−04.3	08.6	0.370E+22	26	1.078	0.00090
0521+166	187.4	−11.3	08.5	0.209E+22	11	1.037	0.00108
0542+498	161.7	+10.3	22.5	0.196E+22	17	1.062	0.00049
0834+555	162.2	+36.6	08.8	0.452E+21	07	1.021	0.00115
0837−198	243.3	+12.6	05.0	0.715E+21	07	1.049	0.00276
2052+365	078.9	−05.1	05.2	0.277E+22	13	1.037	0.00146
2202+422	092.6	−10.4	06.1	0.171E+22	10	1.027	0.00268

[a] The source names are as in the VLA calibrator manual.

[b] The quoted 20 cm flux density is from the VLA calibrator manual.

[c] N(H I) is the column density from the LAB survey H I emission spectra.

[d] Fit summary includes the number of Gaussian components (n), Reduced chi-square (χ^2_r) and the residual RMS for each case.

single dish observations may be seriously affected by issues like non-uniformity of emission across the beam, self-absorption, stray radiation entering via the beam side-lobes etc. Hence, it will be useful to directly compare spectra for the same line of sight obtained from Arecibo telescope (i.e. from Heiles & Troland, 2003a) and interferometric arrays (i.e. from the present GMRT and WSRT observations). It would be good to also compare the GMRT and WSRT spectra for the same line of sight to crosscheck the instrumental behaviour and the consistency. Unfortunately, there is no source in the present sample that has been observed with all three telescopes. Nevertheless, there are sources which are observed with two of these telescopes and a pairwise comparison is possible. For two of the sources ($0137+331$ and $0837-198$), the H I 21 cm spectra were obtained with the GMRT and also the WSRT. There are three more sources ($0318+164$, $0521+166$ and $0534+194$) in the GMRT/WSRT sample which have also been observed by Heiles & Troland (2003a) for the millennium Arecibo 21 cm absorption line survey. These give a chance to compare the spectra for the same line of sight obtained with different telescopes.

For spectra obtained with different telescopes the velocity sampling is different and hence direct comparison is not possible. Instead the best fit model from one telescope was compared with the data from another telescope. Note that it is difficult to compare the models themselves, because a one to one correspondence between the model components is not always present.

In the following section, a detailed comparison of the key results of this study (e.g. fraction of gas in different thermal phase) with the millennium Arecibo 21 cm absorption line survey results have been carried out. This final comparison of the results is based on the best fit model parameters provided in Heiles & Troland (2003a). In a similar spirit, for this comparison also, a refit had not been done for the spectra obtained from the Arecibo survey. Rather, the best fit model parameters given by Heiles & Troland (2003a) had been used. But, before comparison, the best possible amplitude scaling of the Arecibo model had been done to minimize the

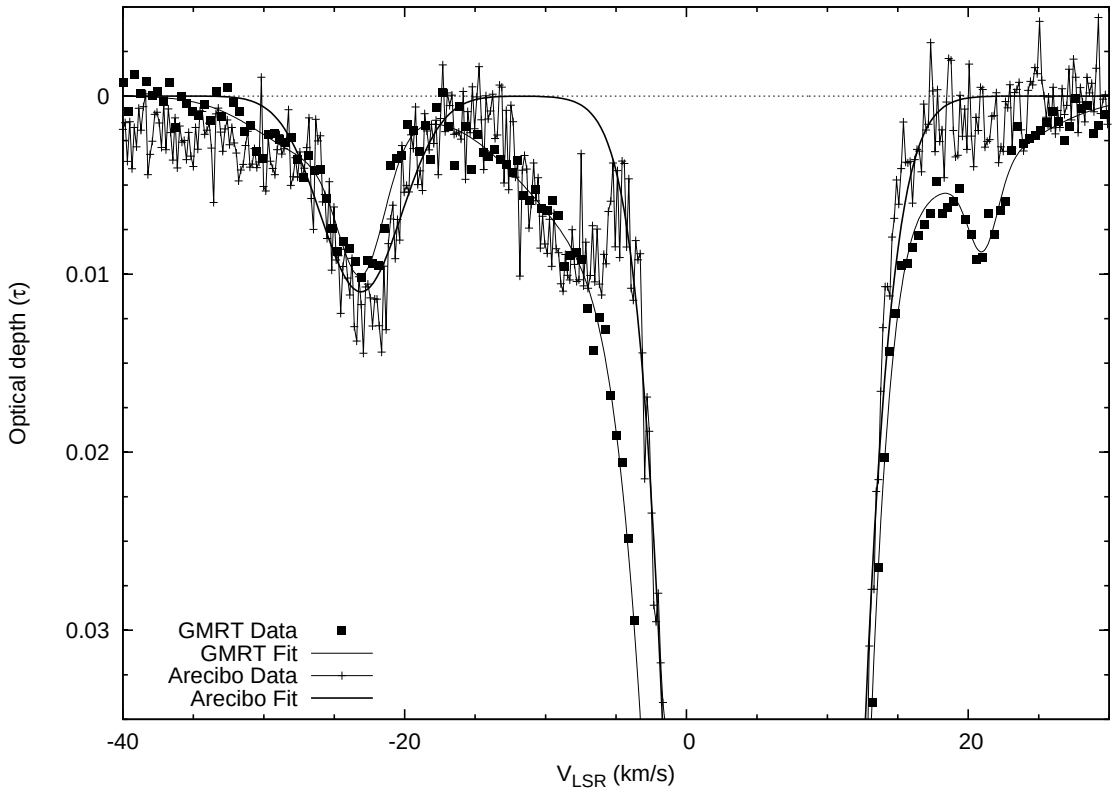

Figure 3.4: H I 21 cm absorption spectra towards $0534 + 194$ obtained with the GMRT and the Arecibo along with the multi-Gaussian models. The Arecibo spectrum and the model is taken from Heiles & Troland (2003a).

difference between two spectra. This permitted amplitude scaling takes care of any offsets in flux density due to (1) error in absolute flux calibration, (2) inaccurate subtraction of H I emission and (3) stray radiation. The residuals of the H I spectra obtained with one telescope after subtracting the best-fit multi-Gaussian model of the spectra obtained with the other telescope are shown in Figure (3.3). Clearly, the agreement of GMRT and WSRT spectra is much better than that of the Arecibo and GMRT/WSRT spectra. Note that the scale is different for the GMRT/WSRT comparison.

The two plausible reasons for such discrepancy are (i) a real difference between the spectra due to effects like inaccurate subtraction of H I emission and (ii) inaccurate modelling of the spectrum. Both of the rea-

sons are relevant in the current situation. An illustrative case, as shown in Figure (3.4), is the Arecibo spectrum towards $0534 + 194$. The absorption component seen in the GMRT spectrum at $V_{LSR} \approx +20.0$ kms^{-1} is not present in the Arecibo spectrum. On the other hand, a component at $V_{LSR} \approx -10.0$ kms^{-1} is clearly present in both the GMRT and the Arecibo spectra, but is not included in the model of Heiles & Troland (2003a).

3.2.5 Optical depth statistics

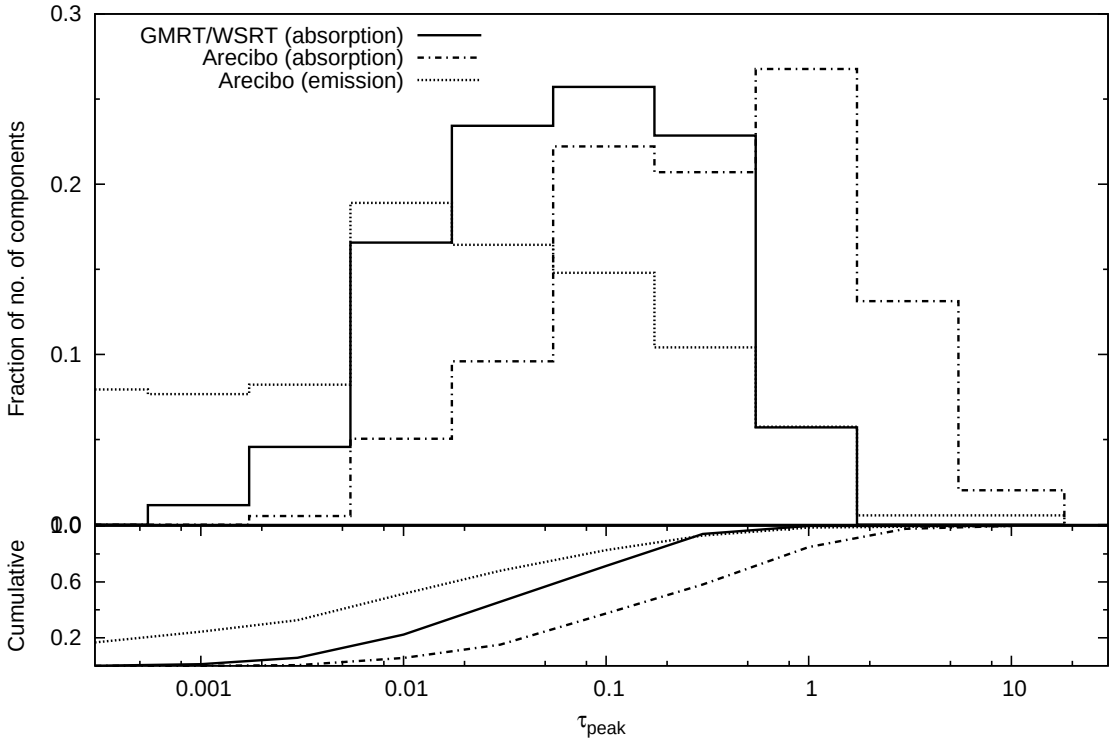

Figure 3.5: The distribution of peak optical depth of the components detected in H I absorption spectra taken with the GMRT/WSRT (solid line). For comparison, the distribution from the millennium Arecibo 21 cm absorption line survey for the components detected in H I absorption and emission spectra (dotted lines) are also shown (see Section 3.2.5 for details).

The components detected in H I absorption spectra obtained with the GMRT and the WSRT have a wide range of optical depth and velocity width. The distribution of peak optical depth for all the components detected in our survey (labelled "GMRT/WSRT (absorption)" in the figure) is shown in Figure (3.5). For comparison, (i) the distribution of observed $\tau_{\rm peak}$ for the components detected in H I absorption (labelled "Arecibo (absorption)" in the figure) and (ii) the distribution of $\tau_{\rm peak}$ inferred from column density N(H I) and upper limit of the kinetic temperature $\rm T_{kmax}$ (labelled "Arecibo (emission)" in the figure) for all the components detected in H I emission from the millennium Arecibo 21 cm absorption line survey (Heiles & Troland, 2003a) are also shown.

Since $\tau_{\rm peak} \propto 1/\rm T_{kmax}$ and $\rm T_{kmax}$ is an upper limit of the temperature, the distribution based on N(H I) and $\rm T_{kmax}$ (i.e. histogram with the dotted line) over-predicts the number of components with small $\tau_{\rm peak}$. Hence, as expected, both the Arecibo survey and the present study with the GMRT and the WSRT detects a smaller fraction of small $\tau_{\rm peak}$ components than predicted by the assumption $\rm T_s = T_kmax$. Note that the present study, however, does detect significantly more components with lower $\tau_{\rm peak}$ than that of the Arecibo survey. This is consistent with the higher sensitivity of the GMRT and WSRT spectra.

3.3 Results

3.3.1 Temperature distribution

It has been found that the best fit models for the absorption spectra towards these lines of sight consist of, along with many narrow components arising from the cold gas, a significant number of wide components which are interpreted as being due to gas in the warm phase. Some of the simpler profiles with the best fit Gaussian components are shown in Figure (3.6) and (3.7). The kinetic temperatures for these components derived from the width of each of the Gaussian components are also given in the respective figure panels.

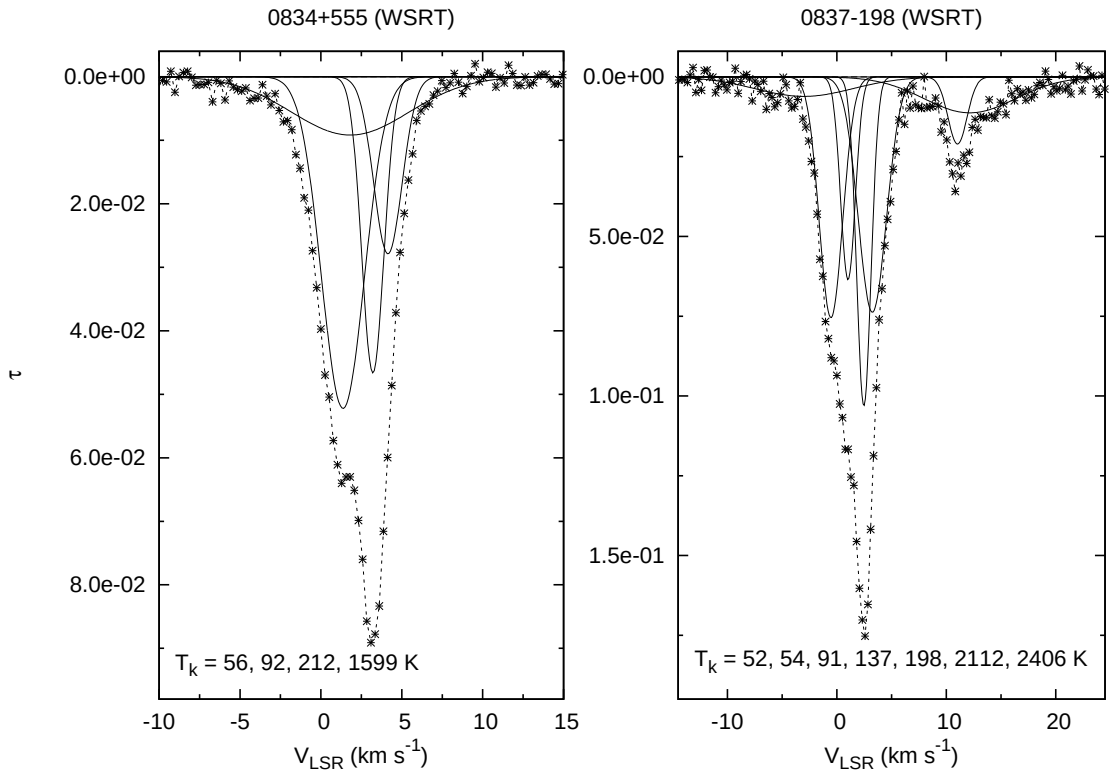

Figure 3.6: Observed H I 21 cm absorption spectra towards $0834+555$ and $0837-198$ along with the Gaussian components from the best fit model.

There are a total of 175 Gaussian components detected in H I absorption spectra towards 18 sources in the sample. The distribution of peak optical depth, $\tau_{\rm peak}$ and velocity width of these components are shown with respect to the Galactic longitude, l and Galactic latitude b in Figure (3.8). It is found that there is a clear trend in $\tau_{\rm peak}$ with both l and b. H I 21 cm absorption is deeper towards Galactic center and anti-centre compared to that at the other Galactic longitude. Absorption components are also significantly deeper, as expected, for the lines of sight close to the Galactic plane (small values of $|b|$). There is no significant correlation of width of the components with l or b.

The correlation between peak optical depth and velocity width for these

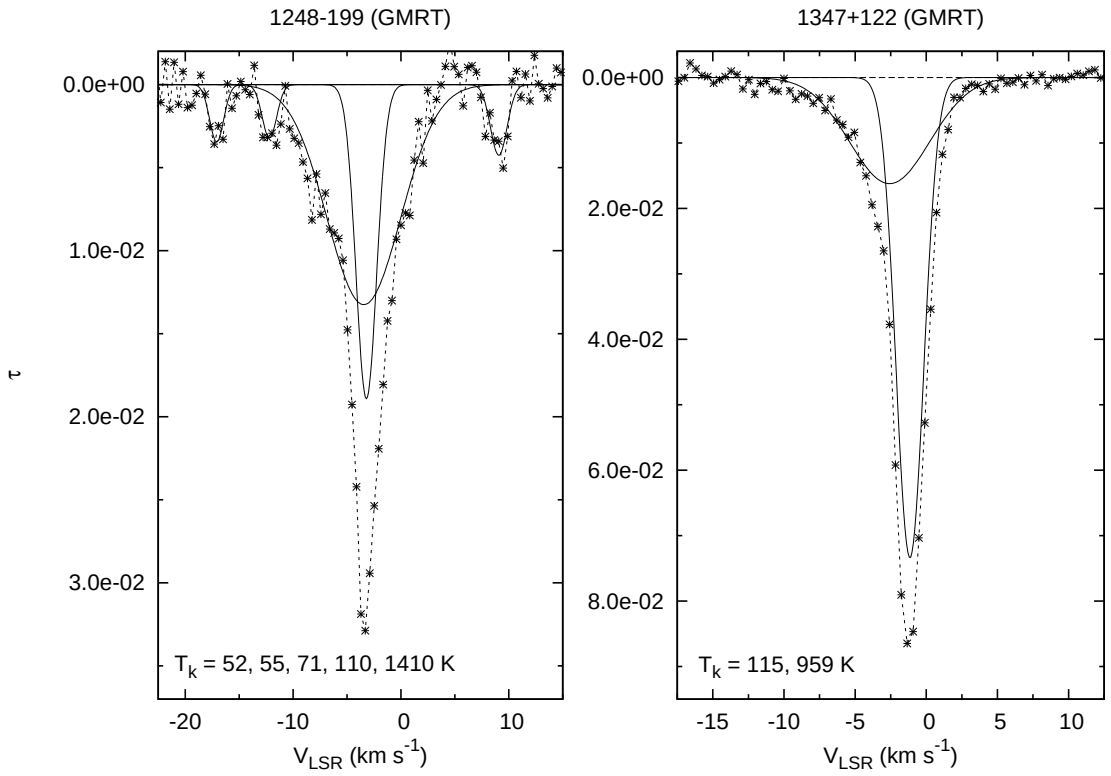

Figure 3.7: Observed H I 21 cm absorption spectra towards $1248-199$ and $1347+122$ along with the Gaussian components from the best fit model.

components was also checked for. As shown in Figure (3.9), there is a clear anti-correlation between these two quantities (at the 5σ level) and the velocity width scales as $\tau_{\rm peak}^{-0.24}$. This anti-correlation is quite natural since the wide "warm" components are generally expected to have lower optical depth. If the width is assumed to be only thermal, then this imply that there is a correlation between the kinetic temperature and peak optical depth ("T$-\tau$ correlation") and $T_k \propto \tau_{\rm peak}^{-0.48}$.

Out of these 175 components, $\sim 75\%$ of the components are in the cold phase ($T_k < 500$ K), $\sim 22\%$ are in the warm unstable phase (T_k between $500-5000$ K) and $\sim 3\%$ of are in stable warm phase ($T_k > 5000$ K). The H I column density fractions are ~ 14, 72 and 14% in cold, unstable warm

Table 3.2: H I column density percentage in different phases

Subsample	n_{los}	N_{comp}	CNM[a]	WNM[a]	
			(stable)	(unstable)	(stable)
GMRT	9	62	17 ± 06	54 ± 21	29 ± 18
WSRT	9	113	13 ± 03	81 ± 05	06 ± 04
$\|b\| > 10^\circ$	15	125	17 ± 03	61 ± 11	22 ± 10
$\|b\| < 10^\circ$[b]	3	50	09	91	–
$n_{comp} \leq 7$	9	55	14 ± 04	66 ± 14	20 ± 17
$n_{comp} > 7$	9	120	15 ± 03	73 ± 10	12 ± 09
All	18	175	14 ± 03	72 ± 08	14 ± 07
Simulation[c]	18	175	16 ± 03	63 ± 06	18 ± 05
All (corrected)[d]	18	175	49 ± 07	51 ± 07	< 14

[a] Errors are estimated using bootstrapping.

[b] No errors are estimated since there are only 3 lines of sight with $|b| < 10^\circ$.

[c] Using 10^6 Gaussian realization of the width for each component.

[d] Statistics after correcting non-thermal line width (see Section 3.3.2 for details).

and stable warm phases respectively. The H I column density fractions in different phases were also calculated for subsamples consisting of (i) only the GMRT/WSRT observations, (ii) only sources with $|b| > 10^\circ$ and $|b| < 10^\circ$, (iii) sources with simpler H I absorption profile with 7 or less Gaussian components and (iv) complex absorption profile with more than 7 components. The result is summarized in Table (3.2). We have used bootstrap resampling to estimate the errors (sample bias) in each case. For $|b| < 10^\circ$, no errors were estimated since there are only 3 lines of sight in this case. The H I column density fractions (with errors) in different phases were also estimated taking care of the errors on individual component parameters. For this, a large number of realizations of each component was made using the best fit values and estimated Gaussian errors of the

widths. Since the H I column density is quite well-determined from the multi-Gaussian fit of the absorption spectra, in this simulation the column density for each component was left unchanged and only the width (i.e. T_k) of the components was changed. Then the distribution of column density fraction in different phases was estimated from these realizations. About 63% of the total detected H I column density is found to be in the unstable thermal phase. Errors on the H I column density fractions in different phases due to parameter uncertainties and due to sample bias are found to be comparable.

3.3.2 Correcting for the non-thermal line width

All this statistics is, however, based on the assumption that the broadening of the components is purely thermal. In reality, the width of the components gives only the upper limit of the kinetic temperature. As it has been shown earlier in Chapter 2, the contribution of non-thermal processes like turbulence to the observed line width may be significant. It is found that the non-thermal line width $v_{nt}^2 \propto (T_{Kmax} - T_S)$ has a Kolmogorov-like power law scaling with the derived length scale $l \propto$ N(H I) T_S. This will result in an overestimation of the temperature of the absorbing gas and the inferred temperature distribution will not be correct.

To take care of this, here the spin temperature T_S of each of the components was derived from the observed parameters using the above-mentioned correlation (see Chapter 2 for details). We also have calculated the total H I column density detected in absorption for these 18 lines of sight before and after correcting for the non-thermal line width. For most of the cases, the upper limit of the N(H I), calculated using the upper limit of the kinetic temperature T_{Kmax} based on the observed line width, is found to be significantly more than the N(H I) calculated from the LDS emission spectrum for the same line of sight. However, as shown in Figure (3.10), after correcting for the non-thermal line width, the derived H I column density detected in absorption is less than the N(H I) detected in emission. A plausible reason for this may be that some fraction of warm gas with a very low optical

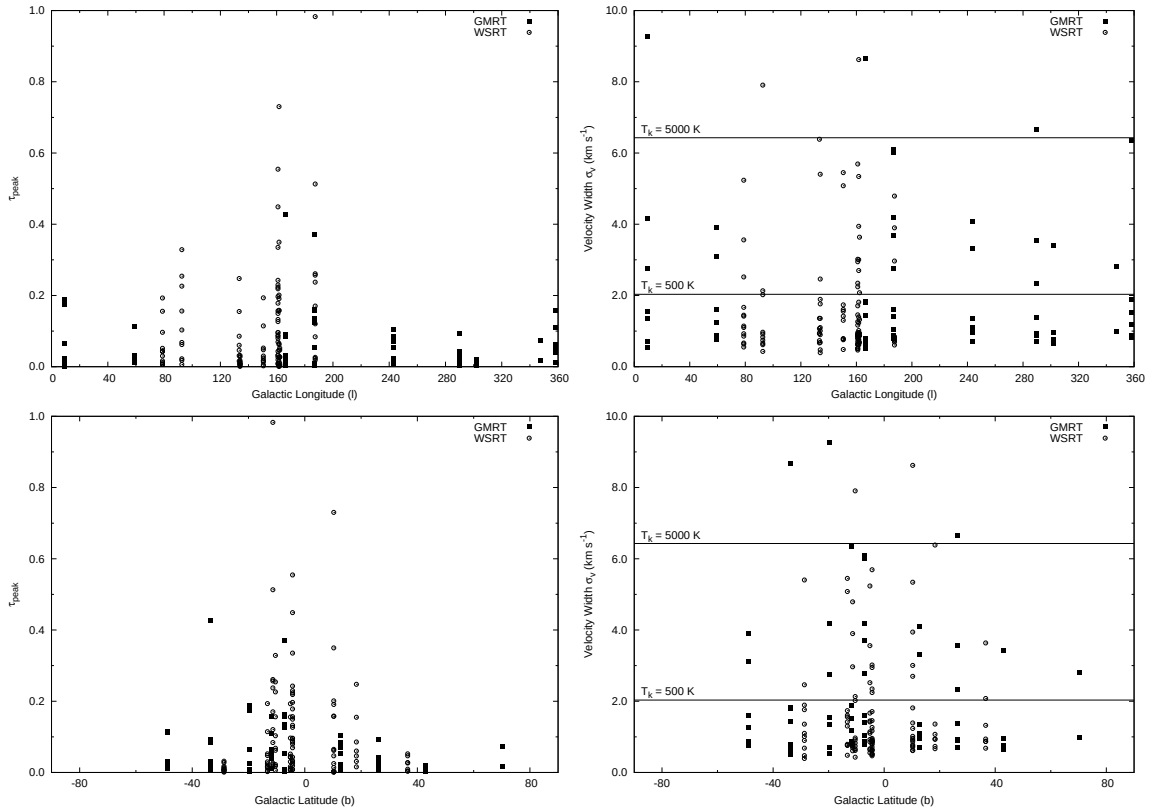

Figure 3.8: Distribution of component parameters (peak optical depth and velocity width) with Galactic longitude and latitude. Velocity widths corresponding to $T_{\rm k} = 500$ and 5000 K are marked on the panels.

depth is not detected in absorption but is seen only in emission. However, for ~ 8000 K gas, the 3σ upper limit of H I column density for these observation is 2×10^{20} cm^{-2} for typical optical depth RMS of 10^{-3} per ~ 0.4 kms^{-1}. To explain N(H I) $\sim 10^{21}$ cm^{-2} seen in emission but not in absorption, about 10 WNM "clouds" are needed for a given line of sight. Hence, it is very unlikely that there is a substantial fraction of WNM which is not detected in absorption. The other explanation is that the bigger beam of the emission survey should detect, along with all the strong components with significant H I column density detected in absorption, some additional components outside the narrow beam of the absorption survey. However, the possibility, that the non-thermal line widths have been over-corrected,

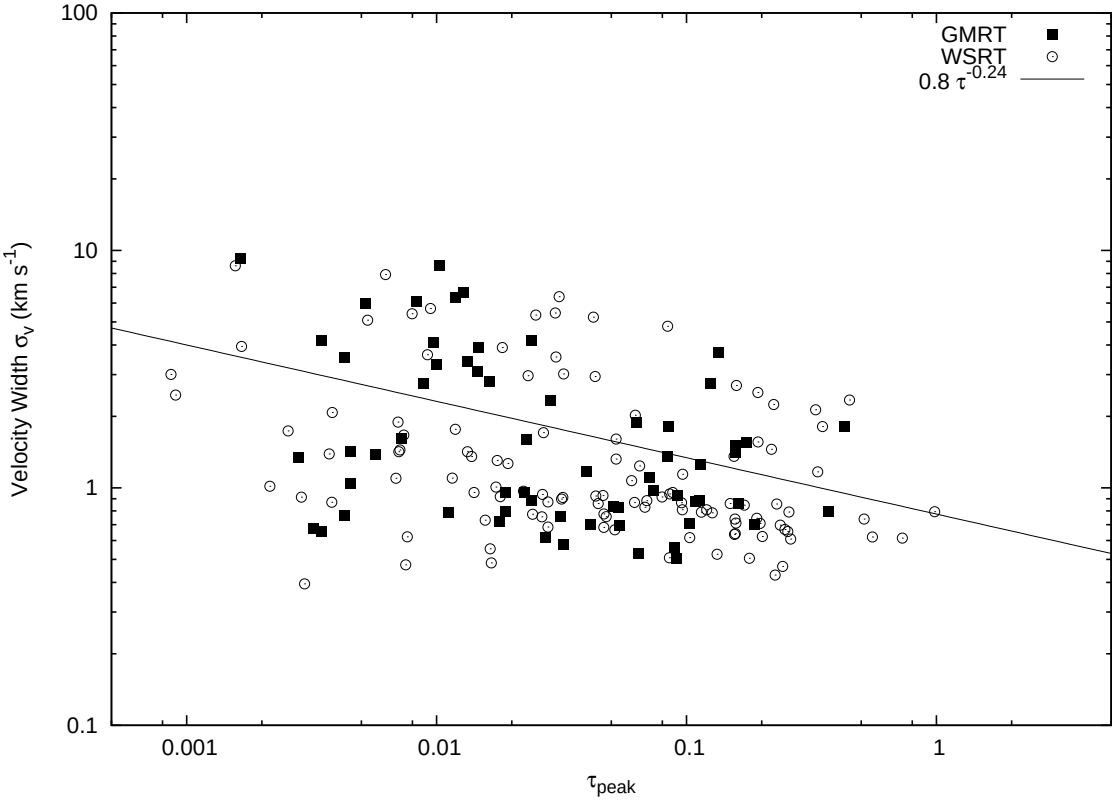

Figure 3.9: Correlation between peak optical depth and velocity width. The line is the best fit power law showing that the velocity width scales as $\tau_{\rm peak}^{-0.24}$.

cannot be ruled out completely.

Using the spin temperature derived from the power law scaling of the non-thermal line width, the fraction of gas in different thermal phases was recomputed (see Table 3.2). It is found that $\sim 49 \pm 07\%$ of the total column density is in the stable cold phase ($T_S \leq 500$ K) and the rest of the gas is in the unstable warm phase. No detection of WNM in stable phase is very striking and this can be explained if the typical optical depth for the WNM is below the sensitivity of these observations ($\sim 10^{-3}$ per ~ 0.4 km s^{-1} channel). As mentioned earlier, for $\sim$ 8000 K gas, the 3σ upper limit of N(H I) is 2×10^{20} cm^{-2}. So, for the typical lines of sight with $\sim 10^{21}$ cm^{-2} H I column density, $< 20\%$ of the total gas at warm phase may be missed due

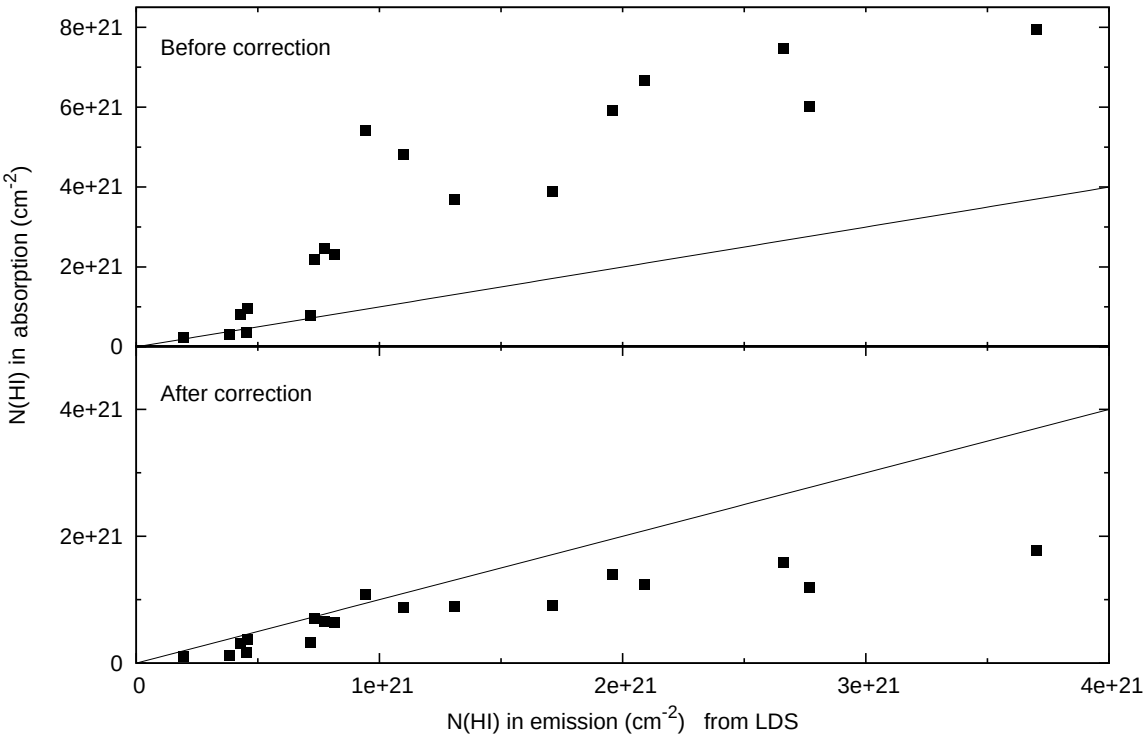

Figure 3.10: Comparing H I column density derived from LDS emission spectra with that inferred from the absorption spectra. The top and bottom panels are results respectively before and after correcting for the non-thermal line widths. The lines represent equal column density detected in absorption and emission.

to the sensitivity limitation.

The T–τ correlation is found to be slightly steeper after the correction and the corrected spin temperature $T_S \propto \tau_{\rm peak}^{-0.57\pm0.08}$. It is noted that a similar correlation between spin temperature $T_{\rm cl}$ and optical depth $\tau_{\rm cl}$, evaluated for each "cloud" at $v_{\rm cl}$, the velocity for which $\tau(v)$ has its maximum, has been reported by Payne et al. (1983). But they have found a significantly shallower power law with power law index -0.34 ± 0.05. A plausible reason for this may be the errors in the correction (over-correction) for non-thermal line width. Another cause for this difference may be that the temperature indicator ($T_{\rm cl}$) that they have used is derived only at the peak

of the component. This may be quite different from T_S, the spin temperature of the component (derived assuming isothermal cloud), or the upper limit of the kinetic temperature T_{Kmax} derived from the observed line width.

3.4 Conclusions

Sensitive H I 21 cm absorption study towards 18 sources was carried out with the GMRT and the WSRT. The observed H I absorption spectra were modelled as a combination of multiple Gaussian components. This is a more sensitive study than the previous single dish H I survey i.e., the millennium Arecibo 21 cm absorption line survey. The interferometric H I absorption spectra are also not affected by issues like stray radiation, self-absorption and inaccurate subtraction of H I emission. Using the sources common to the GMRT/WSRT sample and the Arecibo survey, it is shown that the Arecibo survey measurements have error due to inaccurate subtraction of emission and inaccurate modelling of the spectra with inadequate number of components. Due to higher sensitivity of the present survey, more components with lower optical depth were detected. As a result, the distribution of diffuse H I in different thermal phases, based on the upper limits of the kinetic temperature derived from the line widths, is found to be different from the distribution derived from the Arecibo survey measurements. It is found that more than 80% of neutral gas has T > 500 K and $\sim 65\%$ gas is in warm unstable thermal phase (as opposed to the Arecibo survey results of $\sim 60\%$ with T > 500 K and $\sim 30\%$ warm unstable gas). The observed WNM fraction is more than an order of magnitude higher than the predicted fraction based on steady state model (McKee & Ostriker, 1977). The prediction of the McKee & Ostriker (1977) model, however, refers to gas only on the Galactic plane ($z = 0$) whereas our statistics are based on all values of z.

After correcting for the non-thermal contribution to the line width using the observed power law scaling of non-thermal velocity dispersion with the length scale, it is found that approximately half of the gas is in warm

unstable phase and the rest of the gas is in stable CNM phase (as opposed to the Arecibo survey results of ~ 60, 30 and 10% in CNM, unstable warm and stable warm phase). After the correction, the T$-\tau$ correlation is also found to be significantly steeper than that reported earlier.

Qualitatively, however, these results are consistent with the Arecibo survey results and other recent interferometric studies towards a very limited number of lines of sight, that the a large fraction of the diffuse neutral ISM is in the thermally unstable phase. This is a strong indication of the possibility that the steady state has not been achieved in the diffuse ISM. This may be due to intermittent injection of energy into the medium on a timescale shorter than that required for the WNM phase to reach steady state. The possibility includes supernova-dominant time-dependent models (Gerola et al., 1974), turbulence dominated models with various types of forcing, and models of ISM with stellar energy injection, magnetic field, rotation, self-gravity etc. (Vázquez-Semadeni et al., 2000). Based on numerical simulations, these models suggest the possibility of accommodating a good fraction of gas in the "unstable" phase. There is, however, no detailed modelling and robust quantitative prediction on the fraction of gas in the unstable phase to compare with the observations. In light of these results, it is, hence, a necessary and urgent exercise to check if non-steady state models can explain the observations consistently.

Chapter 4

Magnetohydrodynamic turbulence in supernova remnants

4.1 Introduction

Supernovae and supernova remnants play a very important role in astrophysics at the galactic scale. They cause the heating of the interstellar medium, acceleration of cosmic rays and enrichment of the interstellar medium with heavy elements created in the stellar core or in the supernova explosion. The shock wave traveling through the interstellar medium may also cause the gas clouds to collapse to form new stars. Thus, they work as a link between the gaseous and stellar components of the Galaxy. Based on their large scale structure, supernova remnants are broadly classified into three types: shell-type remnants, filled-centre remnants (or plerions) and composite remnants (Weiler & Sramek, 1988). In addition to the large scale shell-like or filled-centre structures, all these remnants show a very rich and complicated structure over a wide range of scale and frequency of observation.

Although there have been many high resolution and high sensitivity multiwavelength observations of Galactic supernova remnants, there has

not been, to the best of our knowledge, any systematic study to quantify the fine scale structure. Here we present 6 and 20 cm observations and estimates of the angular power spectra of the intensity fluctuation over a wide range of angular scales for the supernova remnants Cas A and the Crab Nebula.

The Crab Nebula (G184.6−5.8) is a supernova remnant in the constellation of Taurus in the third Galactic quadrant. It is a filled-centre nebula, $7' \times 5'$ in size (van den Bergh, 1970) at a distance of approximately 2 kpc (Trimble, 1973). The remnant is of the famous supernova of 1054 AD and the Crab pulsar is observed to be at the centre of this nebula. At radio wavelengths the source is quite strong with a flux density of 1040 Jy at 1 GHz and, beside its filled centre structure, shows faint jet or tube like extension from the north edge of the remnant. Cassiopeia A or Cas A (G111.7−2.1) is in the constellation Cassiopeia in the second Galactic quadrant. This is a shell type supernova remnant of diameter $5'$ at a distance of approximately 3.4 kpc (Reed et al., 1995). The shell thickness estimated from the radial brightness profile at radio wavelengths is found to be approximately $30''$. At these wavelengths, it shows a clear shell like structure with compact emission knots and is one of the strongest radio sources in the sky with a flux density of 2720 Jy at 1 GHz. It is most probably the remnant of a late 17th century supernova (Fesen et al., 2006). There is some spectroscopic evidence that Cas A was a type IIb supernova (Krause et al., 2008). More details of both these supernova remnants can be found in the Galactic supernova remnants catalogue (Green, 2004)[1].

At radio wavelengths, the dominant contribution to the supernova remnants' emission comes from the synchrotron radiation emitted by the relativistic electrons in the presence of magnetic fields. The observed structures over a wide range of scales are most probably a result of the magnetohydrodynamic turbulence in the emitting plasma. Since the synchrotron radiation intensity fluctuation will depend on fluctuation of both density and magnetic field strength, it is expected that the power spectrum will re-

[1]See http://www.mrao.cam.ac.uk/surveys/snrs/ for an updated version.

veal interesting information on the density and magnetic field fluctuations as well as on the nature of the turbulence in the plasma.

We present, here, the estimates of the power spectrum obtained directly from the interferometric measurements of the visibility function of the sources. The analysis technique is briefly described in §4.2. In §4.3, we present the details of the observational data and the results. Finally, we summarize and present our conclusions in §4.4.

4.2 Analysis technique

Assuming that the angular extent of the source is small, the angular power spectrum, $P(u,v)$, of the intensity fluctuation of synchrotron radiation $\delta I(l,m)$ can be written as

$$P(u,v) = \int\int \xi(l,m) e^{-2\pi i(ul+vm)} dldm \tag{4.1}$$

where (l,m) are coordinates in the sky plane, (u,v) are coordinates in the telescope plane (with dimension of inverse angular separation) and ξ is the autocorrelation function of the intensity fluctuation

$$\xi(l-l', m-m') = \langle \delta I(l,m) \delta I(l',m') \rangle. \tag{4.2}$$

Here the angular brackets imply an average across different positions and directions on the sky. If the angular extent of the source is not small enough then, instead of taking the Fourier transform, a spherical harmonic decomposition of the autocorrelation function is to be done to get the angular power spectrum. Throughout this analysis, it is assumed that the angular size of the source is small and the statistical properties of the small scale intensity fluctuations are homogeneous and isotropic. Hence, the intensity fluctuation power spectrum $P(u,v)$ is a function of the magnitude $U = \sqrt{u^2+v^2}$ only and is independent of the direction.

Since the complex visibility function $V(u,v)$ measured by an interferometer is the Fourier transform of the source brightness distribution $I(l,m)$,

$$V_s(u,v) = \int\int I(l,m) e^{-2\pi i(ul+vm)} dldm \tag{4.3}$$

where (u, v) is the baseline or the projected antenna separation in units of the wavelength of observation and is associated with an inverse angular scale, one can estimate the angular power spectrum directly from the measured visibility function. It can be easily shown that the squared modulus of the visibility is a direct estimator of the intensity fluctuation power spectrum

$$P(u, v) = \langle V_s(u, v) V_s^*(u, v) \rangle \tag{4.4}$$

where the angular brackets denote an average over all possible orientations of the baselines.

This method for estimating the power spectrum from the complex visibility function has been used earlier by Crovisier & Dickey (1983) and Green (1993). The technique of direct visibility based estimation of power spectrum has also been used and discussed in literature in various contexts like the analysis of interferometric observations of the Cosmic Microwave Background Radiation (e.g. Hobson et al., 1995), the large-scale H I distribution at high redshifts (Bharadwaj & Sethi, 2001) and the interferometric H I observations to detect the epoch of reionization (Morales & Hewitt, 2004; Bharadwaj & Ali, 2005). Technical issues like the effect of a window function corresponding to the size of the source on the power spectrum estimator and the method of avoiding the noise bias by correlating the visibilities at two different baselines are described in detail in Begum et al. (2006). The actual algorithm of estimating the power spectrum from the measured visibility function is outlined in Dutta et al. (2008). A similar algorithm, slightly modified to further reduce the noise bias, is used for the present work. To minimize the contribution of correlated noise power to the power spectrum estimator, we have correlated visibilities at two different baselines with slightly different time-stamp for which the noise is expected to be uncorrelated. Begum et al. (2006) have shown that the real part of the measured visibility correlation directly estimates the power spectrum at long baselines compared to the inverse angular size of the source, and at short baselines the true power spectrum is convolved with the window function. The error of the power spectrum is estimated

Table 4.1: Details of the VLA and the GMRT data

Source	Wavelength	Array	Project	Date of observation
The VLA archival data:				
Cas A	6 cm	A	AR0435	09 Dec., 2000
Cas A	6 cm	A	AR0435	10 Dec., 2000
Cas A	6 cm	B	AR0435	25 Mar., 2001
Cas A	6 cm	B	AR0435	29 Apr., 2001
Cas A	6 cm	C	AR0435	25 Apr., 2000
Cas A	6 cm	D	AR0435	07 Sep., 2000
Crab	6 cm	A	AH0337	19 Oct., 1988
Crab	6 cm	A	AH0337	08 Nov., 1988
Crab	6 cm	B	AB0876	09 Aug., 1998
Crab	6 cm	C	AB0876	27 Jan., 1999
Crab	6 cm	D	AH0625	19 Nov., 1997
The GMRT data:				
Cas A	20 cm	–	11NRb02	03 Dec., 2006

accounting for both the noise in the measured visibility function and the finite number of independent estimates of the true power spectrum (cosmic variance).

4.3 Data and Results

4.3.1 Summary of the data

The Giant Metrewave Radio Telescope (GMRT; Swarup et al., 1991) L-band (20 cm) receiver was used to observe the supernova remnant Cas A. The unique hybrid array configuration of the GMRT allows one to probe structures on both large and small angular scale in a single observation. Scans on standard calibrators were used for flux calibration, phase calibration and also to determine the bandpass shape. The Very Large Array (VLA)

archival C-band (6 cm) data are also used for both the supernova remnant Cas A and Crab Nebula. A summary, including the observation band, the telescope array configuration, the original programme code and the dates of observation, of the GMRT and the VLA data used for this work is given in Table (4.1). Data analysis was carried out using standard AIPS. After flagging out bad data, the flux density scale and instrumental phase were calibrated. The calibrated visibility data of the target sources were then used to estimate the angular power spectra and the errors.

4.3.2 Results for the Crab Nebula and Cas A

For the Crab Nebula, the angular power spectrum as a function of inverse angular scale is found to be a power law with an index of -3.24 ± 0.03. Since the effect of the convolution with a window function is more significant on the shorter baselines, the power law index is extracted by fitting the power spectra in the longer baseline range of $6 - 60$ kλ. Figure (4.1) shows the spectra derived from the VLA 6 cm observation with different array configuration and at two different "intermediate frequencies" (IFs) . The best fit power law, with an offset introduced in amplitude for clarity, is also shown in the same figure. The four panels in Figure (4.2) show the power spectra with $\pm 1\sigma$ errorbars derived using the data from different VLA array configuration and IFs. The noise in the measured visibility function dominates at long baselines whereas cosmic variance is the significant source of error at small baselines. It is clear from these figures that for a wide range of scales (about $1 - 100$ kλ which corresponds to an angular scale of $2.5 - 250$ arcsec), the intensity fluctuation angular power spectra is a power law function of inverse angular scale. The power spectra derived using data from different array configurations and different IFs are in very good agreement.

The power spectrum for Cas A is also found to be a power law with a similar power law index at small angular scales. But, as shown in Figure (4.3), there is a break in the spectrum at about 10.6 kλ (~ 25 arcsec) and the power law index changes significantly at smaller U. The best fit power

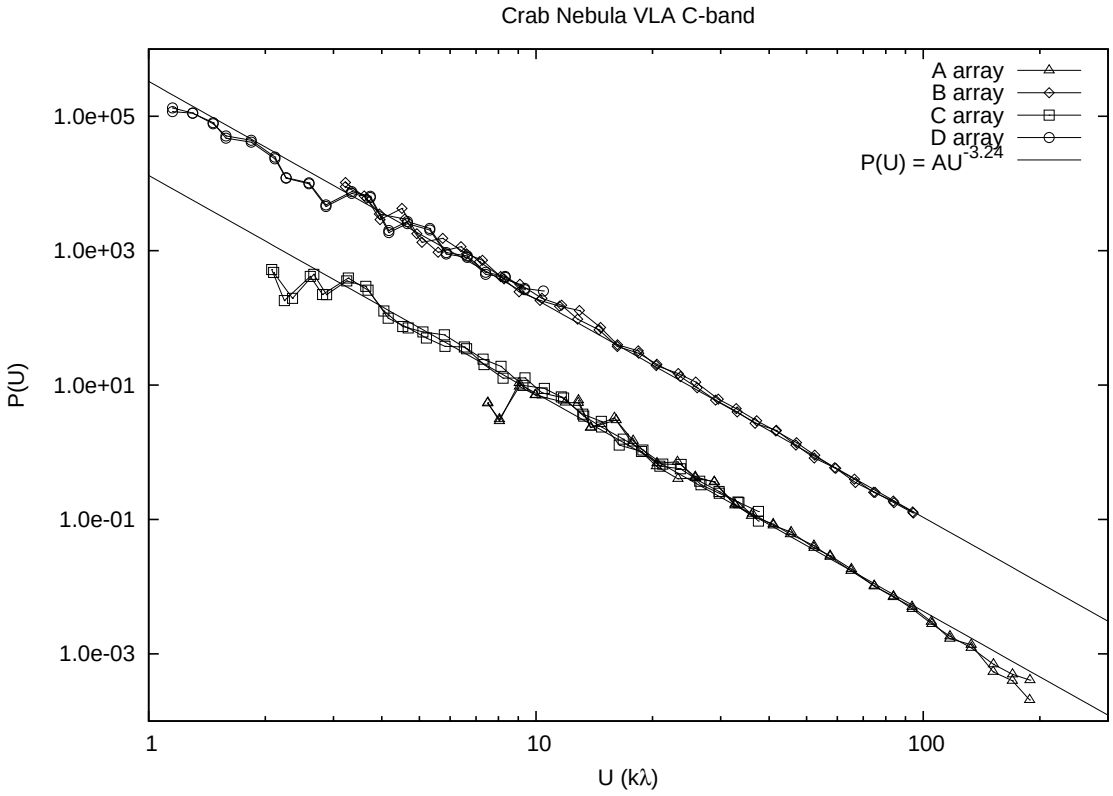

Figure 4.1: Intensity fluctuation power spectra for the Crab Nebula. The data points are from the VLA 6 cm (C-band) observation with different array configurations and at two different IFs. The line is the best fit power law with the power law index of -3.24. Data from different array configuration and the best fit power law are shown here with an offset in amplitude for clarity.

law function for the power spectrum derived from the GMRT 20 cm data has a power law index of -2.22 ± 0.03 in the shorter baseline range ($1.6 - 10$ kλ). After the break, the index changes to -3.23 ± 0.09 (estimated from the range $11 - 30$ kλ) and the power spectrum retains this index all the way up to the smallest angular scale (~ 5 arcsec) probed in this observation. These results for Cas A are consistent with the power spectra derived from the VLA 6 cm archival data of Cas A. The 6 cm power spectrum is also a broken power law with the same power law index and the break at the same angular scale as in the 20 cm power spectrum. The VLA 6 cm power

spectra obtained using data from different array configurations and two different IFs are plotted in Figure (4.4). This shows that the steeper power law at the long baseline range is in fact extended upto 100 kλ (~ 2.5 arcsec). The four panels in Figure (4.5) show the power spectra with $\pm 1\sigma$ errorbars derived using the data from four different VLA array configuration and two IFs. Clearly, for Cas A also, the power spectra derived from 20 cm and 6 cm data with different array configurations and different IFs are in good agreement.

4.3.3 Interpretation of the results

The power law index of the steeper part of the Cas A angular power spectrum is consistent, within measurement errors, with the power law index of the Crab Nebula power spectrum. The break in the Cas A power spectrum and the change of the power law index at small baseline range (or large angular scale) is very interesting. We have analytically verified that the shell type geometry of Cas A will affect the power spectrum significantly only at very small U by convolving it with a window function which is the Fourier transform of the two dimensional projection of this optically thin shell. The same is also true for the optically thin spherical geometry of the Crab Nebula. For the long baseline range around 10 kλ, the effect will be negligible and cannot explain the sharp break and change of power law index by ~ 1.

It appears that a plausible explanation is a transition from three dimensional at small scales ($U > 10$ kλ) to two dimensional turbulence at large scales ($U < 10$ kλ). The shell thickness sets the angular scale of the transition. On length scales smaller than the shell thickness, the shell can have modes of perturbation in all three independent directions. But on length scales larger than the shell thickness, there will be no modes perpendicular to the shell thickness. This results in the three dimensional turbulence being effectively transformed to a two dimensional turbulence and hence the power law index changes by 1. This change in slope might be related to the change in the slope of the velocity power spectrum from $-11/3$ to

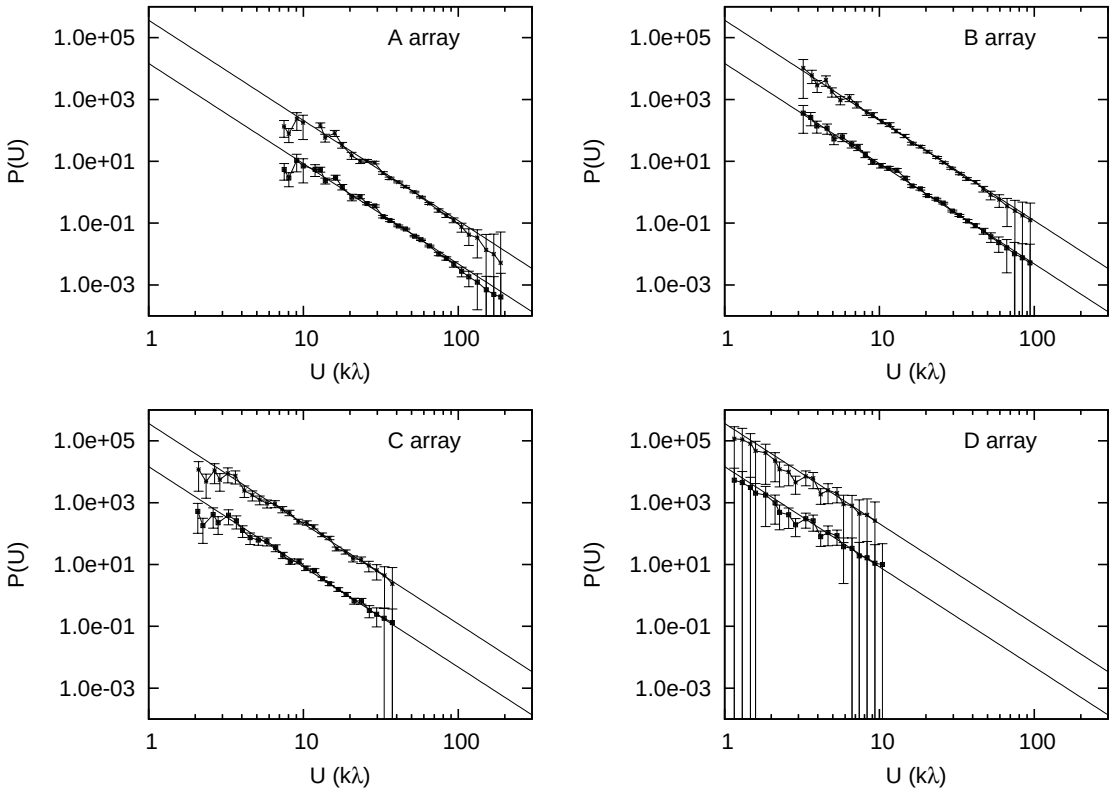

Figure 4.2: Intensity fluctuation power spectra with $\pm 1\sigma$ errorbars for the Crab Nebula. The VLA 6 cm (C-band) power spectra derived from the observation with different array configurations are shown in different panels. Results from two different IFs are plotted in the same panel with an offset in amplitude. The line is same as in Figure (4.1).

$-8/3$ in going from 3D to 2D for incompressible, Kolmogorov turbulence (Kolmogorov, 1941). The density power spectrum is predicted to follow the velocity power spectrum in the Goldreich & Sridhar (1995) model of MHD turbulence. The observation, that the angular scale of this break matches approximately with the shell thickness, is indicative of the consistency of this picture. A similar difference of ≈ 1 in the power law index has also been observed and interpreted as a transition from three dimensional turbulence to two dimensional turbulence in the power spectrum of H I 21 cm emission intensity fluctuations of the Large Magellanic Cloud (Elmegreen

et al., 2001) and the galaxy NGC 628 (Dutta et al., 2008).

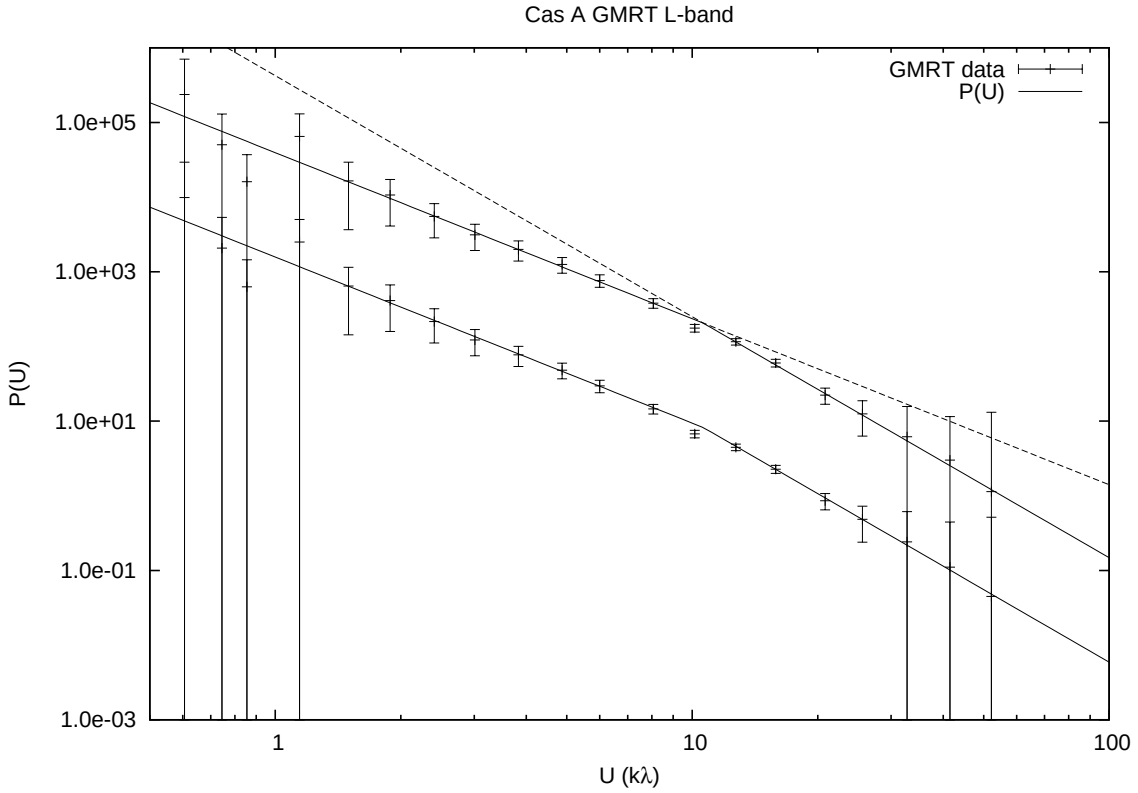

Figure 4.3: Intensity fluctuation power spectra for the supernova remnant Cas A. The points with $\pm 1\sigma$ errorbars are from the GMRT 20 cm (L-band) data with two different observation frequencies. The line is showing the best fit power law with power law index of -2.22 and -3.23 before and after the break (at 10.6 kλ) respectively. Power spectra derived from different frequency ranges and the best fit function are plotted with an offset in amplitude.

The scale-free nature of the power spectra over a wide range of scales and a similar value of the power law index for power spectra of two different types of supernova remnants suggests the universality of the physical process responsible for the observed intensity fluctuations. We propose that the fluctuation is most probably due to turbulence in the synchrotron emitting plasma that gives rise to the power law spectrum. The interaction of the propagating shock with the turbulent interstellar medium is

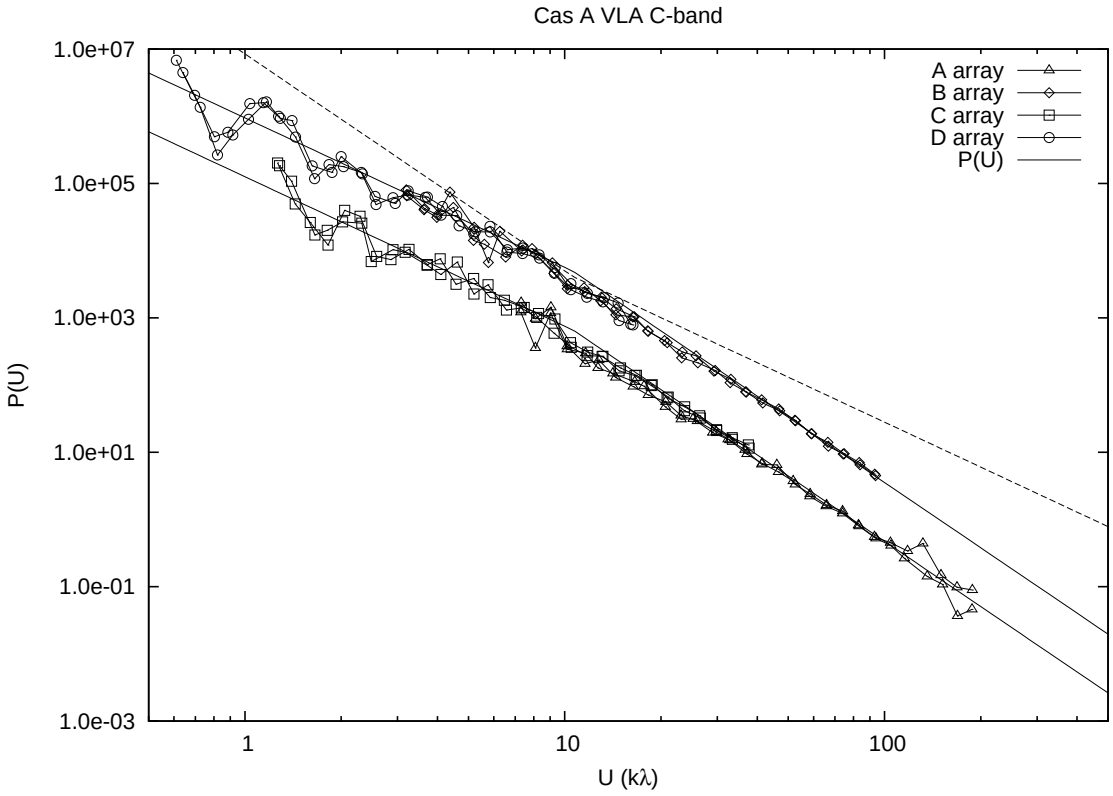

Figure 4.4: Intensity fluctuation power spectra for Cas A. The data points are from the VLA 6 cm (C-band) observation with different array configurations and at two different IFs. The line is the best fit function as in Figure (4.3). Data from different array configuration and the best fit function are shown here with an offset in amplitude.

known to enhance the turbulence in the postshock region and cause the spatial variation of emission in supernova remnants (Balsara et al., 2001). We investigate here whether the observed power spectrum $P(k) \propto k^{-3.2}$ (where k is the magnitude of the wave vector), or equivalently the energy spectrum $E(k) = k^2 P(k) \propto k^{-1.2}$, is consistent with our present understanding of astrophysical turbulence. The observed intensity fluctuation power spectrum is related to the density and magnetic field power spectra which, in turn, are found, from numerical simulations, to closely follow the velocity fluctuation power spectra. For incompressible and nonmagnetized

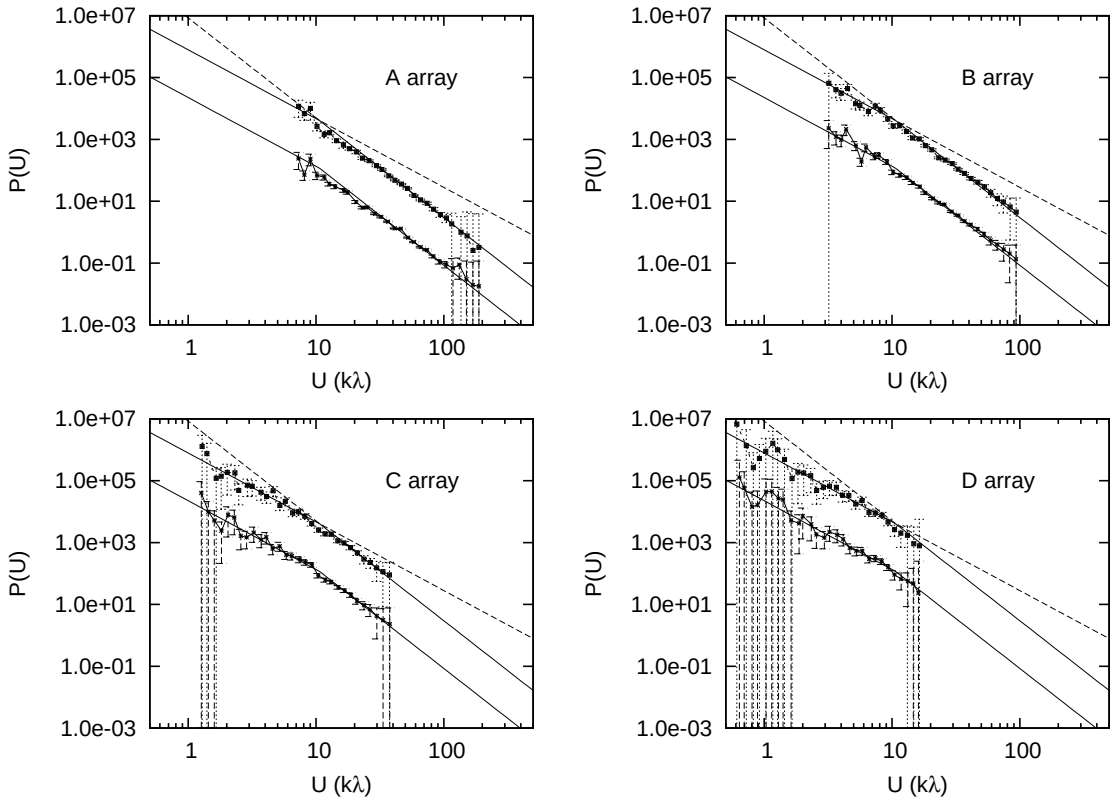

Figure 4.5: Intensity fluctuation power spectra with $\pm 1\sigma$ errorbars for Cas A. The VLA 6 cm (C-band) power spectra derived from the observation with different array configurations are shown in different panels. Results from two different IFs are plotted in the same panel with an offset in amplitude. The line is same as in Figure (4.3).

turbulence, Kolmogorov theory suggests an isotropic power law velocity fluctuation energy spectrum $E_v(k) \propto k^{-5/3}$ (Kolmogorov, 1941). Irosnikov (1964) and Kraichna (1965) gave a model of magnetic incompressible turbulence (IK theory) that predicts, even in the presence of magnetic fields, an isotropic power law energy spectra $E(k) \propto k^{-3/2}$ for both velocity and magnetic field. Without assuming an isotropic energy distribution, Goldreich & Sridhar (1995) proposed a model of incompressible magnetohydrodynamic turbulence that predicts a Kolmogorov-like energy spectrum $E_v(k_\perp) \propto k_\perp^{-5/3}$ where $k_\perp$ is the component of the wave vector perpendicular

to the local magnetic field direction. It also predicts an anisotropy condition $k_{\parallel} \propto k_{\perp}^{2/3}$ where $k_{\parallel}$ is the component of the wave vector parallel to the local magnetic field direction. But, even if there is anisotropy in the system of reference defined by the local magnetic field, it is worth keeping in mind that there will only be moderate anisotropy in the observer's reference.

For compressible magnetohydrodynamics turbulence, there is, unfortunately, no widely-accepted theory and much of the present understanding has come from numerical results. Recent numerical simulation indicates that, for compressible magnetohydrodynamic turbulence, both the velocity and magnetic field energy spectra and anisotropy in Alfvén modes and slow modes are as predicted by Goldreich & Sridhar (1995). But the energy spectra for fast modes are isotropic and the scaling is as predicted in IK theory (Cho & Lazarian, 2002b). It is also found that, in the case of incompressible magnetic turbulence, viscous damping on scales larger than the magnetic diffusion scale can make the magnetic energy spectrum significantly less steep. Cho et al. (2002) report a magnetic energy spectrum of the form $E_b(k) \propto k^{-1}$ implying a rich structure of magnetic fields on small scales.

The synchrotron emissivity $i_s \propto n_e |B_{\perp}|^{(p+1)/2}$ where n_e is the electron number density, $B_{\perp}$ is the magnetic field component perpendicular to the line of sight and the typical value of the power law index p of electron energy distribution in supernova remnants is about 2 (Green, 1991). One dimensional numerical analysis suggests that if the magnetic field power spectrum is a power law, then $|B|^{(p+1)/2}$ will also have a power law spectrum with the same index for the values of p in the range of our interest. But, because of this nonlinearity, in general it is not straightforward to derive the magnetic field fluctuation power spectrum from the intensity fluctuation power spectrum. It is also not necessarily true that the density distribution and magnetic field are strongly coupled. Numerical simulations and analytical studies, in fact, suggest that in compressible magnetohydrodynamic turbulence, the magnetic field strength and density are only weakly correlated (Passot & Vázquez-Semadeni, 2003). Beresnyak et al. (2005)

also report a flat and isotropic density spectrum from numerical simulation of supersonic magnetohydrodynamic turbulence. But, if the electron density distribution smoothly follows the magnetic field inhomogeneities in the supernova remnants, the synchrotron intensity fluctuation power spectrum is directly related to the magnetic field power spectrum. In this condition, following the analysis of Deshpande et al. (2000), one can conclude that if the intensity fluctuation has a power law spectrum then the magnetic field fluctuation will also have a power law spectrum with the same power law index, provided that the magnetic field perturbation amplitude is small. The effect of the nonlinear law of synchrotron emission on the power spectrum is not clear in situations when the perturbation amplitude is high or correlation between the magnetic field strength and density is weak.

The observed intensity fluctuation power spectrum is somewhat shallower than the expected spectrum of the magnetic field. From the above discussion, one can identify three plausible reasons for this discrepancy. They are (i) viscous damping on scales larger than the magnetic diffusion scale, (ii) weak or no correlation between the magnetic field and the density distribution and (iii) large amplitude of magnetic field perturbation which may affect via the nonlinearity of synchrotron emissivity.

Interestingly, numerical, observational and theoretical studies of synchrotron emission fluctuations are carried out in a completely different context to understand the effect of the Galactic foreground emission on the angular power spectrum of the cosmic microwave background (see Cho & Lazarian, 2002a, and references therein for details) and in some of the cases the intensity fluctuations are attributed to turbulence (Chepurnov, 1998; Tegmark et al., 2000; Cho & Lazarian, 2002a). Though in a very different range of angular scale, the energy spectrum of the Galactic synchrotron foreground is found to be a range of power laws with power law index ~ -1 for higher latitudes (Cho & Lazarian, 2002a, and references therein). This is less steep than the expected $k^{-5/3}$ energy spectrum of the magnetic field. Clearly, a similar discrepancy is evident in this case also.

But, in spite of this discrepancy, one can say that the near-Kolmogorov power law power spectrum is broadly consistent with our present understanding of the magnetohydrodynamic turbulence.

4.4 Conclusions

We have analysed the data from GMRT 20 cm and VLA 6 cm observations of two supernova remnants Cas A and Crab Nebula and estimated the angular power spectra of the synchrotron radiation intensity fluctuation over a wide range of angular scales. We report, for the first time, a power law power spectrum of the synchrotron radiation intensity fluctuations in supernova remnants. The power law index is found to be -3.24 ± 0.03 for both these sources with very different large scale morphology. For Cas A, there is a break in the power spectrum and the power law index changes from -3.2 to -2.2 at angular scale larger than the size of the shell thickness. This change is a result of the anisotropy of the perturbation at length scales larger than the shell thickness. This power law power spectrum is consistent with our present understanding of the magnetohydrodynamic turbulence derived mostly from existing numerical simulation results.

Chapter 5

H I opacity fluctuations towards Cassiopeia A

5.1 Introduction

It is now well established that the H I 21 cm opacity in the Galaxy shows measurable small scale structure. VLBI observations show opacity fluctuations on angular scales as small as 20 milli arc seconds corresponding to a projected separation ~ 10 AU, if one assumes that the opacity variations occur in a thin screen (Brogan et al., 2005). Similarly, multi-epoch observations of some high velocity pulsars show evidence for H I 21 cm opacity variation on scales of 5 - 100 AU (Frail et al., 1994). Several other pulsars however do not show opacity variations (Johnston et al., 2003), leading to suggestions that the occurrence of fine scale structure in the galaxy may be rare. Much of these observed fluctuations on AU scales were earlier believed to be originating from H I "clouds" which are small scale physical structures with densities $\sim 10^4 - 10^5$ cm^{-3}. It was hard to explain the existence of these structures in equilibrium with other orders of magnitude lower density components of the diffuse ISM. Deshpande (2000) has recently shown that the observed small scale transverse variations have contributions from structure on all scales and the fluctuations at larger scales may account for the measured small scale fluctuations.

On the other hand, there are some observational and numerical simulation results supporting the existence of tiny scale structures (e.g. Braun & Kanekar, 2005; Vázquez-Semadeni et al., 2006; Hennebelle & Audit, 2007). With an evaporation timescale of ~ 1 Myr, these structures can survive if either the ambient pressure is much higher or they are formed continuously with a comparable timescale. The detail of their origin and physical properties are, however, still unknown.

On somewhat larger scales, Deshpande et al. (2000) measured the opacity variations of the absorption across Cassiopeia A and Cygnus A, and found that the power spectrum of these fluctuations could be fairly well represented by a power law. The index of the power law was similar for the absorption in the Perseus arm and the Outer arm, but substantially different from that of the Local arm opacity fluctuation power spectrum.

The scale free behavior of fluctuation power spectra of a variety of tracers (H I 21 cm emission intensity, dust emission) is the main observational evidence for the existence of turbulence in the atomic interstellar medium (ISM). The slope of the power law of H I 21 cm emission and absorption in our own Galaxy, H I 21 cm emission from the Large Magellanic Cloud, the Small Magellanic Cloud and DDO 210 are all ~ -3 (Crovisier & Dickey, 1983; Green, 1993; Stanimirović et al., 1999; Elmegreen et al., 2001; Begum et al., 2006). Recently Dutta et al. (2009a,b) have reported that the H I 21 cm intensity fluctuation power spectra for a sample of dwarf and nearby spiral galaxies have a power law index of ~ -2.6 and ~ -1.5 on scales respectively smaller and larger than the scale height of the galaxy disk. This is interpreted as the effect of a transition from three dimensional to two dimensional turbulence at scales larger than the disk thickness. The observed fractal structure of H I in several dwarf galaxies in the M 81 group is also consistent with the self-similar hierarchical structure of the turbulent ISM without any preferred length scale (Westpfahl et al., 1999).

On the theoretical side, fine scale structure in the neutral gas is naturally expected in turbulent models of the ISM. The fluctuations in the H I 21 cm opacity in a particular velocity range depend on the fluctuations in

the density, spin temperature and velocity of the gas. Deshpande et al. (2000) show that, in the case of small fluctuations of density, the dependence on temperature is small. Turbulence however, gives rise to fluctuations in both the density and velocity of the gas and both of these contribute to the observed opacity fluctuations. Lazarian & Pogosyan (2000) show that the slope of the observed power spectrum changes depending on whether the H I 21 cm emission is averaged over a velocity range that is large ("thick slices") or small ("thin slices") compared to the turbulent velocity dispersion. Observations with high enough spectral resolution can hence disentangle the statistical properties of the velocity and the density fluctuations.

There have been many studies of the ISM towards Cassiopeia A using the H I 21 cm absorption (e.g. Clark et al., 1962; Clark, 1965; Schwarz et al., 1986; Bieging et al., 1991) and a variety of other tracers like H_2CO and OH (Goss et al., 1984; Bieging & Crutcher, 1986) revealing the small scale structure. A recently developed formalism for statistically robust extraction of the fluctuation power spectrum from interferometric data is used here to re-examine the issue and to constrain the H I 21 cm opacity fluctuation power spectrum towards Cas A. In essence, since the visibilities measured by an interferometer are already samples in Fourier space, we use a second order visibility statistic (the correlation between adjacent visibilities) to estimate the power spectrum. This method is particularly useful because one can completely avoid the complications of deconvolution and imaging the strong background source. We note that the opacity power spectrum towards Cas A has been obtained earlier by Deshpande et al. (2000). They used the data from the Very Large Array B, C and D configurations but with only 18 antennas in each configuration because of software restrictions. However, estimating the power spectrum using the visibility based formalism for the same line of sight will allow us to compare the results from two very different methods to cross-check different techniques. We also plan to apply this simpler visibility based method to estimate the power spectra for other lines of sight to derive a more com-

plete understanding of the density and velocity fluctuations in the ISM. The analysis technique used here is briefly described below in §5.2. In §5.3, the details of the observational data and the results are given. Finally, we summarize and present our conclusions in §5.4.

5.2 Analysis technique

As mentioned in Chapter 4, since the complex visibility function $V(u,v)$ measured by an interferometer is the Fourier transform of the brightness distribution $S(l,m)$, one can estimate the angular power spectrum directly from the measured visibility function. It can be easily shown that the squared modulus of the visibility is a direct estimator of the intensity fluctuation power spectrum. For a detailed discussion on the actual algorithm to estimate the power spectrum from the visibility function and on technical issues including the effect of the window function (corresponding to the source size), the method of avoiding the noise bias, the method of estimating the errors of the power spectra etc., see Section 4.2 and references therein.

In the case of H I absorption measurement towards extended source, if the continuum background source intensity is $I_c(l,m)$ then, for the channels with H I absorption, the signal is

$$S(l,m) = I_c(l,m)e^{-\tau(l,m)} \tag{5.1}$$

where $\tau(l,m)$ is the H I optical depth. As $I_c(l,m)$ and $\tau(l,m)$ are not correlated, we can write

$$\xi_S = \langle I_c(l,m)I_c(l',m')\rangle \times \langle e^{-\tau(l,m)}e^{-\tau(l',m')}\rangle. \tag{5.2}$$

Both $I_c(l,m)$ and $\tau(l,m)$ can be decomposed into the sum of a constant average value and the fluctuation around that value (as a function of l,m)

$$\begin{aligned} I_c(l,m) &= I_c^0 + \delta I_c(l,m) \\ \tau(l,m) &= \tau^0 + \delta\tau(l,m) \end{aligned} \tag{5.3}$$

and hence Equation (5.2) can be re-written as

$$\xi_S = (I_c^{0\,2} + \xi_{I_c}) \times e^{-2\tau^0} \langle e^{-\delta\tau(l,m)} e^{-\delta\tau(l',m')} \rangle \tag{5.4}$$

where ξ_{I_c} is the autocorrelation function of continuum intensity fluctuation

$$\xi_{I_c}(l - l', m - m') = \langle \delta I_c(l,m) \delta I_c(l',m') \rangle. \tag{5.5}$$

If $\delta\tau$ is Gaussian random variable then the autocorrelation function $\xi(e^{-\delta\tau}, e^{-\delta\tau'})$ can be written as

$$\langle e^{-\delta\tau} e^{-\delta\tau'} \rangle = \langle e^{-(\delta\tau+\delta\tau')} \rangle = \exp\left(-\mu_{\delta\tau+\delta\tau'} + \sigma^2_{\delta\tau+\delta\tau'}/2\right) \tag{5.6}$$

where $\mu_{\delta\tau+\delta\tau'}$ and $\sigma_{\delta\tau+\delta\tau'}$ are the mean and the variance of the distribution of $(\delta\tau + \delta\tau')$. Since, both $\delta\tau$ and $\delta\tau'$ are Gaussian random variable with $\mu = 0$ and $\sigma = \sigma_\tau$, $\mu_{\delta\tau+\delta\tau'} = 0$ and $\sigma^2_{\delta\tau+\delta\tau'} = 2(\sigma^2_\tau + \langle \delta\tau\delta\tau' \rangle)$. So, $\xi(e^{-\delta\tau}, e^{-\delta\tau'})$ can be reduced to

$$\langle e^{-\delta\tau} e^{-\delta\tau'} \rangle = \exp\left(\sigma^2_\tau + \langle \delta\tau\delta\tau' \rangle\right) \tag{5.7}$$

where $\langle \delta\tau\delta\tau' \rangle = \xi_\tau$ is the opacity autocorrelation function. The power spectrum measured from the frequency channels with H I absorption signal can be written as

$$P_S = \mathcal{F}\{\xi_S\} = e^{-2\tau^0+\sigma^2_\tau}(I_c^{0\,2} + P_{I_c}) \otimes \mathcal{F}\{e^{\xi_\tau}\} \tag{5.8}$$

where $P_{I_c} = \mathcal{F}\{\xi_{I_c}\}$ is the power spectrum measured from the frequency channels with the continuum background but without any H I absorption signal. Note that this continuum power spectrum P_{I_c} is already derived from "line-free" channels (see Chapter 4 and Roy et al., 2009, for details). Further, it is possible to estimate the constant part of the specific intensity I_c^0 using independent single dish observations.

If it is assumed that the H I opacity fluctuation $\delta\tau$ has a power law power spectrum given by

$$P_\tau = \mathcal{F}\{\xi_\tau\} = AU^{-\alpha} \tag{5.9}$$

then, given the continuum power spectrum and the value of α, one can predict the power spectrum of intensity fluctuation in the presence of H I

absorption using Equation (5.8). On the other hand, the measured power spectra of intensity fluctuation with and without H I absorption can also be used to numerically constrain the value of α. Here the latter technique is used to derive the H I opacity fluctuation power spectrum from the measured intensity fluctuation power spectra from the frequency channels with and without H I absorption.

5.3 Data and Results

5.3.1 Summary of the data

The Giant Metrewave Radio Telescope (GMRT) L-band (21 cm) receiver was used to observe the H I in absorption towards supernova remnant Cas A. The observation was carried out on December 03, 2006 and the total duration was about 13 hours with on-source time of about 8 hours. VLA calibrator sources 2148+611 and 2355+498 were used for phase calibration. One of the phase calibrators was observed for 3 minutes for every 20 minutes observation of Cas A. A total baseband bandwidth of 0.5 MHz divided into 256 frequency channels centered at 1420.5973 MHz was used for the observation. The spectral resolution of the observation was ~ 0.4 km s^{-1} per channel and the total bandwidth was sufficient to cover the H I 21 cm absorption produced by gas both from the Perseus spiral arm and the solar neighbourhood. Total flux density of the source in different velocity channels plotted in Figure (5.1) for the relevant part of the band clearly shows both these absorption features.

Standard flux calibrators 3C48 and 3C286 were observed for about 20 minutes in every 4 hours during the observation. The frequency switching technique was used to avoid the Galactic H I absorption by changing the frequency by 5 MHz for the scans of these flux calibrators which were also used to determine the bandpass shape. Data analysis was carried out using standard AIPS. After flagging out bad data, the flux density scale, instrumental phase and frequency response were calibrated. The calibrated

visibility data of Cas A were then used to estimate the angular power spectra and the errors.

5.3.2 H I opacity fluctuation power spectrum

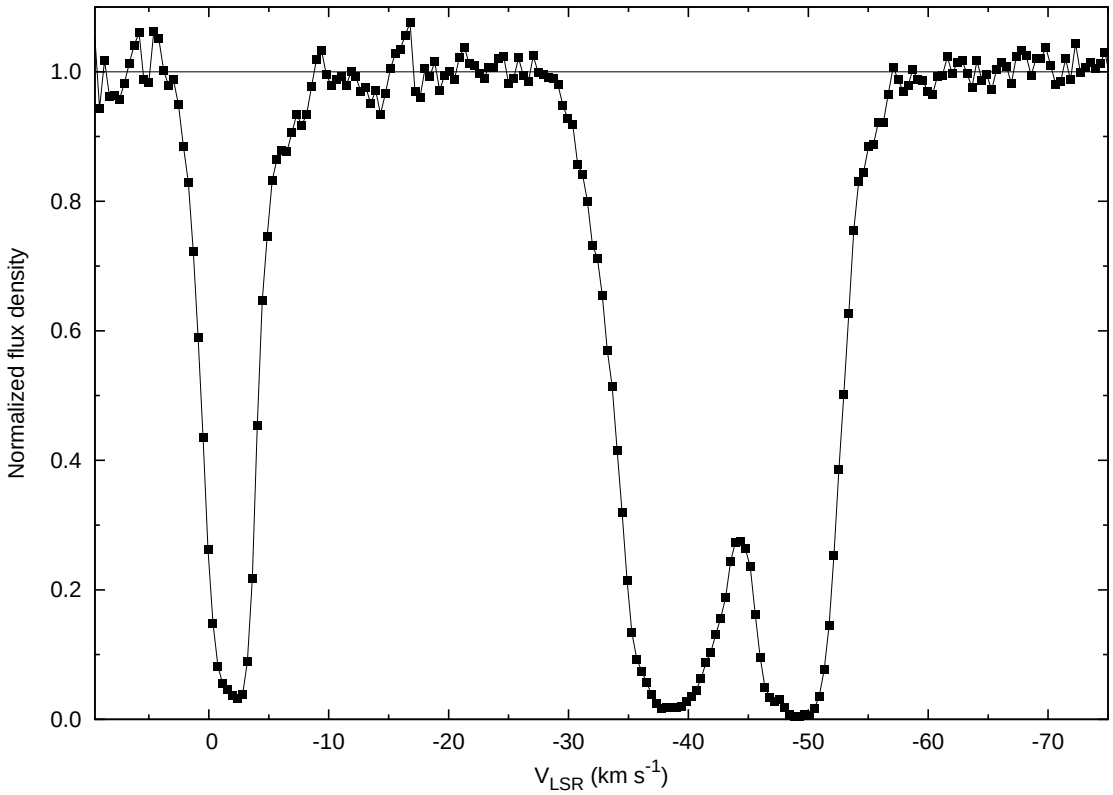

Figure 5.1: Integrated H I 21 cm absorption spectrum towards the supernova remnant Cas A. The continuum corresponds to the total flux density of Cas A. The wide absorption feature at negative LSR velocity is the absorption produced by gas from the Perseus spiral arm and the absorption near zero LSR is from the solar neighbourhood gas.

We have used the best fit broken power law model of continuum intensity fluctuation power spectrum P_{I_c},

$$\begin{aligned} P_{I_c} &= CU^{-2.22} \quad \text{for} \quad U < 10.6 \quad \text{k}\lambda \\ &= 10.6^{1.01} CU^{-3.23} \quad \text{for} \quad U > 10.6 \quad \text{k}\lambda \end{aligned} \tag{5.10}$$

and a scale free power law model of the opacity fluctuation power spectrum P_τ defined in Equation (5.9). The observed power spectrum for individual velocity channels are then used to constrain the value of the power law index of P_τ following standard chi-square minimization technique. As an example case, the data and the best fit model for a single channel with H I absorption is shown in Figure (5.2).

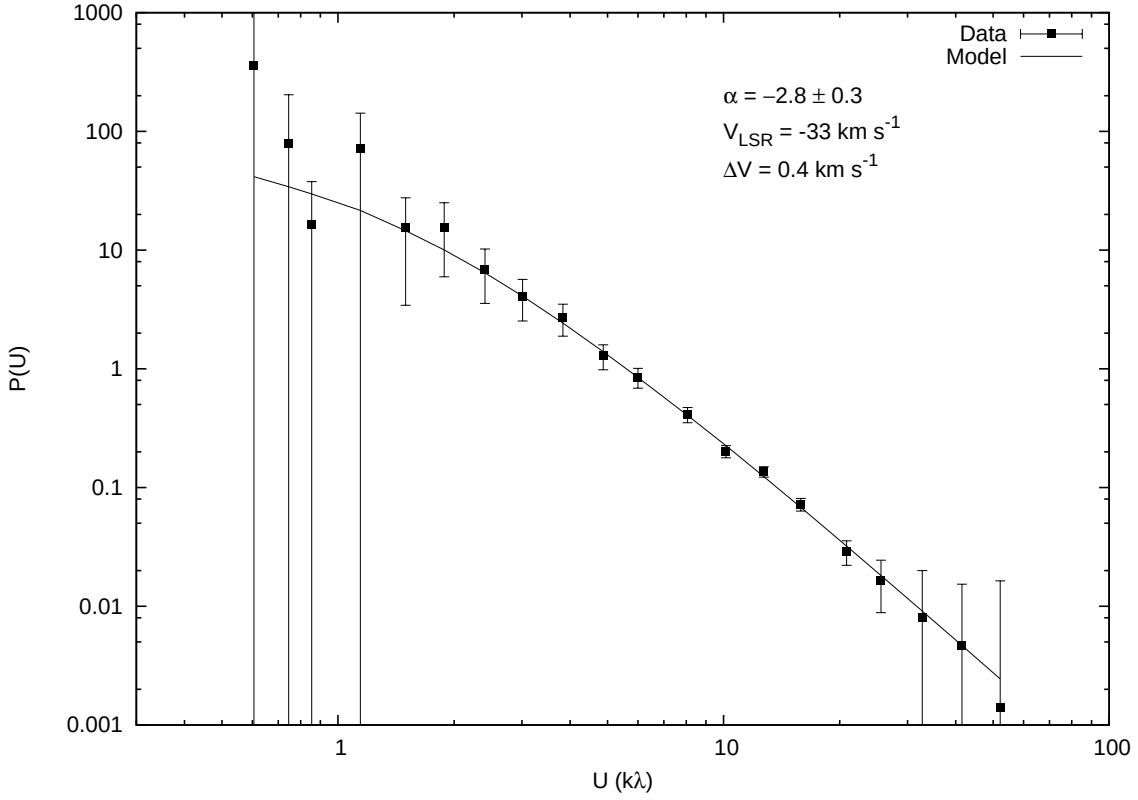

Figure 5.2: Intensity fluctuation power spectrum for a "thin" velocity channel with H I absorption. The absorption in this channel is due to the H I gas in the Perseus arm. The best fit model power spectrum is plotted with the data.

The reduced chi-square values for the best fit model are, however, not close to 1.0 but are about 0.3. We conclude that this is most probably because of an overestimation of the errors. The errors of the power spectrum are estimated to account for both the noise in the measured visibility function and the finite number of independent estimates of the true power

spectrum (cosmic variance). The estimated errors are significantly more than, for example, the variation of the continuum power spectra across velocity channels. This is a very conservative estimate of errors and it may result in a smaller value of the reduced chi-square even when the model represents the observed spectrum quite well. Hence, we have scaled down the errors of the observed spectra so that the reduced chi-square is close to 1.0. The quoted errors of the power law index correspond to a change of the reduced chi-square by $+1$ from its minimum value.

The best fit value of α is found to be $\sim 2.86 \pm 0.30$ for the angular scale of $5 - 250$ arcsec probed in this observation. For a distance of 3 kpc, the corresponding linear scale range is $0.07 - 3.6$ pc. The channel to channel variation of the best fit value of α is, however, much smaller than this error. From independent estimates from different velocity channels, we can constrain the value of α to be $\sim 2.86 \pm 0.10$ (3σ error). There is no significant difference in α between the velocity channels with absorption produced by gas from the Perseus spiral arm and from the solar neighbourhood. Though there is a very weak trend, the change of α for velocity width ranging from $\sim 0.4 - 12.8$ km s^{-1}, as shown in Figure (5.3), is also within the estimation errors. We also note that, if the density fluctuation is small compared to the mean density, then for gas in pressure equilibrium, the slope of the opacity fluctuation power spectrum will be nearly the same as that of the density fluctuation power spectrum (Deshpande et al., 2000).

Our estimate of the power law index for the H I opacity (or equivalently density) fluctuation power spectrum is consistent with the power law index of the power spectra (-2.75 ± 0.25) for the Perseus arm toward Cas A reported by Deshpande et al. (2000) for a very similar range of linear scales. It is also very close to the value (~ -3) reported from the Galactic H I emission observations (Green, 1993) probing the scales of $50 - 200$ pc. This spectrum is significantly shallower than the Kolmogorov spectrum (with power law index of $11/3$) expected from an incompressible turbulent medium (Kolmogorov, 1941). This may be because of the fact that the turbulence in H I is compressible and magnetohydrodynamic in nature (see

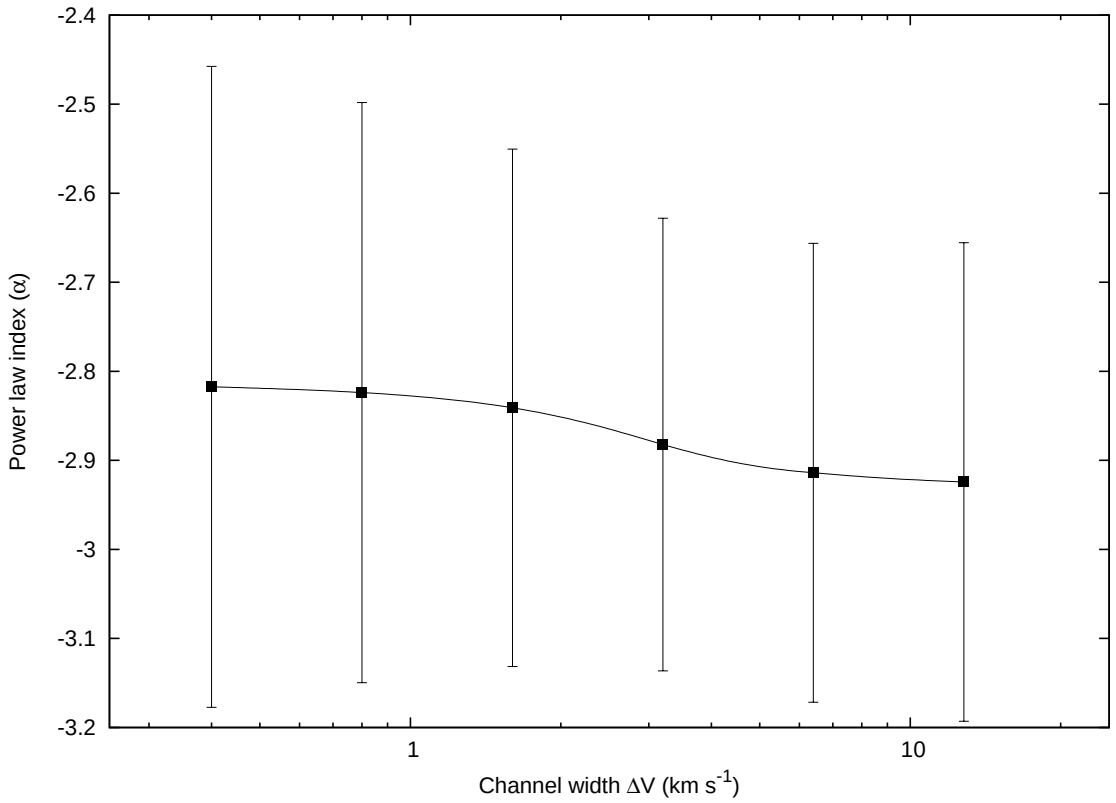

Figure 5.3: Power law index of the opacity fluctuation power spectrum for different velocity width of a channel centred at $V_{LSR} = -33$ km s^{-1}. The change of α for velocity width ranging from $\sim 0.4 - 12.8$ km s^{-1} is within the estimation errors.

Chapter 4 for discussion on this issue).

Fluctuations in both the density and velocity fields produced by the turbulence in the medium contribute to the observed H I opacity fluctuations. It can be shown that for the power spectrum estimated from "thick slices" with velocity width larger than the turbulent velocity dispersion, the contribution comes only from the density fluctuations, and all velocity information gets averaged out (Lazarian & Pogosyan, 2000). For "thin slices", the power law index of the observed power spectrum is $n + \beta/2$, where n is the index of the density fluctuation power spectrum and β is that of the velocity structure function. Here, the change of α is within the estimation errors for a wide range of velocity width. Since α remains

unchanged for "thin slices" with velocity width as small as ~ 0.4 km s^{-1}, there is a possibility that the turbulence velocity dispersion is smaller than 0.4 km s^{-1}. This, however, contradicts earlier observational result that the typical value of turbulent dispersion in Galactic cold H I is ~ 4.0 km s^{-1} (Radhakrishnan et al., 1972). Hence, we conclude that the effect of averaging over velocity is not significant in this case. But, with the present data, we cannot rule out a value of $\beta = 0.2 \pm 0.6$ which is consistent with the value of $\beta = 2/3$ predicted for turbulence in an incompressible medium (Kolmogorov, 1941).

5.4 Conclusions

In this work, we have studied the H I 21 cm opacity fluctuation towards Cas A. A simple but robust method of directly estimating the opacity fluctuation power spectrum from the observed visibilities is outlined. In this analysis technique we can avoid the complications of imaging the bright and extended continuum source, of subtracting the continuum and of making optical depth image for channels with H I absorption.

We have found that the H I opacity fluctuation power spectrum can be modelled as a power law with a power law index of $\sim 2.86 \pm 0.10$. This is consistent with earlier observational results. We have not found any significant difference of the power law index between velocity channels with absorption produced by the cold H I gas from the Perseus spiral arm and from the solar neighbourhood. We have also checked, by smoothing the visibility data for adjacent channels, if there is variation of the power law index with the velocity width of channels. It is found that, within the estimation errors, the power law index remains constant for a wide range of velocity widths. We cannot, however, rule out contribution of velocity fluctuations to the observed opacity fluctuations if the power law index of the velocity structure function $\beta = 0.2 \pm 0.6$. We plan to apply, in future, this visibility based method to estimate the power spectra for other lines of sight to study the opacity fluctuations in different regions of the Galaxy.

Chapter 6

C II radiative cooling of the diffuse interstellar medium

6.1 Introduction

The classical description of the Galactic interstellar medium (ISM) is that it consists of cold neutral medium (CNM), warm neutral medium (WNM), warm ionized medium (WIM) and a hot ionized phase (e.g. McKee & Ostriker, 1977). The diffuse ISM exhibits a vast range of densities, temperatures, ionization fractions and molecular abundances. The physical conditions in some given region of the ISM are, in turn, determined by a host of factors, including the local radiation field and cosmic ray energy density, the dust grain abundance, composition and size distribution, as well as mechanical energy input from both impulsive disturbances such as supernova explosions (McKee & Ostriker, 1977) as well as more steady sources such as stellar winds (Abbott, 1982). The heating and cooling balance of the ISM leads to different phases of a multi-phase medium coexisting in thermal pressure equilibrium even at very different temperatures (Field, Goldsmith & Habing, 1969; McKee & Ostriker, 1977).

Here we focus on understanding the origin of the C II* absorption line. CII 157.7 μm transition is the dominant contributor to the cooling in the ISM because of (1) the high abundance of carbon (second most abundant

metal in gas phase), (2) high abundance of its singly ionized stage in the diffuse CNM, WNM and WIM, and (3) the easy excitation of the $^2P_{3/2}$ fine-structure state ($h\nu/k = 91$ K) by collisions under typical conditions in the diffuse ISM. The C II radiative cooling rate can be determined directly from the C II line intensity of the $^2P_{3/2}$ to $^2P_{1/2}$ 157.7 μm transition in the far infra-red (FIR). Alternately, the measured column density of C II* per H I atom is also believed to be a direct measure of the cooling rate of the gas (Pottasch, Wesselius & van Duinen, 1979; Wolfe, Prochaska & Gawiser, 2003; Lehner, Wakker & Savage, 2004). C II* column density can be measured from the C II* absorption lines originating in the $^2P_{3/2}$ state at 1037.018 Å and 1335.708 Å in the far ultraviolet (FUV). In steady state the cooling rate is equal to the heating rate, which in turn depends on the flux of ultraviolet (UV) photons and cosmic rays, and thus on the star formation rate. Based on this reasoning, observations of C II* in high redshift damped Lyman-α systems (DLAs) have been used to deduce the star formation rate in these systems (Wolfe et al., 2003).

In detail however, the UV and cosmic ray flux required to maintain a given heating rate crucially depends on the physical conditions of the gas. Whether the gas is in the CNM or WNM phase, for example, is one of the important issues in this regard. The calculations of the star formation rate in DLAs by Wolfe et al. (2003) were based on the assumption that most of the gas that gives rise to the C II* absorption is in the CNM phase. Otherwise, if it is assumed that all the gas is in the WNM phase, then the inferred star formation rate per unit area in DLAs is significantly higher than that of the Milky way. On the other hand, Lehner et al. (2004) studied the C II* absorption along high Galactic latitude extra-galactic sources, and in conjunction with observations of the diffuse Hα emission along these same line of sight concluded that most of the C II* absorption occurs in the WNM or WIM. Their conclusion that most of the C II* along high Galactic latitudes comes from the WIM rests in large part on the assumption that there is negligible amount of gas in the CNM phase along these sight lines. However, there exist several high latitude lines of sight with a high CNM

fraction. One way to resolve the issue of the origin of the C II* absorption would be to directly measure the temperature in individual components that are responsible for the C II* absorption.

In the radio regime, the classical method to determine the kinetic temperature of the gas consists of observing the H I 21 cm line in absorption towards a bright radio continuum source; this, in conjunction with observations of the emission spectrum along a nearby line of sight allows one to measure the spin temperature (T_s) of the H I (see e.g. Kulkarni & Heiles, 1988, for details). While the H I spin temperature, strictly speaking, characterizes the population distribution between the two hyperfine levels of the hydrogen atom, it is often used as a proxy for the kinetic temperature of the gas. This is because, in high density regions, T_s is expected to be tightly coupled to the kinetic temperature via collisions, while in low density regions, resonant scattering of Lyman-α photons again may couple the spin temperature to the kinetic temperature (Field, 1958).

In this work we present the results of GMRT (Swarup et al., 1991) 21 cm H I observations toward 7 high Galactic latitude extra-galactic radio sources for which both H I 21 cm single dish emission spectra and UV spectroscopic data covering C II* absorption are available.

6.2 Observation and data analysis

In the complete sample of Lehner et al. (2004), there are seven radio-loud high Galactic latitude sources with flux density at 1420 MHz $\gtrsim 100$ mJy in the sky accessible to GMRT. For all these sources, substantial flux comes from the compact components. This forms the sample for the present study. The details of the sources are summarized in Table 6.1. The columns in Table 6.1 are: (1) the background radio source, (2) the IAU name of the source, (3) the Galactic latitude, (4) the Galactic longitude and (5) extinction $E(B-V)$ from Lehner et al. (2004). The GMRT radio observations for six of these sources (except 3C 273) were conducted in the 8th observation cycle between June – August, 2005 with the observa-

tion frequency centered at the frequency of the H I 21 cm line. For these sources, the total bandwidth was 2.0 MHz (for Mrk 421), 0.5 MHz (for NGC 1068) and 1.0 MHz (for the rest of the sources) with 128 spectral channels (i.e. a velocity resolution of $\sim$ 3.3, 0.8 and 1.6 km s^{-1} respectively) to cover the complete velocity range of H I emission detected from LDS. The total on-source time was 6–8 hour on each source. Scans on standard calibrators were used for flux calibration, phase calibration and also to determine the bandpass shape. Data analysis was done using AIPS. After flagging out bad data, the flux density scale and instrumental phase were calibrated. The continuum emission was then subtracted from the multi-channel visibility data set. Any residual continuum was subtracted in the image plane by fitting a linear baseline to line-free regions. The absorption spectra were extracted from the high resolution image cubes where the the smooth emission was resolved out. Typical RMS optical depth achieved was few times 10^{-3} for these observations.

For 3C 273, the 21 cm H I absorption spectrum has been taken from Dwarakanath, Carilli & Goss (2002) who observed from Westerbork Synthesis Radio Telescope (WSRT) with a velocity resolution of $\sim$ 2.1 km s^{-1}. The 21 cm emission spectra, for all the sources, were taken from the Leiden-Dwingeloo survey (LDS; Hartmann & Burton, 1997). The angular resolution of the LDS survey is $\sim 35'$ and the spectral resolution is 1.030 km s^{-1}.

6.3 Calculations

First the H I emission and absorption spectra were independently decomposed into multiple Gaussian components for the complete available velocity range using least-square minimization with minimum number of components. It was noted that although the decomposition was done independently for the emission and absorption spectra, for each of the components detected in absorption, within the spectral resolution there was always a corresponding emission component with the same central veloc-

Table 6.1: Details of our sample

Background Sources	IAU Name	(l, b)	$E(B-V)^a$ (mag)
3C 273[b]	J122906+020305	289.95, +64.36	0.021
3C 351	J170443+604449	090.09, +36.38	0.023
Mrk 421	J110427+381232	179.83, +65.03	0.015
NGC 1068	J024240−000047	172.10, −51.93	0.034
NGC 4151	J121032+392420	155.08, +75.06	0.028
PG 1302−120	J130533−103320	308.59, +52.16	0.043
PKS 2155−304	J215852−301330	017.73, −52.25	0.022

[a] From Lehner et al. (2004)

[b] H I absorption spectrum from Dwarakanath et al. (2002)

ity. For five out of seven of these lines of sight, H I absorption was detected in these observations.

For a homogeneous cloud, the emission and absorption spectra uniquely yield the spin temperature, i.e.

$$T_s = \frac{N(HI)}{1.823 \times 10^{18} \int \tau(v) \mathrm{dv}} \tag{6.1}$$

with N(H I) being determined from the (off source) emission spectrum and $\tau(\mathrm{v})$ being determined from the absorption spectrum. Application of Equation (6.1) to the observed spectrum produced by a set of optically thin multiple components along the line of sight will yield a column density weighted harmonic mean temperature of the individual components. This equation is used to obtain an average $\mathrm{T_s}$ and the total H I column density detected in absorption (includes only the components detected in both emission and absorption) from the H I 21 cm emission and absorption spectra for these five lines of sight. We have also calculated, for individual lines of sight, $\mathrm{N(H\ I)_{100}}$, a limit of total H I column density in cold phase if all the components have temperature below 100 K. This has been done by using the actual $\mathrm{T_s}$ for components with $\mathrm{T_s} \leq 100$ K and assuming a

Table 6.2: Summary of our results - I

Background Sources	N(H I)$^a_{\rm abs}$ 10^{19} cm^{-2}	N(H I)$^a_{100}$ 10^{19} cm^{-2}	N(H I)^b 10^{19} cm^{-2}	$\frac{N(H\ I)_{\rm abs}}{N(H\ I)_{\rm tot}}$
3C 273	8.87±1.20	1.88	14.9±1.3	0.59±0.10
3C 351	1.36±0.43	2.20	15.8±1.1	0.09±0.03
Mrk 421	1.21±0.29	9.70	15.0±0.8	0.08±0.02
NGC 1068	5.58±0.53	3.20	26.1±0.7	0.22±0.02
NGC 4151	–	8.61	24.1±3.2	–
PG 1302−120	15.51±3.23	7.81	30.2±5.2	0.51±0.14
PKS 2155−304	–	2.38	12.4±0.2	–

[a] Components within the velocity range of the C II* absorption line

[b] From Leiden-Dwingeloo Survey H I emission spectra

spin temperature of 100 K for the rest of the components (includes all the components detected in emission spectra).

6.4 Results and Conclusions

For five out of seven lines of sight, we detect H I absorption. We present our results in Table 6.2 and Table 6.3. The columns in Table 6.2 are: (1) the background radio source, (2) the total H I column density detected in the absorption spectra, (3) the limits of total H I column density in cold phase if all the components have temperature $T_s \leq 100$, (4) the integrated line of sight H I column density from LDS emission spectra and (5) the fraction of total H I column density detected in absorption spectra, N(H I)$_{\rm abs}$/N(H I)$_{\rm tot}$. The columns in Table 6.3 are: (1) the background radio source, (2) column density weighted line of sight spin temperature calculated from all the components detected in absorption, (3) the column density of C II* from Lehner et al. (2004), (4) and (5) the estimated star formation rate for the "CNM" and "WNM" model (explained in the following paragraphs). All

Table 6.3: Summary of our results - II

Background Sources	T_s^a K	log N(CII*)^b (dex)	SFR ($M_\odot$ yr^{-1} kpc^{-2})^c CNM model	WNM model
3C 273	487± 80	14.07	2.0×10^{-3}	50×10^{-2}
3C 351	173± 83	14.28	2.0×10^{-2}	32×10^{-2}
Mrk 421	65± 31	13.91	7.9×10^{-3}	13×10^{-2}
NGC 1068	151± 40	14.02	3.2×10^{-3}	13×10^{-2}
NGC 4151	–	14.16	–	16×10^{-2}
PG 1302−120	441±123	14.28	2.0×10^{-3}	32×10^{-2}
PKS 2155−304	–	13.81	–	13×10^{-2}

[a] Average T_s^a calculated from all the components detected in absorption

[b] From Lehner et al. (2004)

[c] See text in Section 6.4 for details.

the H I column density mentioned above are calculated from the components with central velocity within the velocity range of the C II* $\lambda1037$ or $\lambda1335$ far ultraviolet absorption lines detected in spectra obtained from *Far Ultraviolet Spectroscopic Explorer* (FUSE) and the Space Telescope Imaging Spectrograph (STIS) onboard of the *Hubble Space Telescope* (HST). We summarize our results in Figure (6.1). In panel (a) the fraction of H I detected in absorption for individual lines of sight (solid circles) are plotted against the total H I column density derived from the LDS emission spectra. The upper limits for cold H I fraction for $T_s \leq 100$ are also shown (empty boxes) in the same panel. Total H I column density detected in absorption N(H I)$_{abs}$, extinction $E(B-V)$ and total H I column density derived from the LDS emission N(H I)$_{tot}$ are plotted against the observed C II* column density N(C II*)$_{obs}$ in panels (b), (c) and (d) respectively.

It is clear from the plot that the fraction of "cold" gas has a wide range and a good fraction of high galactic latitude gas can be in cold phase. For these 7 lines of sight, there is no significant correlation between N(C II*) and N(H I)$_{abs}$, N(H I)$_{tot}$ or $E(B-V)$. Though it is not possible to derive

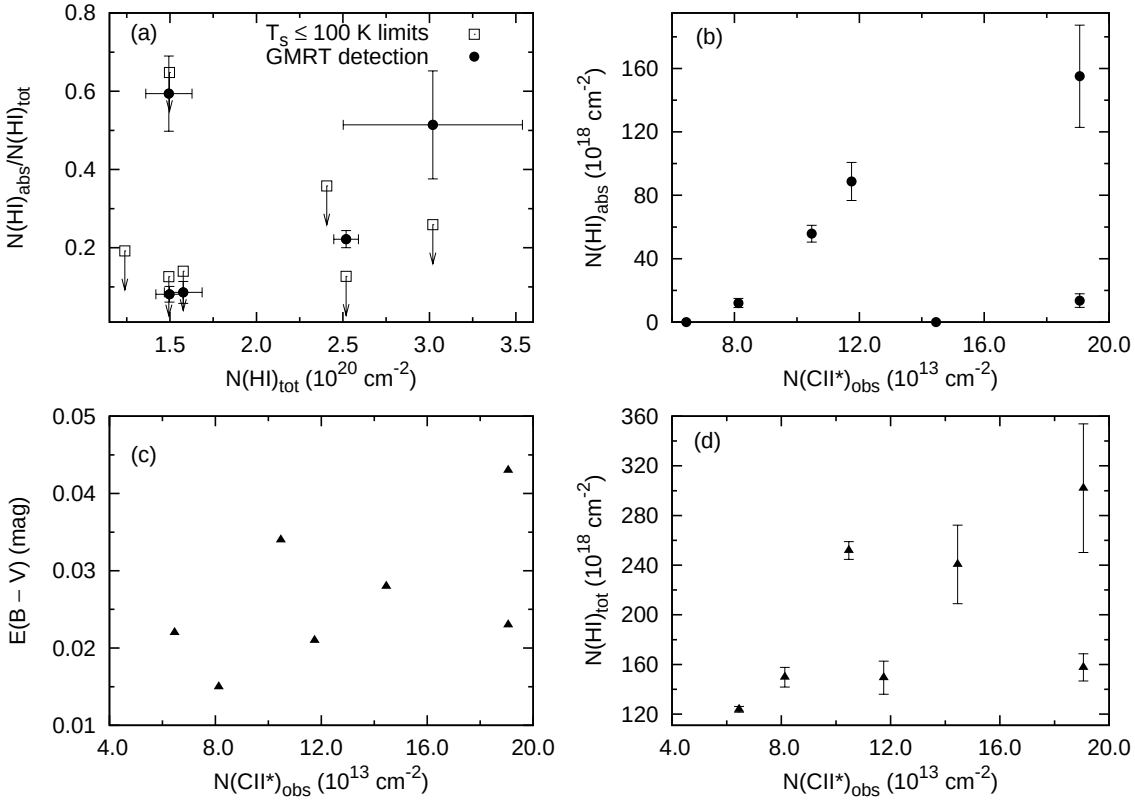

Figure 6.1: (a) N(H I)$_{\rm abs}$/N(H I)$_{\rm tot}$ as a function of N(H I)$_{\rm tot}$ (detections are shown as solid circles, 3σ upper limits for $T_s \leq 100$ are shown as empty boxes). (b) N(H I)$_{\rm abs}$ plotted against N(C II*). (c) $E(B-V)$ as a function of N(C II*) and (d) N(H I)$_{\rm tot}$ as a function of N(C II*).

a statistically significant result because we have observations for a small number of lines of sight, detection of H I absorption for 5 out of 7 of these lines of sight and a direct measurement of spin temperature for these components has significant implications. It shows that there exist high Galactic latitude lines of sight with C II* absorption for which H I absorption is produced by cold gas and a non-negligible fraction of the H I components have spin temperature in the CNM range ruling out the theory that all or most of the C II* absorption must originate in the WNM or WIM. But, at the same time, since there is no significant correlation of the cold H I column density and the C II* column density, one cannot assume that all of the

C II* absorption occurs in the CNM.

We have also estimated the star formation rate per unit area for these lines of sight assuming the extreme situations where all of the observed C II* absorption originate (i) only in WNM and (ii) only in CNM. Following the calculations of Wolfire et al. (1995), the photoelectric heating rate from dust grains is assumed to be approximately equal to the C II fine structure cooling rate in the CNM and about an order of magnitude higher in the WNM. The estimated star formation rate is $0.1 - 0.5$ $M_\odot$ yr^{-1} kpc^{-2} for the "WNM model", and $2.0 \times 10^{-3} - 2.0 \times 10^{-2}$ $M_\odot$ yr^{-1} kpc^{-2} for the "CNM model" (excluding the two lines of sight with no detected H I absorption for the second case). Clearly, for the lines of sight with very less or no detected cold H I absorption, the star formation rate is more than an order of magnitude higher than the observed rate of $\sim 4 \times 10^{-3}$ $M_\odot$ yr^{-1} kpc^{-2} (Kennicutt, 1998).

From direct detection of H I absorption, we can conclude that the assumption, that there is no CNM along these lines of sight, is not correct. On the other hand, the fact that C II* column density does not correlate with cold CNM column density makes one doubt that C II* absorption arises *solely* in CNM. Rather, it is more likely to be a mixture of gas in both cold and warm phase. A higher value of the inferred star formation rate for WNM dominated lines of sight also does not necessarily mean that most of the C II* absorption arise from gas in the CNM phase. However, the constraint on the upper limit of CNM column density from non-detection of H I absorption is not very strong. It is hence necessary to carry out more sensitive observations for a larger sample of suitable lines of sight.

Chapter 7

Summary of the thesis

I have presented, in this thesis, my work on the ISM temperature, turbulence and the interplay of these two, concentrating mostly on the science of the diffuse neutral ISM. First we have investigated the issue of non-thermal broadening of linewidth and its implications on temperature measurements along with the distribution of diffuse gas in different thermal phases from both single dish and interferometric observations. Next, we have studied the nature of turbulence in two different components of the ISM (namely in supernova remnants and in diffuse neutral gas). Finally, we have considered an illustrative example to show the importance of temperature measurements. The main results that are reported in this thesis are summarized below. Further, scope for future work related to these studies is also discussed briefly.

7.1 Key results

7.1.1 Diffuse neutral ISM - Temperature and turbulence

The temperature of the neutral hydrogen is classically measured from the H I emission and absorption spectrum. The derived spin temperature is found to be a very good proxy of the gas kinetic temperature. The temperature can also be inferred from the observed line width. But this gives only an upper limit to the kinetic temperature, since there may be significant

non-thermal broadening of the line due to processes like turbulence in the gas. We have found that the non-thermal contribution to the H I line width has a power law scaling with the derived length scale and the power law index is consistent with what one would expect from a turbulent medium with a Kolmogorov scaling. Using this scaling relation for the millennium Arecibo 21 cm absorption-line survey measurements, we have also determined the corrected H I kinetic temperature and found that $\sim 30\%$ of the total H I column density is in the warm unstable phase.

These results, derived from the millennium Arecibo 21 cm absorption-line survey measurements, are, however, based completely on single dish observations of H I emission and absorption spectra. Single dish spectra are known to be affected by stray radiation entering via the side-lobes of the telescope beam, self-absorption of background H I emission by foreground gas and inaccurate subtraction of the H I emission in the beam to obtain the H I absorption spectrum. Interferometric 21 cm absorption studies of lines of sight towards compact sources are not affected by the above issues.

We have hence carried out deep, high resolution interferometric absorption observations towards 18 compact sources to obtain absorption based estimates of the distribution of diffuse ISM in different thermal phases. Based on the upper limits of the kinetic temperature derived from the line widths, it is found that more than 80% of neutral gas has $T_{kmax} > 500$ K and $\sim 65\%$ gas is in warm unstable thermal phase (as opposed to the Arecibo survey results of $\sim 60\%$ with $T_{kmax} > 500$ K and $\sim 50\%$ warm unstable gas). After correcting for the non-thermal contribution to the line width using the above-mentioned power law scaling of non-thermal velocity dispersion with the length scale, we found that approximately half of the gas is in warm unstable phase and the rest of the gas is in stable CNM phase (as opposed to the Arecibo survey results of ~ 60, 30 and 10% in CNM, warm unstable and warm stable phase respectively). Derived temperature and peak optical depth are found to be anti-correlated which is qualitatively consistent with earlier reported results. In details, however, the $T-\tau$ cor-

relation is found to be significantly steeper than that reported earlier.

Direct measurement of properties like temperature, pressure, density and ionization fraction of the ISM is very important in understanding various physical processes related to the ISM physics. As an illustrative example, we have considered the case of the cooling of diffuse ISM. CII 157.7 μm is a major coolant of the diffuse interstellar gas. The inferred heating rate of interstellar gas estimated from CII radiative cooling crucially depends on physical conditions like the temperature of the gas. It is generally assumed that most of the gas that gives rise to the C II* absorption is in the cold or warm phase. This is, however, an *ad hoc* assumption. Our direct observations of the Galactic H I for lines of sight with C II* absorption clearly show that one cannot assume that all or most of the C II* absorption occurs in the cold or warm gas. Rather, it is more likely to be a mixture of gas in both cold and warm phases.

7.1.2 Turbulence and structure in different ISM phases

The ISM is believed to have a clumpy hierarchical structure over scales of several orders of magnitude. The self-similar turbulent structure in different phases of the ISM has also been observationally established using a variety of techniques. The indication that thermal steady state models are not applicable for the ISM may be related to the turbulent nature of the ISM. Hence, this exercise of measuring the ISM temperature from the HI observations is very much coupled with understanding in detail the nature of turbulence in the ISM. Turbulence in two different components of the ISM (namely in supernova remnants and in the cold diffuse neutral gas) is probed as a part of this thesis work.

On the galactic scale, supernovae and supernova remnants play a very important role as a link between the gaseous and stellar components of the Galaxy. In addition to the large scale shell-like or filled-centre structures, supernova remnants show a very rich and complicated structure over a wide range of scales. For the first time, we provide a quantitative estimate of the fine scale structure. We have found that the angular power spec-

tra of the synchrotron radiation intensity fluctuations for the shell type supernova remnant Cas A and the filled-centre Crab supernova remnant can be described as a power law with index -3.24 ± 0.03. This power law power spectrum is consistent with magnetohydrodynamic turbulence in the synchrotron emitting plasma. For Cas A, there is a break in the power spectrum and the power law index changes from -3.2 to -2.2 at large angular scales. This transition occurs at an angular scale that corresponds to the shell thickness of Cas A. We interpret this as a transition from three dimensional turbulence to two dimensional turbulence on scales that are smaller and larger than the shell thickness respectively.

We have also studied opacity fluctuation of the H I 21 cm absorption towards Cas A. From similar studies using H I emission observations, the intensity fluctuation power spectrum was found to be a power law with an index of ~ -3. We have found that the opacity fluctuation power spectrum has a power law index of $\sim 2.86 \pm 0.10$ over the scales of $0.07 - 3.6$ pc. This is consistent with previously reported observational results based on both H I emission (over somewhat larger scales) and absorption studies (over a similar range of scales). Power spectra derived for the gas from the Perseus spiral arm and from the solar neighbourhood show no significant difference. The variation of the power law index with the velocity width of the channel is also within the estimation error ruling out any significant effect of averaging over velocity. We cannot, however, rule out contribution of velocity fluctuations to the observed opacity fluctuations if the power law index of the velocity structure function is $\beta = 0.2 \pm 0.6$.

7.2 Scope for future work

In the light of the investigations and the results reported in this thesis, the following are the natural extension of this work, which we plan to do in near future.

Direct detection of H I 21 cm absorption from cold gas towards high Galactic latitude lines of sight has shown that C II 157.7μm radiative cool-

ing occurs in both cold and warm phases of diffuse ISM. But, we have observations for only a few lines of sight which prevents us from statistically checking whether the C II* column density has any significant correlation with cold H I column density. This is primarily because there are not many lines of sight towards strong background source suitable for H I 21 cm absorption study and with known C II* column density. But we plan to increase the sample size in near future by carrying out deep 21 cm absorption studies towards some of the weak sources. This can be complemented with the high-sensitivity and high angular resolution archival H I emission survey data to determine the physical properties of the gas. Analysis of archival optical and ultraviolet spectroscopic data for a few such lines of sight will also allow detailed modelling of the physical condition of halo ISM.

We have direct observational evidence that a large fraction of diffuse neutral ISM is in the thermally unstable phase. Our result is based on deep, interferometric observations of H I 21 cm absorption. But, it is important to establish this observational result even more strongly. We are currently carrying out a deep H I absorption survey using GMRT and WSRT to acquire high spectral resolution interferometric absorption spectra towards ~ 30 more compact sources, to increase the statistical significance of our result. It is also necessary to check if non-equilibrium models can explain the observations properly.

We have shown that the intensity fluctuation power spectra at radio wavelengths for both the Cas A and the Crab Nebula is a power law. This is consistent with our present understanding of the magnetohydrodynamic turbulence. We plan to analyse, in near the future, radio and X-ray archival data of a number of Galactic supernova remnants to systematically measure fluctuations in the density and magnetic fields. The synchrotron intensity fluctuation power spectrum at radio wavelengths will depend on both the density and magnetic field fluctuations whereas at X-ray wavelengths the power spectrum will depend only on the density fluctuations. Thus, a comparison between radio and X-ray observa-

tions will allow one to disentangle the structures of density and magnetic fields. Comparing the power spectra for a number of SNRs at different wavelengths will also help us to check the universality of the nature of turbulence which is most probably responsible for these structures.

Finally, we have outlined a simple but robust method of directly estimating the opacity fluctuation power spectrum from the observed visibility function completely avoiding the complications of imaging the bright and extended continuum source, of subtracting the continuum and of making optical depth image for channels with H I absorption. We have used this technique to study the H I 21 cm opacity fluctuation towards Cas A. Our result is consistent with earlier observational evidence of a power law fluctuation power spectrum (with power law index ~ -3) of cold H I gas in our Galaxy. This assures us of the consistency of our analysis technique. We plan to apply this simple visibility based method to estimate the power spectra for other lines of sight to study the opacity fluctuations in different regions of the Galaxy and to derive a more complete understanding of the density and velocity fluctuations in the ISM.

7.3 Concluding remarks

As a whole, in this work, a couple of issues related to the science of the ISM have been studied, primarily from an observer's point of view. For some of the aspects, within the limited scope of this thesis work, interesting results are derived and definitive conclusions are drawn. But, as expected, many things still remain elusive. This is simply because of the fact that the physical properties of the ISM on any scale are determined by various processes over a range of scales. Hence, the associated physics is quite complex, complicated and entangled. Then again, it is this complexity that also makes it extremely *interesting*.

Epilogue

or why am I doing what I am doing?

I have now put together the work that I have done during last five years or so, on the science of the interstellar medium. Hopefully, this thesis will soon be submitted for the degree of Doctor of "*Philosophy*". After writing approximately a hundred pages, I strongly feel that I deserve the right to write down at least a couple of pages on *philosophy*. This is not to fulfill any official requirement of the university and hence, I guess, should not undergo a review. This is rather a reflection of personal opinions and ideas. In some sense this is an explanation of *why am I doing what I am doing*, an honest and sincere answer from my personal point of view. From the very first day when I joined NCRA-TIFR as an astronomy student, I have faced, as expected, a wide variety of questions from many of my friends, relatives, acquaintances and family members. Why am I trying to be a *doctor* when I have already got an engineering degree? Am I going to go to the moon boarding one of those NASA rockets? Can I predict when will someone get married? Do I also do palmistry? Have I invented or discovered anything new? And finally, will what I do ever be of any use to anyone?

I have often ignored these questions to hide my incapability of properly addressing these questions. But now, when I am about to finish my thesis work, I strongly feel that they deserve to get an appropriate, honest and satisfactory answer - not just because they are my friends or relatives, but for ages *they*, as in "common people", have significantly contributed, in their own way, to the progress of science. Though there is no guarantee that this time I will be able to answer all or any of the questions satisfac-

torily, I must try honestly for the completeness of this thesis work.

Well, all these questions other than the very last one can probably be handled without much effort. For historical reasons this advanced academic degree is called Doctor of Philosophy (for the Latin *philosophiæ doctor*). Here *doctor* means teacher and philosophy, used in a broad sense, includes all academic disciplines outside the professional fields of theology, medicine and law. I have no intention of practicing astrology and am also not very keen to travel to the moon. So, what am I really doing?

Do you remember the beautiful opening narration from the movie Stardust (2007)? *A philosopher once asked, "Are we human because we gaze at the stars, or do we gaze at them because we are human?"* I believe the first one to be correct. What do you think? Anyway, fortunately gazing at the stars is both a passion and a profession for me. I am a student of astronomy. Astronomy (literally means "the laws of stars") is the *scientific study* of "objects and matter outside the earth's atmosphere and of their physical and chemical properties" (Merriam-Webster). By scientific study I mean the method of studying nature to derive empirical theories on the basis of experiments and/or observations following the logic of reproducibility, predictivity and parsimony. In this framework, theories are perpetually open to falsification on the basis of experiments and observations. It is crucial to appreciate the significance of this scientific framework which helps in differentiating science from non-science and, most importantly, pseudo-science.

Let us consider, as an example, the difference between predicting the timing of the next total solar eclipse and predicting "when someone will get married" from the position of stars and planets at the time of her birth. The theory that is used to predict eclipses has gone through repeated re-examinations by comparing observational evidence with theoretical predictions. Even after centuries of success, the theory remains open to review and, if necessary, modifications. Even when a theory has undergone a large number of tests so that it can be considered fully verified and can be called a *law*, it is still not sacred and is allowed to be modified or even

abandoned based on observational evidence. One of the critical aspects of science is that the collected observational evidence and details of the theory are publicly available making it possible for anyone to check the reliability and repeatability, ruling out personal biases. Above all, there is a parsimonious underlying theory (the theory of Gravitation governing the motion of planets and satellites) that is used for these predictions. Contrary to this, the theory of predicting the marriage time has never been open to any such review or repeated comparison of observation and prediction. All such past efforts, though rare, have instead shown the lack of any reproducibility and predictivity and thus the theory does not qualify to be considered as science.

So, to summarize, I am one of those, who carry out scientific studies of the cosmos. As an individual, I get the chance to work only on some limited aspects. However, the field of interest of the community is everything out there - the sun and the solar system, the stars, the Milky Way (i.e., our Galaxy), the (other) galaxies and the whole Universe. This is probably the oldest branch of natural science and, in some sense, is the one closest to religion addressing questions related to the creation, evolution and governing laws of the Universe. In the context of religion, I still remember my awe when, in one of the graduate school lectures, Jayaram, my thesis supervisor, did the calculations to show that the formation of micron size dust grains in space takes about 100000 years! As if that was not enough, almost in the soothing voice of one of the sages from ancient India, he then commented that this is anyway a very “small” timescale. The overwhelming feeling soon turned into my strongest source of inspiration for doing astronomy.

For my thesis, I have done observational study of the properties of the interstellar medium. The interstellar medium (or ISM in short) is very low density material that fills the space in between the stars. Even if the density is very low, it can be “seen” using various astronomical techniques. I have observed, using different telescopes, electromagnetic radiation from the ISM of the Milky Way (mainly from the neutral hydrogen gas in the ISM

emitting at radio frequencies). From these observations, I have inferred the physical properties of the gas. I must clarify here that all these works are collaborative in nature where many people have contributed but I have taken a leading role doing a major fraction of the job. So, when I say "I have done", it really means that a team of people have done this.

Of course, before me, many others have observed the ISM to study the physical properties. What I have specifically done, is to try to find out whether the ISM is in a thermal steady state and whether the turbulence plays any role in different components of the ISM. It is not a *discovery* in the true sense, but we have found that the laws of turbulence derived from laboratory experiments and theoretical understanding are also applicable even at these very large scales. There is also strong evidence based on our observations that the ISM is not in thermal equilibrium. These are, however, not completely new results. Some earlier observations have also indicated the same thing. But the present results are derived from independent observations and different analysis techniques. These cross-checks and re-examinations are, as I have already pointed out, very crucial steps in developing any scientific theory. So, I have not *discovered* anything fascinatingly new, but I have been working as a part of the framework to ensure the *true* scientific nature of the study to derive an understanding of the properties of the ISM.

The question that may come to ones mind next is "So what?". Well, the *basic* aim of astronomy (and of all other natural sciences) is to derive empirical theories and to understand the laws of nature. Our main driving force for research in basic science is our dream to understand, in detail, how nature works. There are various astrophysical processes that couple stars and the ISM, and hence the ISM plays a crucial coupling role in relating stellar and galactic scales. Hence, the study of the properties of the ISM is very important to understand the stellar and galactic phenomenon.

Now, one may still not be convinced with this. Will it ever be of any use to anyone? Otherwise, what is the point? One may not see an apparent and immediate usefulness of this whole exercise. Let me point out, these

issues are not specific to just astronomy and can, in general, be raised for any fundamental research. This is also the key question that I want to address here from my personal point of view. It is indeed true that the "usefulness" of astronomy (or any of the basic sciences and mathematics) have been discussed quite elaborately by many people in the past. Some of the *giants* of the community have talked and written about it. Why then am I trying to rush in *where angels fear to tread*? The arguments for fundamental research (in astronomy) still lack wide acceptability. I am not hoping that this article will solve the problem once and for all, but "there is no harm in repeating a good thing". I also found the arguments of some of the renowned persons from the field in this regard to be completely unacceptable and feel the need for this repetition more strongly.

I was fortunate to attend a lecture delivered by an eminent astronomer and cosmologist on "How Astronomy has Contributed to Enrichment and Survival of Human Societies" in the 27th annual meeting of the Astronomical Society of India held at the Indian Institute of Astrophysics, Bangalore (February, 2009). He elaborated on how astronomy has helped in the developing space technologies which in turn have contributed in the fields of health, education, entertainment, communication (via satellites), weather prediction and agriculture, navigation and military purposes. In the same way, he argued, current research with no apparent practical use may in future be the key to "the survival of our civilization on Earth".

I am sorry to say, I was very disappointed. Is it just this? I do not quite agree. Before I explain why, let us listen to this dialogue between Socrates and Glaucon (from Plato's The Republic, Book VII):

> **Socrates:** Shall we set down astronomy among the subjects of study?
>
> **Glaucon:** I think so, to know something about the seasons, the months and the years is of use for military purposes, as well as for agriculture and for navigation.

The same reasons - military purposes, agriculture and navigation! It seems as if the general perception of the usefulness of astronomy has not

changed at all over the past 2400 years. Remember that in both the cases, this line of justification is presented in an academic discussion session. Neither Glaucon nor the eminent astronomer I have mentioned was addressing politicians or bureaucrats to justify any funding, and that is what is more surprising. Let us go back to *The Republic* for Socrates' opinion in this regard:

> **Socrates:** It amuses me to see how afraid you are, lest the people should accuse you of recommending useless studies.

Then Socrates goes on justifying how astronomy should be done "in the right way" that *compels the soul to look upwards*, to apprehend the laws of nature by reason and intelligence and to *make the natural gift of reason to be of any real use*. It is a pity that many of the scientists are hesitant to strongly put forward this cultural argument.

So, are we "useful" people or just some sort of parasites for the society? In this regard, let me put a personal perspective on *why am I doing what I am doing*. It is pointless to debate on the amount of money spent for basic research - it is not a very big share of the annual budget and we can afford it. The debate is on its justification. I agree that if there is no *use* of astronomy, then putting any effort to it is unjustified, but I disagree that "there is no use". I think that cultural upliftment alone is important enough to justify doing astronomy. I also agree that there are indirect uses of the derived knowledge that have added, sometimes in a very pivotal way (like in the case of satellite communication for example), comfort to our daily life. But the vulgarity lies in suppressing the most important contribution, namely the cultural upliftment, and purposefully replacing it (sometimes dishonestly) with popular secondary bi-products - agriculture, navigation, military purposes etc.

I consider astronomy to be a *normal* profession - like any other profession - where the immediate return is *job* satisfaction in addition to just earning a living. I enjoy the freedom that I get in this profession and love the feeling that *I don't work for anybody; I am just having fun*. Whether by profession you are a farmer, an engineer, a pilot or an astronomer, the

"social benefit" out of this work is merely a bi-product. The passion and motivation may come from the awareness of the usefulness, but that is a different thing. No one probably gets up in the morning and goes farming just because it will be *useful to the society*. In most of the cases, one is doing what one is doing because, within ones capabilities, that is the best (and/or easiest) way of earning a living. Can the possible future application of my current research in the field of "agriculture, navigation and military purposes" be the source of my motivation?

For me, astronomy is my passion because I find it really fascinating that, despite of all our limitations, through scientific study we are trying to understand natural laws of the creation and evolution of the Universe and are trying to make sense of our very existence. The motivation here is just our craving for knowledge, "not faith, not supposition, but knowledge". To me this seems like the most logical and obvious replacement of religion. All the great discoveries of astronomy put things into a perspective that help us in realizing, with all our greed and power, how pathetically insignificant we all are in the big picture. But, on the other hand this apprehension makes us proud of the triumph of pure knowledge and intelligence despite of our physical insignificance. The joy of *looking upwards* fills my heart when I think that I am also taking part, even if in a very insignificant way, in search of this Holy Grail.

Bibliography

Abbott D. C., 1982, ApJ, 263, 723

Arnal E. M., Bajaja E., Larrarte J. J., Morras R., Pöppel W. G. L., 2000, A&AS, 142, 35

Arons J., Max C. E., 1975, ApJ, 196, L77

Audit E., Hennebelle P., 2005, A&A, 433, 1

Bajaja E., Arnal E. M., Larrarte J.J., Morras R., Pöppel W. G. L., Kalberla P. M. W., 2005, A&A, 440, 767

Balsara D., Benjamin R. A., Cox D. P., 2001, ApJ, 563, 800

Barnard E. E., 1919, ApJ, 49, 1

Begum A., Chengalur J. N., Bhardwaj S., 2006, MNRAS, 372, L33

Beresnyak A., Lazarian A., Cho J., 2005, ApJ, 624, L93

Bharadwaj S., Ali S. S., 2005, MNRAS, 356, 1519

Bharadwaj S., Sethi S. K., 2001, JA&A, 22, 293

Bieging J. H., Crutcher R. M., 1986, ApJ, 310, 853

Bieging J. H., Goss W. M., Wilcots E. M., 1991, ApJS, 75, 999

Braun R., Kanekar N., 2005, A&A, 436, L53

Brogan C. L., Zauderer B. A., Lazio T. J., Goss W. M., De Pree C. D., Fasion M. D., 2005, AJ, 130, 698

Burkert A., Bate M. R., Bodenheimer P., 1997, MNRAS, 289, 497

Carilli C. L., Dwarakanath K. S., Goss W. M., 1998, ApJ, 502, L79

Chepurnov A. V., 1998, Astron. Astrophys. Trans., 17, 281

Cho J., Lazarian A., 2002a, ApJ, 575, L63

Cho J., Lazarian A., 2002b, Phys. Rev. Lett., 88, 245001

Cho J., Lazarian A., Vishniac E. T., 2002, ApJ, 566 L49

Cho J., Lazarian A., Yan H., 2002, in Taylor A. R., Landecker T. L., Willis A. G., eds., Seeing Through the Dust: The Detection of H I and the Exploration of the ISM of Galaxies, San Francisco: Astronomical Society of the Pacific, Vol. 276, p.170

Clark B. G., Radhakrishnan V., Wilson R. W., 1962, ApJ, 135, 151

Clark B. G., 1965, ApJ, 142, 1398

Condon J. J., Cotton W. D., Greisen E. W., Yin Q. F., Perley R. A., Taylor G. B., Broderick J. J., 1998, AJ, 115, 1693

Crovisier J., Dickey J. M., 1983, A&A, 122, 282

Crovisier J., Dickey J. M., Kazès I., 1985, A&A, 146, 223

Deshpande A. A., 2000, MNRAS, 317, 199

Deshpande A. A., Dwarakanath K. S., Goss W. M., 2000, ApJ, 543, 227

Dickey J. M., Lockman F. J., 1990, ARA&A, 28, 215

Dickey J. M., Terzian Y., Salpeter E. E., 1978, ApJS, 36, 77

Dieter N. H., Welch W. J., Romney J.D., 1976, ApJ, 206, L113

Dutta P., Begum A., Bharadwaj S., Chengalur J. N., 2008, MNRAS, 384, L34

Dutta P., Begum A., Bharadwaj S., Chengalur J. N., 2009, MNRAS, 397, L60

Dutta P., Begum A., Bharadwaj S., Chengalur J. N., 2009, MNRAS, 398, 887

Dwarakanath K. S., Carilli C. L., Goss W. M., 2002, ApJ, 567, 940

Elmegreen B. G., Falgarone E., 1996, ApJ, 471, 816

Elmegreen B. G., Kim S., Staveley-Smith L., 2001, ApJ, 548, 749

Ewen H. I., Purcell E. M., 1951, Nature, 168, 356

Faison M.D., Goss W.M., Diamond P.J., Taylor G.B., 1998, AJ, 116, 2916

Falgarone E., Puget J-L., Perault M., 1992, A&A, 257, 715

Ferrière K. M., 2001, Rev. Mod. Phys., 73, 1031

Fesen R. A., Hammell M. C., Morse J., Chevalier R. A., Borkowski K. J., Dopita M. A., Gerardy C. L., Lawrence S. S., Raymond J. C., van den Bergh S., 2006, ApJ, 645, 283

Field G. B., 1958, Proc. IRE, 46, 240

Field G. B., 1965, ApJ, 142, 531

Field G. B., Goldsmith D. W., Habing H. J., 1969, ApJ, 155, L149

Frail D. A., Weisberg J. M., Cordes J. M., Mathers C., 1994, ApJ, 436, 144

Gazol A., Vázquez-Semadeni E., Kim J., 2005, ApJ, 630, 911

Goldreich P., Sridhar S., 1995, ApJ, 438, 763

Gerola H., Kafatos M., McCray R., 1974, ApJ, 189, 55

Goodman A. A., Barranco J. A., Wilner D. J., Heyer M. H., 1998, ApJ, 504, 223

Goss W. M., Kalberla P. M. W., Dickel H. R., 1984, A&A, 139, 317

Green D. A., 1991, PASP, 103, 209

Green D. A., 1993, MNRAS, 262, 327

Green D. A., 2004, Bull. Astron. Soc. India, 32, 335

Hartmann J., 1904, ApJ, 19, 268

Hartmann D., Burton W. B., 1997, Atlas of Galactic Neutral Hydrogen, Cambridge University Press, Cambridge, NY

Heiles C., 2001, ApJ, 551, L105

Heiles C., Troland T., 2003a, ApJS, 145, 329

Heiles C., Troland T., 2003b, ApJ, 586, 1067

Heiles C., Troland T., 2005, ApJ, 624, 773

Heithausen A., Bensch F., Stutzki J., Falgarone E., Panis J.F., 1998, A&A, 331, L65

Hennebelle P., Audit E., 2007, A&A, 465, 431

Hennebelle P., Audit E., Miville-Deschênes, M.-A., 2007, A&A, 465, 445

Hill A. S., Stinebring D. R., Asplund C. T., Berkwick D. E., Everett W. B., Hinkel, N. R., 2005, ApJ, 619, L171

Hobson M. P., Lasenby A. N., Jones M., 1995, MNRAS, 275, 863

Hoyle F., 1953, ApJ, 118, 513

Iroshnikov P., 1964, Sov. Astron., 7, 566

Johnston S., Koribalski B., Wilson W., Walker M., 2003, MNRAS, 341, 941

Kalberla P. M. W., Burton W. B., Hartmann D., Arnal E. M., Bajaja E., Morras R., Pöppel W. G. L., 2005, A&A, 440, 775

Kanekar N., Subrahmanyan R., Chengalur J. N, Safouris V., 2003, MNRAS, 346, L57

Kennicutt R. C., 1998, ARA&A, 36, 189

Kim S., et al., 2007, ApJS, 171, 419

Klessen R.S., Burkert A., Bate M.R, 1998, ApJ, 501, L205

Kolmogorov A., 1941, Dokl. Akad. Nauk SSSR, 31, 538

Koyama H., Inutsuka S., 2002, ApJ, 564, L97

Krause O., Birkmann S. M., Usuda T., Hattori T., Goto M., Rieke G. H., Misselt K. A., 2008, Science, 320, 1195

Kraichnan R., 1965, Phys. Fluids, 8, 1385

Kulkarni S. R., Heiles C., 1988, in Verschuur G., Kellerman K., eds., Galactic and ExtraGalactic Radio Astronomy (2nd edition), Springer-Verlag, Berlin and New York, p95

Langer W. D., Velusamy T., Kuiper T. B. H., Levin S., Olsen E., Migenes V., 1995, ApJ, 453, 293

Larson R. B., 1981, MNRAS, 194, 809

Lazarian A., Pogosyan D., 2000, ApJ, 537, 720

Lehner N., Wakker B. P., Savage B. D., 2004, ApJ, 615, 767

McKee C. F., Ostriker J. P., 1977, ApJ, 218, 148

Mebold U., 1972, A&A, 19, 13

Mebold U., Winnberg A., Kalberia P. M. W., Goss W. M., 1982, A&A, 115, 223

Minter A., Spangler S., 1997, ApJ, 485, 182

Mohan R., Dwarakanath K. S., Srinivasan G. & Chengalur J. N. 2001, JApA, 22, 35

Morales M. F., Hewitt J., 2004, ApJ, 615, 7

Nagashima M., Inutsuka S.-I., Koyama H., 2006, ApJ, 652, 41

Passot T., Vázquez-Semadeni E., 2003, A&A, 398, 845

Payne H. E., Salpeter E. E., Terzian Y., 1983, ApJ, 272, 540

Pottasch S. R., Wesselius P. R., van Duinen R. J., 1979, A&A, 74, L15

Radhakrishnan V., Murray J. D., Lockhart P., Whittle R. P. J., 1972, ApJS, 24, 15

Reed J. E., Hester J. J., Fabian A. C., Winkler P. F., 1995, ApJ, 440, 706

Roshi D. A., 2007, ApJ, 658, L41

Roy N., Chengalur J. N., Srianand R., 2006, MNRAS, 365, L1

Roy N., Dutta P., Bharadwaj S., Chengalur J. N., 2009, MNRAS, 393, L26

Roy N. & Kanekar N., Frequency-switched bandpass calibration at the GMRT, 2007, NCRA Technical Report, R00228

Roy N., Peedikakkandy L., Chengalur J. N., 2008, MNRAS, 387, L18

Schwarz U. J., Troland T. H., Albinson J. S., Bregman J. D., Goss W. M., Heiles Carl, 1986, ApJ, 301, 320

Semelin B., Combes F., 2000, A&A, 360, 1096

Stanimirović S., Staveley-Smith L., Dickey J. M., Sault R. J., Snowden S. L., 1999, MNRAS, 302, 417

Stanimirović S., Heiles C., 2005, ApJ, 631, 371

Spitzer L., 1978, Physical Processes in the Interstellar Medium, Wiley-Interscience publication, New York

Swarup G., Ananthakrishnan S., Kapahi V. K., Rao A. P., Subrahmanya C. R., Kulkarni V. K., 1991, Curr. Sci., 60, 95

Tegmark M., Eisenstein D. J., Hu W., de Oliveira-Costa A., 2000, ApJ, 530, 133

Trimble V., 1973, PASP, 85, 579

van den Bergh S., 1970, ApJ, 160, L27

Vázquez-Semadeni E., Gazol A., Scalo J., 2000, ApJ, 540, 271

Vázquez-Semadeni E., Ryu D., Passot T., González R., Gazol A., 2006, ApJ, 643, 245

Weiler K. W. & Sramek R. A., 1988, ARA&A, 26, 295

Westpfahl D. J., Coleman P. H., Alexander J., Tongue T., 1999, AJ, 117, 868

Wolfe A. M., Prochaska J. X., Gawiser E., 2003, ApJ, 593, 215

Wolfire M. G., Hollenbach D., McKee C. F., Tielens A. G. G. M., Bakes E. L. O., 1995, ApJ, 443, 152

Wolfire M. G., McKee C. F., Hollenbach D., Tielens A. G. G. M., 2003, ApJ, 587, 278